

Maja Morawska

An Experimental Study of Anisotropic Stiffness of Tiller-Flotten Quick Clay Using Bender Elements

Master's thesis in Geotechnics and Geohazards

Supervisor: Steinar Nordal

June 2019

NTNU
Norwegian University of Science and Technology
Faculty of Engineering
Department of Civil and Environmental Engineering



Norwegian University of
Science and Technology

Maja Morawska

An Experimental Study of Anisotropic Stiffness of Tiller-Flotten Quick Clay Using Bender Elements

Master's thesis in Geotechnics and Geohazards
Supervisor: Steinar Nordal
June 2019

Norwegian University of Science and Technology
Faculty of Engineering
Department of Civil and Environmental Engineering

 **NTNU**
Norwegian University of
Science and Technology

Preface

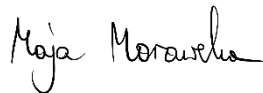
This study was performed as a Master's Thesis as part of MSc in Civil Engineering and was written at the Geotechnical Division of the Department of Civil and Environmental Engineering at the Norwegian University of Science and Technology (NTNU).

This study, performed during the Spring of 2019 over the period of 20 weeks, is a continuation of the author's specialization project thesis regarding the evaluation of bender elements system.

The main supervisor for the study was Professor Steinar Nordal with a co-supervisor, Professor Jean-Sebastien L'Heureux.

Since my first days in Trondheim, I had been fascinated by this unique material known as quick clay. So naturally, when the opportunity arose to research a topic that piqued my interest, I was excited to accept this challenge.

Trondheim, June 2019



Maja Morawska

Acknowledgments

I would like to thank the following persons for their help during this study:

My supervisor Professor Steinar Nordal and co-supervisor Professor Jean-Sebastien L'Heureux, for the valuable discussions and support throughout the study.

Senior engineer Per Asbjørn Østensen, for his help with the bender elements program.

Senior engineer Karl Ivar Volden Kvisvik and engineer Espen Andersen, for their help with the soil samples and triaxial equipment.

Beatriz Almarza Galdon and Katherine Emily Robinson, for their help with index testing and the laboratory equipment.

Abstract

Stiffness anisotropy at small strains is a distinctive feature of many natural soils. The nature of the soil is dependent on the geological processes that occur during soil formation. Stress conditions and depositional environment contribute to the variations of soil properties in different planes, resulting in soil anisotropy. Small strain stiffness anisotropy is crucial in understanding soil behaviour and is widely used in geotechnical numerical modelling. Therefore, there is a need for detailed investigations in this area.

Stiffness anisotropy of quick clay is of particular interest in this study. Due to their low shear strength and extremely high sensitivity, these deposits of sensitive marine clays are extremely challenging in geotechnical engineering. Further analysis on this material is conducted for a stronger understanding of the clay behaviour and to advance the research currently undergoing in the Tiller-Flotten area.

The main objective of this study is to investigate the small strains stiffness anisotropy of Tiller-Flotten quick clay. Using a bender element system, the small strain shear modulus was determined in different planes of the samples. Shear wave velocity measurements were performed on triaxial specimens obtained from mini-block samples. Vertical and horizontal samples were tested with bender elements in an unconfined state and during the consolidation in a triaxial apparatus.

The study results suggest that the Tiller-Flotten quick clay is inherently anisotropic. Shear waves propagate faster in the plane parallel to the bedding plane than in the normal plane. It is therefore concluded, that the stiffness anisotropy is a consequence of the clay's structure. The cross-anisotropic behaviour of Tiller-Flotten quick clay is however, not conclusively supported by the experimental findings of this study. Further investigations are required to verify this assumption.

Contents

List of Figures	xiii
List of Tables	xv
List Symbols and Abbreviations	xvi
Chapter 1 Introduction	1
1.1 Background.....	1
1.2 Objectives	2
1.3 Limitations.....	2
1.4 Research approach.....	2
1.5 Structure of the report.....	2
Chapter 2 Background	5
2.1 Wave propagation.....	5
2.2 Small strain stiffness.....	6
2.2.1 Factors influencing G_{\max}	6
2.2.2 Measurement of soil stiffness	11
2.3 Stiffness Anisotropy	12
2.3.1 Isotropy	12
2.3.2 Transverse isotropy	12
2.3.3 Stiffness anisotropy in clays.....	14
2.4 Sampling and sample disturbance	17
2.4.1 Sampling methods	17
2.4.2 Evaluation of sample quality	18
Chapter 3 Bender elements	21
3.1 Construction and operating principle.....	21
3.2 Travel time determination	22
3.2.1 First Arrival Method.....	23
3.2.2 Peak-to-peak Method	24
3.2.3 Cross Correlation Method	24
3.2.4 Phase Cross Spectrum Method.....	25
3.3 Travel distance determination.....	25
3.4 Factors influencing bender element testing	26
3.4.1 Resonant frequency	26
3.4.2 Near-Field Effect.....	27
3.4.3 P-wave component	30
3.4.4 Sample geometry.....	31
3.5 Anisotropy investigations with bender elements	32
Chapter 4 Tiller-Flotten Testing Site	33
4.1 Norwegian Geo-Test Sites	33

4.2	Site location	33
4.3	Engineering geology	34
4.3.1	Geological setting.....	34
4.3.2	Stress history	35
4.4	Stratigraphy and index properties	35
4.5	Shear wave velocity measurements	36
4.6	Clay mineralogy and structure.....	37
Chapter 5	Laboratory Investigations.....	39
5.1	Bender element equipment	39
5.2	Soil specimens	42
5.2.1	Division of the samples	42
5.2.2	Preparation for testing	45
5.3	Index testing	46
5.3.1	Water content	46
5.3.2	Density	46
5.3.3	Atterberg limits	47
5.3.4	Salinity	47
5.3.5	Fall cone.....	47
5.3.6	Grain size distribution	47
5.3.7	Degree of saturation, porosity and void ratio	47
5.4	Bender elements testing.....	48
5.4.1	Methodology	48
5.4.2	Overview of tests performed	49
Chapter 6	Overview of results	51
6.1	Index testing results	51
6.2	Bender elements testing results	51
6.2.1	Preliminary testing on the unconfined specimen.....	51
6.2.2	Main tests	54
6.3	Sample quality	62
Chapter 7	Discussion	63
7.1	Waveform analysis	63
7.1.1	Preliminary testing	63
7.1.2	Frequency changes	65
7.1.3	Signal distortion and near-field effect	66
7.2	Shear wave velocity.....	70
7.2.1	Shear wave velocity with depth.....	70
7.2.2	Shear wave velocity with time of consolidation.....	70
7.3	Small strain shear modulus.....	71
7.3.1	Effect of effective stress on shear modulus	71
7.3.2	Development of G_{max} with consolidation time	71

7.3.3	Correlations between G_{\max} and index parameters.....	75
7.3.4	Comparison of V_s and G_{\max} between in-situ and laboratory tests.....	78
7.4	Stiffness anisotropy	79
7.4.1	Discussion of stiffness anisotropy in Tiller-Flotten clay	80
7.4.2	Effect of consolidation stress on the anisotropy of G_{\max}	81
7.4.3	Anisotropy with depth	82
7.4.4	Effect of consolidation time on the anisotropy of G_{\max}	82
7.4.5	Influence of plasticity index on stiffness anisotropy	83
Chapter 8	Summary	85
8.1	Summary and Conclusions	85
8.2	Recommendations for Further Work	86
References	89
Appendices	95

List of Figures

Figure 2.1: Seismic wave types (Kramer, 1996).....	5
Figure 2.2: Relationship between shear modulus and shear strain according to (PLAXIS, 2018).....	6
Figure 2.3: Shear modulus vs confining stress relationships for normally and overconsolidated clays (Kokusho et al., 1982)	8
Figure 2.4: Correlations between G_{max} and void ratio (L'Heureux and Long, 2016)	8
Figure 2.5: Effect of I_p on the parameter k (Towhata, 2008)	9
Figure 2.6: Relations between G/G_{max} vs γ_c and soil plasticity for normally and overconsolidated soils (Vucetic and Dobry, 1991)	9
Figure 2.7: Effect of time of consolidation on small strain shear modulus (Anderson and Stokoe, 1978)	10
Figure 2.8: Different techniques of measurement of shear wave velocity in-situ: a) invasive; b) non-invasive...	11
Figure 2.9: Clay particle arrangement: a) clay deposited in fresh water; b) marine clay (Pusch, 1970)	14
Figure 2.10: Shear moduli values versus σ'_h / σ'_v (OCR>30) (Pennington et al., 1997).....	15
Figure 2.11: Shear moduli ratio for the shallow and deep blocks (Kim i Finno, 2012)	16
Figure 2.12: Shear wave velocity measurement on Boston Blue Clay, Ønsoy Clay and Burswood Clay (Landon and DeGroot, 2006).....	17
Figure 2.13: Technical drawing of the mini-block sampler (Emdal et al., 2016).....	18
Figure 2.14: Sample quality evaluation based on $Lvs-Lu$ criterion (Donohue and Long, 2010).....	20
Figure 3.1: Bender elements: a) parallel; b) series (Dyvik and Madshus, 1985)	21
Figure 3.2: Operating principle of BE system (Camacho-Tauta et al., 2012).....	22
Figure 3.3: Piezoelectric bender element (Kramer, 1996)	22
Figure 3.4: Travel time determination in first arrival method (Yamashita et al., 2009).....	23
Figure 3.5: Picking of the wave first arrival (Lee and Santamarina, 2005).....	23
Figure 3.6: Travel time determination in peak-to-peak method	24
Figure 3.7: Travel time determination in cross correlation method (Yamashita et al., 2009)	24
Figure 3.8: Example of phase cross spectrum method (Yamashita et al., 2009).....	25
Figure 3.9: Experimental determination of the travel distance (Brignoli et al., 1996)	26
Figure 3.10: Vector nomenclature adapted from (Arroyo et al., 2003).....	27
Figure 3.11: Waves generated by a bender element (Lee and Santamarina, 2005).....	30
Figure 3.12: Sample behaviour models according to Rio (2006).....	31
Figure 3.13: Anisotropy investigations with bender elements: a) Teng et al., 2014; b) Jovicic and Coop (1998)	32
Figure 3.14: Bender elements configuration and consequent wave polarization (Rio, 2006).....	32
Figure 4.1: Location of the NGTS sites (ngi.no).....	33
Figure 4.2: NGTS Tiller-Flotten Quick Clay Test Site location (norgeskart.no)	34
Figure 4.3: NGTS Flotten Quick Clay Test Site quaternary geology (ngu.no)	34
Figure 4.4: In-situ groundwater pressure, effective stress profile and preconsolidation stresses at Tiller-Flotten site (L'Heureux et al., In press).....	35
Figure 4.5: Basic soil profile and index properties at Tiller-Flotten site (L'Heureux et al., In press).....	36

Figure 4.6: Shear wave velocity (V_s) and small strain shear modulus (G_{max}) with depth at Tiller-Flotten Site (L'Heureux et al., In press).....	37
Figure 4.7: Split core section with visible varves at Tiller-Flotten site (L'Heureux et al., In press)	37
Figure 5.1: Bender element testing system at the geotechnical laboratory at NTNU: a) full view of the testing system; b) bender elements; c) data acquisition device.....	39
Figure 5.2: Schematic work of the bender element system.....	40
Figure 5.3: Example of the output from the LabVIEW program	40
Figure 5.4: Example of the matching process: a) sent and received signals b) least squares, best match c) result of matching.....	41
Figure 5.5: Mini-block 9,75-10,10 m depth: a) sample in a PVC tube; b) sample after opening the tube; c) mini-block prepared for cutting	42
Figure 5.6: Example of the disturbance near the edge of the mini-block sample: a) view from the top; b) cross-section	42
Figure 5.7: Visible varves and layering in clay: a) Sample 2hv; b) Sample 1vh; c) Sample 4hv; d) Sample 4vh; e) Sample 3vh.....	43
Figure 5.8: Division of the mini-block samples	44
Figure 5.9: Preparation of the specimen for bender elements testing in the triaxial cell.....	45
Figure 5.10: Arrangement of samples and bender elements for measurements of shear wave velocities in different planes	48
Figure 5.11: Preliminary bender element tests on the unconfined specimen	49
Figure 6.1: Effects of input signal frequency on output signals for the preliminary tests on unconfined specimen	52
Figure 6.2: Shear wave velocity, frequency, expelled water data during consolidation for samples at 9,75-10,10 m depth.....	56
Figure 6.3: Shear wave velocity, frequency, expelled water data during consolidation for samples at 10,80-11,05 m depth	57
Figure 6.4: Shear wave velocity, frequency, expelled water data during consolidation for samples at 12,80-13,15 m depth	58
Figure 6.5: Shear wave velocity, frequency, expelled water data during consolidation for samples at 19,45-19,70 m depth	59
Figure 6.6: Shear wave velocity (V_s) with depth	60
Figure 6.7: Small strain shear modulus (G_{max}) with depth	60
Figure 6.8: Variations in G_{max} with time of consolidation	61
Figure 7.1: Analysis of the received signal, unconfined specimen; frequencies 1 kHz, 2 kHz, 3 kHz	64
Figure 7.2: Illustration of changes in frequency of the input signal before and during consolidation for sample 3vh	65
Figure 7.3: Effect of shear wave velocity on the frequency.....	66
Figure 7.4: Variation in received signal for different consolidation stresses	67
Figure 7.5: Examination of near-field effect for sample 4vh, $\sigma'_v=134$ kPa.....	68
Figure 7.6: Relationship between shear wave velocity and d/λ for the tests on sample 4vh, $\sigma'_v=134$ kPa	70

Figure 7.7: Shear modulus versus average effective confining pressure.....	71
Figure 7.8: Shear modulus changes with time of consolidation for Sample 2	72
Figure 7.9: Shear modulus changes with time of consolidation for Sample 3	73
Figure 7.10: Shear modulus changes with time of consolidation for Sample 4	73
Figure 7.11: Shear modulus changes with time of consolidation for Sample 3vh2	74
Figure 7.12: Relationship between normalized shear modulus increase with time (N_G) and void ratio (e).....	75
Figure 7.13: Relationship between G_{max} and water content	76
Figure 7.14: Normalized shear modulus g_{max} versus water content (Langø, 1991).....	76
Figure 7.15 Shear modulus versus void ratio	76
Figure 7.16: Relationship between G_{max} according to Leroueil and Hight (2003) and e	77
Figure 7.17: Shear modulus versus plasticity index.....	78
Figure 7.18: Shear wave velocity (V_s) and small strain shear modulus (G_{max}) with depth - comparison between field and laboratory measurements	79
Figure 7.19: G_{vh}/G_{hv} and G_{hh}/G_{vh} ratios versus average confining pressure.....	81
Figure 7.20: Anisotropy ratio versus depth.....	82
Figure 7.21: G_{vh}/G_{hv} development during sample consolidation.....	82
Figure 7.22: G_{hh}/G_{vh} development during sample consolidation.....	83
Figure 7.23: Anisotropy ratio G_{hh}/G_{vh} versus plasticity index I_p	83

List of Tables

Table 2.1: Parameters influencing G_{max} in normally consolidated and moderately overconsolidated clays (Vucetic and Dobry, 1991).....	7
Table 2.2: Summary of the G_{hh}/G_{vh} ratios of London Clay (Wongsaroj et al., 2004)	15
Table 2.3: Sample quality evaluation based on ϵ_{vol} (Andresen and Kolstad, 1979)	19
Table 2.4: Sample quality evaluation based on $\Delta e/e_0$ (Lunne et al., 2006)	19
Table 2.5: Sample quality evaluation using V_{vh}/V_{SCPTU} (Landon et al., 2007).....	19
Table 5.1: Summary of performed bender element tests.....	50
Table 6.1: Index testing results	51
Table 6.2: Summary of V_s and G_{max} values obtained in bender element testing	54
Table 6.3: Bender element testing results	55
Table 6.4: Sample quality assessment.....	62
Table 7.1: Coefficient of shear modulus increase with time (I_G) and normalized shear modulus increase with time (N_G) for the evaluation of the long-term effect	75
Table 7.2: Anisotropy ratios for different consolidation stages	80

List Symbols and Abbreviations

Roman letters

A	matrix appearing in Stoke's fundamental solution
A	material constant
a	attraction
B	material constant
b	bender element width
b	force vector
c	cementation
D	diameter of the sample
d	effective height
E	Young's modulus
E^*	modified Young's modulus
E_h	young's modulus in horizontal direction
E_b	elastic modulus
E_v	young's modulus in vertical direction
e	void ratio
e_0	initial void ratio
F_A	age factor
$F(e)$	void ratio function
F_p, F_s	far-field p-related and s-related coefficients of Stoke's fundamental solution
f	frequency
f_{lim}	limiting frequency of near-field influence
f_r	resonant frequency
G	shear modulus
GR	green tensor
G_{1000}	shear modulus measured at T=1000 minutes from the start of the primary consolidation
G_{hh}	small strain shear modulus in the horizontal plane
$G_{max,field}$	in-situ small strain shear modulus
$G_{max,primary}$	small strain shear modulus at the end of primary consolidation
G_{max}, G_0	small strain shear modulus
G_{vh}, G_{hv}	small strain shear moduli in the vertical plane
$G_{xy}(f)$	cross-power spectrum
g	gravitational constant
g_{max}	normalized shear modulus
H	height of the sample
h	bender element thickness
I	moment of inertia

I_G	coefficient of shear modulus increase with time
I_L	liquidity index
I_P	plasticity index
K	bulk modulus
K_0	coefficient of earth pressure at rest
k	exponent
k_b	equivalent spring constant
L_b	cantilever length
L_{tt}	tip-to-tip distance between the bender elements
L_u	normalized soil suction parameter for sample quality assessment
L_{vs}	normalized shear wave velocity parameter for sample quality assessment
$L_x(f)$	linear spectrum of the signal X(T)
$L_y(f)$	linear spectrum of the signal Y(T)
$L_y^*(f)$	complex conjugate of the linear spectrum of Y(T)
m	power exponent
m_1	mass of the cup and wet sample
m_2	mass of the cup and dry sample
m_b	cantilever mass
m_c	mass of the cup
m_d	mass of dry specimen
m_d	mass of dry sample
m_w	mass of water
m_{wp}	mass of waterfilled pycnometer
m_{wps}	mass of waterfilled pycnometer and the sample
\bar{m}	mass per unit length
N	number of loading cycles
N	near-field coefficient of Stoke's fundamental solution
N_G	normalized shear modulus increase with time
N_p, N_s	p-related and s-related components of near-field coefficient
n	stress exponent
n	porosity
n_p, n_s	dimensionless s and p ratios
p_a	atmospheric pressure
p_r	reference pressure
p'	mean effective stress
p'_c	preconsolidation pressure
r	radius coordinate
S	dimensionless parameter
S	salinity

S_r	degree of saturation
S_t	sensitivity
$S(\omega, r)$	transfer function for shear movement
s_r	remoulded shear strength
s_u	undrained shear strength
t	shear wave travel time
t	time
t_g	geological age
u	displacement vector
u_r	soil suction
u_p, u_s	displacement vectors of compressive and shear movements
V_0	initial volume
V_{hh}	shear wave propagating horizontally with horizontal polarization
V_{hv}	shear wave propagating horizontally with vertical polarization
V_p	P-wave velocity
V_p	volume of voids
V_{SCPTU}	in-situ shear wave velocity obtained from the seismic piezocone testing (SCPTU)
$V_{s, in situ}$	shear wave velocity measured in-situ
$V_{s, remoulded}$	shear wave velocity measured on remoulded sample
V_s	shear wave velocity
V_{s0}	shear wave velocity measured on unconfined sample
V_{vh}	shear wave propagating vertically with horizontal polarization
V_w	volume of water
w	water content
w_L	liquid limit
w_P	plastic limit
x	power exponent
$x(t)$	time record of the input wave
$y(t)$	time record of the received wave

Greek letters

α	anisotropy factor
α	effective length factor
α	inclination of the line
β	experimentally determined value
γ	shear strain
γ	unit weight
γ_c	cyclic strain
γ_w	unit weight of water

$\dot{\gamma}$	strain rate
ΔG	change in shear modulus
ΔV	volume change
Δe	change in void ratio
Δt	shear wave propagation time
δ	axial deformation
$\delta \varepsilon_{ij}$	Strain increment
$\delta \sigma'_{ij}$	Stress increment
ε_{vol}	volumetric strain
η	mean displacement influence factor
λ	Lamé elastic constant
λ	wavelength
λ_p, λ_s	compressive and shear wavelengths
μ	Lamé elastic constant
ν	Poisson's ratio
ν^*	modified Poisson's ratio
ν_{hh}	Poisson's ratio for vertical strains from a horizontal strain
ν_{hv}	Poisson's ratio for horizontal strains from a horizontal strain
ν_{vh}	Poisson's ratio for horizontal strains from a vertical strain
ρ	bulk density
ρ_b	bender element mass density
ρ_s	density of solids
ρ_w	density of water
σ'_c	effective confining stress
σ'_m	average effective confining pressure
σ'_h	effective horizontal stress
σ'_v	effective vertical stress
σ'_{v0}	in-situ vertical effective stress
τ	time delay between the two signals
ω	angular frequency

Abbreviations

<i>BE</i>	Bender Element
<i>CR</i>	Cross-correlation
<i>CSW</i>	Continuous Surface Waves
<i>DAQ</i>	Data Acquisition Device
<i>EOPC</i>	End of primary consolidation
<i>FFT</i>	Fast Fourier Transform
<i>MASW</i>	Multichannel Analysis of Surface Waves

<i>NGTS</i>	Norwegian Geo-Test Site
<i>NTNU</i>	Norwegian University of Science and Technology
<i>OCR</i>	Overconsolidation ratio
<i>PC</i>	Personal Computer
<i>SASW</i>	Spectral Analysis of Surface Waves
<i>SCPTU</i>	Seismic Cone Penetration Test
<i>SDT</i>	Seismic Dilatometer Test

Chapter 1

Introduction

1.1 Background

Soil properties at small strains are of great interest in geotechnical engineering. The nonlinearity of the stress-strain response, which is characteristic for soil behaviour at small strains, has significant effect on soil behaviour. Small strain shear modulus is a key parameter in the analysis of geotechnical problems such as settlements, deformation and soil-structure interaction. It is also crucial in soil dynamics when predicting ground movement during earthquakes, explosions or machine vibrations.

Anisotropy is recognized as a distinctive feature of soils. The nature of the soil is dependent on the geological processes that occur during soil formation. Geological history, stress conditions and depositional environment all contribute to soil stiffness anisotropy. Since clay behaviour is highly influenced by the clay structure, stiffness anisotropy of clays is of particular interest. The deposition process of clays tends to induce the horizontal bedding plane in the soil layer. Clays will consequently exhibit different behaviour in the horizontal plane and in the planes perpendicular to the bedding plane. Therefore, stiffness of clays is commonly assumed to be cross-anisotropic. In order to analyse the stiffness anisotropy, investigations should be carried out on: the degree of anisotropy, the source of anisotropy, and the parameters influencing the anisotropy.

Soil anisotropy is crucial in understanding soil behaviour and is widely used in geotechnical numerical modelling. In order to improve the prediction of the soil response, soil models which incorporate anisotropy in stiffness should be applied. The cross-anisotropic soil models are used in numerical analysis to simulate ground settlement profiles, tunnel induced ground deformation, or deep excavations in soft clay with nearby structures.

Anisotropy of the small strain shear modulus is commonly investigated using bender elements technique. This method involves measurements of the shear wave velocity propagating through a soil specimen in multiple planes. However, there is currently no standardised practice when interpreting bender elements testing results. Wave dispersion phenomena such as near-field effect and wave reflection have not been fully explained. Variability, therefore, still exists in waveform interpretation and travel time determination between researchers.

Stiffness anisotropy of quick clay is of particular interest in this study. Due to their low shear strength and extremely high sensitivity, these soils are extremely challenging in geotechnical engineering. These deposits of sensitive marine clays can be found mostly in Scandinavia, North America and Russia. Quick clay found in Norway is investigated at the Tiller-Flotten Norwegian Geo-Test Site. Further analysis on this material is conducted for a stronger understanding of the clay behaviour and to advance the research currently undergoing in this area.

1.2 Objectives

The main objective of this study is the investigation of the anisotropy of the small strain shear modulus of Tiller-Flotten clay. The objectives for this study are the following:

- To present relevant literature background for the subject.
- To evaluate the bender elements system performance.
- To carry out index testing.
- To perform shear wave velocity measurements with bender elements on specimens before and during samples' consolidation.
- To determine small strain shear modulus in different directions across the samples and analyse relationships between G_{\max} and other parameters.
- To evaluate anisotropy and analyse the factors influencing anisotropy.
- To compare laboratory results with in-situ data.

1.3 Limitations

A major limiting factor in this study is insufficient quantity of data. Due to errors in preparation and measurements, two of the samples could not be used for further bender elements testing. Therefore, inadequate data relating to the small strain shear modulus with horizontal wave propagation and horizontal polarization G_{hh} was collected. Consequently, it was not possible to verify the anisotropic behaviour of quick clay, and only tentative conclusions could be made.

Furthermore, the mini-block samples used in these investigations may not be completely representative of the quick clay found at Tiller-Flotten Site. Samples were kept for a long storage time of 1,5 years prior to laboratory testing. The samples' quality is significantly affected due to changes in stress distribution, loss of moisture, and chemical effects during storage. This results in the reduction of measured mechanical properties of the clay and therefore the results cannot be deemed completely reliable.

1.4 Research approach

Bender elements technique was used to investigate small strains stiffness anisotropy of Tiller-Flotten quick clay. The shear wave velocity was measured in three different planes across the specimens. The triaxial specimens were obtained from the mini-block samples from Tiller-Flotten NGTS. Each of the samples were tested in unconfined conditions, and during sample consolidation in the triaxial apparatus. Isotropic confining pressure was applied to each of the samples. Small strain shear modulus was determined from shear wave velocity measurements. The stiffness anisotropy was analysed by comparing G_{\max} determined for each of the planes of the samples.

1.5 Structure of the report

The report is structured as follows:

- Chapter 2 presents the background regarding small strain shear modulus and stiffness anisotropy in clays.
- Chapter 3 provides the background concerning bender elements testing.

1.5 *STRUCTURE OF THE REPORT*

- Chapter 4 describes the Tiller-Flotten Quick Clay Site.
- Chapter 5 outlines the performed laboratory investigations.
- Chapter 6 gives a summary of results obtained in the experimental study.
- Chapter 7 discusses the test results.
- Chapter 8 contains a summary of results, relevant conclusions and recommendations for further work.

Chapter 2

Background

This chapter gives the background regarding small strain shear modulus and stiffness anisotropy. The literature review on factors affecting small strain stiffness is additionally presented. Furthermore, sampling methods and sample disturbance are reviewed. In this section the anisotropy of clays is of particular focus.

2.1 Wave propagation

Two categories of seismic waves exist: body waves and surface waves (Kramer, 1996). Body waves may be compressional or shear waves. The compressional wave, also called primary wave (P-wave), has particle motion parallel to the direction of wave propagation (Figure 2.1). The shear wave, also known as secondary wave (S-wave), causes shearing deformations while travelling through a material. The particle displacement of the shear wave (S-wave) is perpendicular to the direction of S-wave travel. S-waves may propagate in vertical direction with horizontal particle motion (VH waves), in horizontal direction with vertical particle motion (HV waves), or in horizontal direction with horizontal particle motion (HH waves).

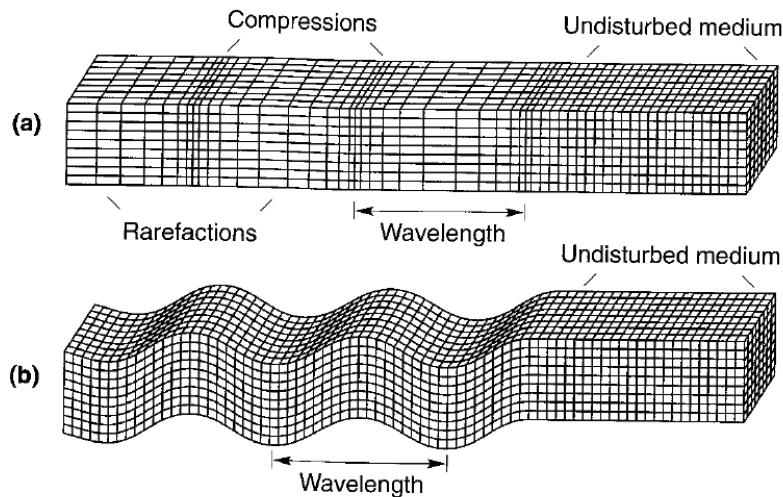


Figure 2.1: Seismic wave types (Kramer, 1996)

The velocity of the body waves varies with the stiffness of the material they travel through. From the differential equation of the S-wave the shear wave velocity of the material may be calculated as:

$$V_s = \sqrt{\frac{\mu}{\rho}} = \sqrt{\frac{G}{\rho}} \quad (2.1)$$

where V_s is shear wave velocity, ρ is density of the medium and μ , G is shear modulus.

2.2 Small strain stiffness

The stiffness characteristic of soils is of great importance in geotechnical analyses. It links the stress and strain increments. Figure 2.2 presents the relationship between the shear modulus and shear strain. With the increasing shear strain the stiffness decays nonlinearly, that is the stiffness is dependent on the strain level. Strain range where soil can be considered elastic is termed as very small strains. This is typically associated with strains lower than 0,001%. The soil stiffness corresponding to this range of strains is identified with the small strain shear modulus G_{max} (G_0). Theory of shear wave propagation through an isotropic elastic medium tells us that the value of the shear modulus G_{max} of the soil is given by:

$$G_{max} = \rho \cdot V_s^2 \quad (Pa) \quad (2.2)$$

where ρ is the density of the soil (kg/m^3) and V_s is the shear wave velocity (m/s).

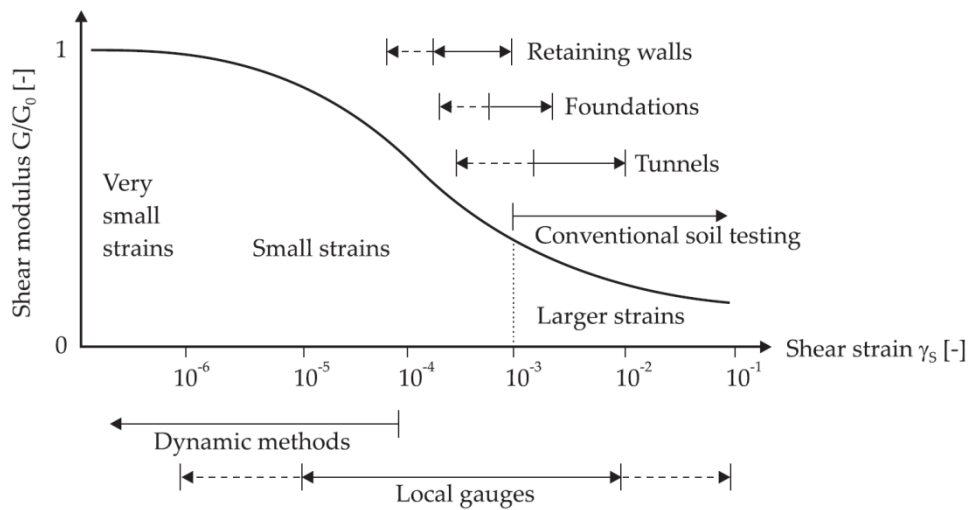


Figure 2.2: Relationship between shear modulus and shear strain according to (PLAXIS, 2018)

The small strain shear modulus is widely considered to be a fundamental soil property in engineering practice. It should be taken into account to accurately predict soil behaviour. It is a key parameter in analysis of geotechnical problems such as settlements, deformation, and soil-structure interaction. It is used in numerical modelling to simulate shallow foundations, piles, excavations and tunnels. It is also important in soil dynamics when predicting ground movement during earthquakes, explosions, and machine vibrations.

2.2.1 Factors influencing G_{max}

The influence of various factors on the stiffness of soils at small strains has been studied by many researchers. It was found that G_{max} is affected by numerous soil properties. A short review of the literature is presented below.

Hardin (1978) suggested that for clays, the small strain shear modulus, G_{max} , depends on applied stress, void ratio, overconsolidation ratio and plasticity index as follows:

$$G_{max} = AF(e)\sigma'_m{}^n p_a^{(1-2n)}(OCR)^k \quad (2.3)$$

where A is a material constant dependent on the soil and reference stress ($A = 625$ is commonly used for atmospheric pressure), $F(e)$ is a void ratio function, σ'_m is the average effective confining pressure, n is the stress

2.2 SMALL STRAIN STIFFNESS

exponent, p_a is the atmospheric pressure, OCR is the overconsolidation ratio, k is an exponent dependent on plasticity index I_p . However, Lerouil and Hight (2003) suggested that the effect of OCR is included in the void ratio function and thus may be neglected. They proposed an empirical equation:

$$G_{max} = SF(e)(\sigma'_v \cdot \sigma'_h)^n p_a^{(1-2n)} \quad (2.4)$$

where S is a dimensionless parameter characterizing the considered soil, $F(e)$ is a void ratio function, σ'_v and σ'_h are the vertical and horizontal effective stresses respectively, n is a parameter indicating the influence of stress and p_a is the atmospheric pressure. Viggiani and Atkinson (1995) proposed the relationship:

$$\frac{G_0}{p_r} = A \left(\frac{p'}{p_r} \right)^n OCR^m \quad (2.5)$$

where p' is the mean effective stress, p_r is the reference pressure, A , m , n are soil parameters dependent on plasticity index I_p . The study by Shiwakoti et al. (2000) focused on investigations of G_0 on the naturally sedimented undisturbed soft marine clays in Japan, Korea, Thailand and United Kingdom. They introduced a correlation to estimate G_{max} :

$$\frac{G_0}{\sigma'_{v0}} = A \cdot B \left(\frac{1}{21} + \frac{1}{1820} I_p \right)^{-2} \quad (2.6)$$

where σ'_{v0} is the in-situ vertical effective stress, A is a parameter related to the soil structure, B is a parameter related to OCR and I_p is plasticity index. Vucetic and Dobry (1991) studied the effects of different factors on G_{max} for normally and moderately overconsolidated clays. The summary of their research is presented in Table 2.1.

Table 2.1: Parameters influencing G_{max} in normally consolidated and moderately overconsolidated clays (Vucetic and Dobry, 1991)

Increasing factor	G_{max}	G/G_{max}
Confining pressure, σ'_0	Increases with σ'_0	Stays constant or increases with σ'_0
Void ratio, e	Decreases with e	Increases with e
Geological age, t_g	Increases with t_g	May increase with t_g
Cementation, c	Increases with c	May increase with c
Overconsolidation ratio, OCR	Increases with OCR	Not affected
Plasticity index, I_p	Increases with I_p if $OCR > 1$ Stays about constant if $OCR = 1$	Increases with I_p
Cyclic strain, γ_c	-	Decreases with γ_c
Strain rate, $\dot{\gamma}$ (frequency of cyclic loading)	Increases with $\dot{\gamma}$	G increases with $\dot{\gamma}$; G/G_{max} probably not affected if G and G_{max} are measured at same $\dot{\gamma}$
Number of loading cycles, N	Decreases after N cycles of large γ_c but recovers later with time	Decreases after N cycles or large

Confining pressure

Shear modulus is considerably affected by confining pressure. With the increase of confining pressure, G_{max} significantly increases. Hardin and Richart (1963) proposed a following relationship between the effective confining stress and G_{max} :

$$G_{max} \propto (p')^m \tag{2.7}$$

where m is a power exponent. The value of this exponent may vary between 0.4 and 1.0 (Benz, 2007). Kokusho et al. (1982) compared the shear moduli for the normally and overconsolidated clays by plotting them versus confining stress. The analysis result is presented in Figure 2.3. They stated that the relationship between $G_0/F(e)$ and σ'_c may be approximated by two linear functions related to the state of consolidation.

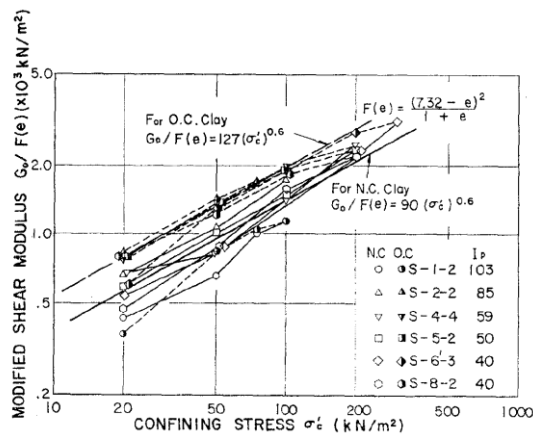


Figure 2.3: Shear modulus vs confining stress relationships for normally and overconsolidated clays (Kokusho et al., 1982)

Void ratio

Most of the relationships between void ratio and G_{max} found in the literature are typically of the form:

$$G_{max} \propto e^{-x} \tag{2.8}$$

where x is an exponent dependent on the soil type. Thus, with increasing void ratio, G_{max} decreases. When the void ratio is low there is more contact between the grains and hence the soil is stiffer. L'Heureux and Long (2016) investigated Norwegian clays by analysing data from different sites in Norway. They normalized the relationship between G_{max} according to Hardin (1978) and Hight and Leroueil (2003) (Figure 2.4).

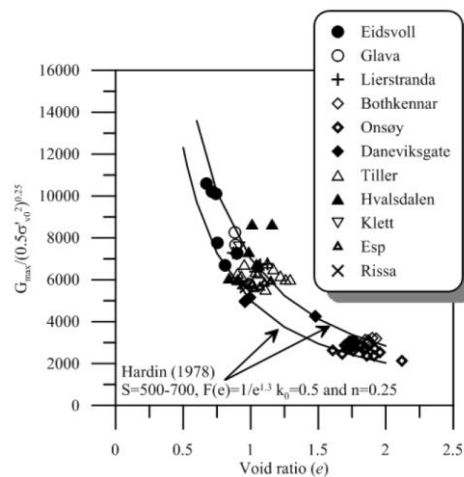


Figure 2.4: Correlations between G_{max} and void ratio (L'Heureux and Long, 2016)

Overconsolidation ratio

There is a discordance between researchers when evaluating the effect of overconsolidation ratio on small strain stiffness. As seen in equations 2.3 and 2.5, G_{max} increases with OCR. According to Benz (2007), in cohesive soils G_{max} increases with OCR and the increase rate depends on the soil plasticity. Kokusho et al. (1982) also noted the effect of OCR on G_{max} and showed how it may differ between normally and overconsolidated clays. However, on the contrary, opposing researches have claimed that the effect of OCR on G_{max} has already been taken into account in the void ratio function $F(e)$; thus, the effect of OCR itself is negligible. Nonetheless, Kokusho et al. (1982) have stated that due to the overconsolidation history, the microstructure of soft clays may be changed: and therefore cannot be fully evaluated with the use of void ratio.

Plasticity index

According to Hardin (1978) the plasticity index influences the exponent k in equation 2.3, which is used to derive shear modulus. The effect of the plasticity index on the exponent k is presented in Figure 2.5. The exponent k increases with plasticity index. However, k is related to OCR, thus the influence of plasticity index on G_{max} itself should not be considered without taking into account OCR.

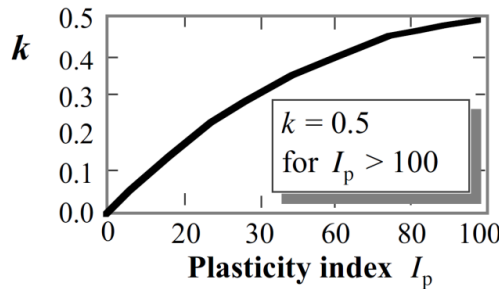


Figure 2.5: Effect of I_p on the parameter k (Towhata, 2008)

The study by Kokusho et al. (1982) showed that the strain-dependent variation of the shear modulus ratio is very sensitive to the plasticity of cohesive soils. Vucetic and Dobry (1991) also found that the plasticity index is the main factor controlling G/G_{max} . They concluded that soils with higher plasticity index tend to have a more linear cyclic stress-strain response at small strains and to degrade less at larger cyclic strains than lower plasticity soils (Figure 2.6). Therefore, greater I_p is related with more linear elastic behaviour.

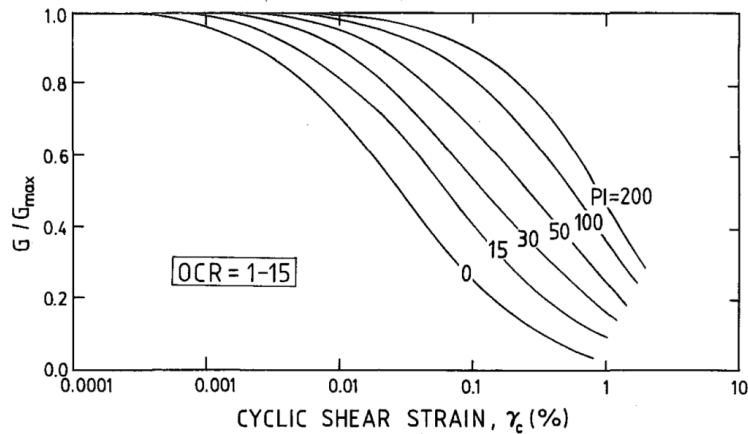


Figure 2.6: Relations between G/G_{max} vs γ_c and soil plasticity for normally and overconsolidated soils (Vucetic and Dobry, 1991)

Confinement time

Duration of the confining pressure is an important parameter in laboratory evaluation of the small strain shear modulus of all soils. G_{max} was found to increase with time of confinement. The consolidation time of fine-grained soils may be divided into two phases: an initial primary consolidation phase and second phase denoted as the long-term time effect (Anderson and Stokoe, 1978). The G_{max} -time relationship depends on the soil type and stress conditions (Anderson and Stokoe, 1978). For most clays G_{max} increases rapidly during primary consolidation phase, while in the second phase it increases approximately linearly with the logarithm of time. Anderson and Stokoe (1978) indicated that the long-term effect of consolidation plays particularly significant role in stiffness investigations of soft marine clays. They expressed the rate of the shear modulus change during secondary consolidation as:

$$I_G = \frac{\Delta G}{\log(t_2/t_1)} \tag{2.9}$$

$$N_G = \left(\frac{I_G}{G_{1000}} \right) 100\% = \left(\frac{\Delta G}{\log(t_2/t_1)} \right) \left(\frac{1}{G_{1000}} \right) 100\% \tag{2.10}$$

where t_1 and t_2 are times after primary consolidation, ΔG is the change in shear modulus from t_1 to t_2 and G_{1000} is the shear modulus measured at $T = 1000$ minutes from the start of the primary consolidation. Typical relationships between G_{max} and confinement time are presented in Figure 2.7.

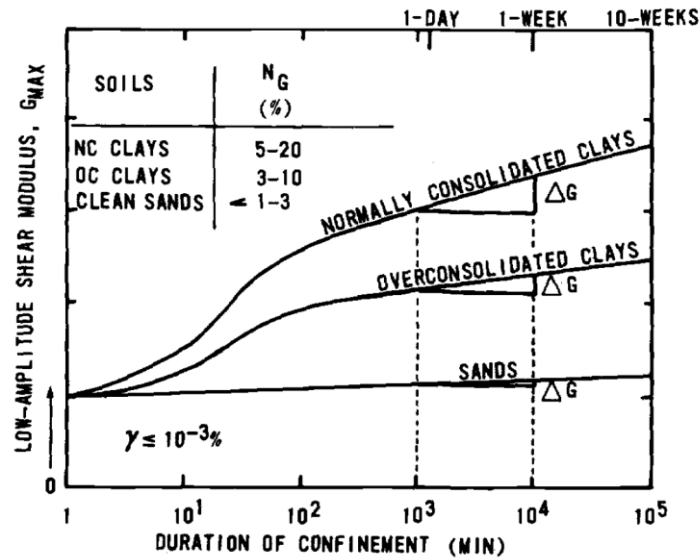


Figure 2.7: Effect of time of consolidation on small strain shear modulus (Anderson and Stokoe, 1978)

Kokusho et al. 1982 performed a series of long term consolidation tests on various soft clay samples. Their research showed that the plasticity index, I_p , is the most influential parameter for the increasing rate of shear modulus. They suggested the relationship given by equation 2.11.

$$\frac{\Delta G}{G_{1000}} = 0,027 \sqrt{I_p} \tag{2.11}$$

According to Anderson and Stokoe (1978) evaluation of the long term consolidation time on small strain shear modulus can be used to estimate the in-situ shear wave velocity according to formula:

$$G_{max,field} = G_{max,primary} + F_A \cdot I_G \tag{2.12}$$

2.2 SMALL STRAIN STIFFNESS

where $G_{max,field}$ is the predicted in-situ small strain shear modulus, $G_{max,primary}$ is the small strain shear modulus at the end of primary consolidation, F_A is an age factor for site and I_G is the coefficient of shear modulus increase with time. However, since the assessment of the age factor for a given site is very difficult and the procedure does not take into account the effect of sample disturbance, this method is not fully reliable.

2.2.2 Measurement of soil stiffness

Determination of the small strain stiffness of soils is frequently made from the shear wave velocity measurements both in the field and the laboratory. Several different methods can be used. The most commonly used laboratory techniques to determine G_{max} are bender element method and the resonant column method. However, in-situ measurement of shear wave velocity is the preferred method of investigating small strain shear properties of soils (L'Heureux & Long, 2017). Field techniques are classified as invasive and non-invasive methods. Invasive methods require preparation of boreholes. They include down-hole logging, cross-hole logging, suspension logging, seismic dilatometer test (SDT) and seismic cone penetration test (SCPTU). The non-invasive testing eliminates the need of penetration to the ground, since the seismic instrumentation is placed on the surface. These methods include multichannel analysis of surface waves (MASW), spectral analysis of surface waves (SASW), continuous surface waves (CSW), seismic refraction and seismic reflection. Figure 2.8 illustrates the concept of each of the methods.

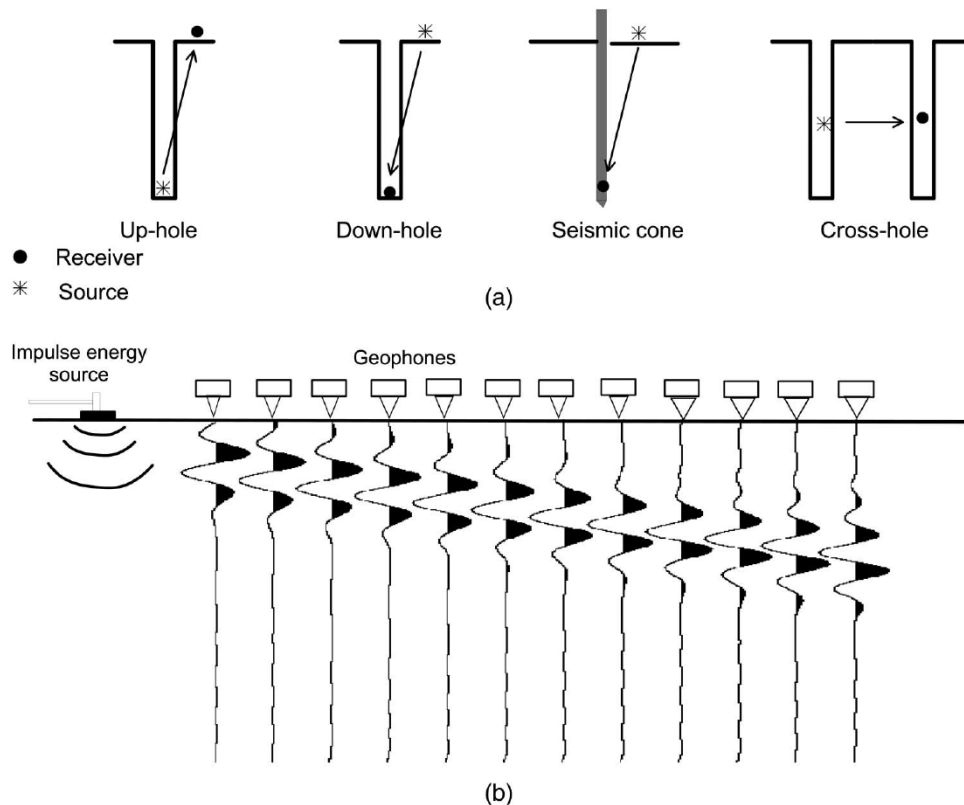


Figure 2.8: Different techniques of measurement of shear wave velocity in-situ: a) invasive; b) non-invasive

2.3 Stiffness Anisotropy

Two sources of stiffness anisotropy may be distinguished: inherent and stress-induced anisotropy (Masin and Rott, 2014). The stress-induced anisotropy is caused by the anisotropy of the stress state. Numerical and experimental analyses showed that shear modulus is influenced by the stresses in the wave propagation plane, while it is relatively independent of the out-of-plane component (Roesler, 1979; Wang and Mok, 2008). Inherent anisotropy is a result of the development of the natural soil structure related to the prevalent orientation of soil particles. The inherent anisotropy can be evaluated after separation from the stress-induced anisotropy, i.e., by subjecting the specimen to isotropic stress state (Jovicic and Coop, 1998).

As shown in previous section, the small strain shear modulus is stress dependent. Therefore, it would be reasonable to assume greater G_{\max} in the vertical plane, i.e., the direction of the major principle stress in-situ, than in the horizontal plane, i.e., the direction of the minor in-situ stress. However, experimental studies show that in most geomaterials G_{hh} is always larger than the shear moduli in other directions due to the presence of fabric anisotropy (Wang and Mok, 2008).

2.3.1 Isotropy

Isotropy is independence of material parameters from the direction. An isotropic elastic material is described by two parameters: the Young's modulus E and the Poisson's ratio ν . These parameters are essential to create the stiffness matrix of the material, thus to define the elastic behaviour of the material. Using Hooke's law the volumetric modulus and the shear stiffness may be derived and expressed with the formulas:

$$K = \frac{E}{3(1 - 2\nu)} \quad (2.13)$$

$$G = \frac{E}{2(1 + \nu)} \quad (2.14)$$

The volumetric modulus K , also known as the bulk modulus, describes the relation between the mean stress and the volumetric strain. In isotropic elasticity the change in volume is a result of the change of the mean stress. In consequence, when the average stress is constant, there is no change in volume of the material. The shear modulus G describes the relationship between the shear stress and the shear strain.

2.3.2 Transverse isotropy

An anisotropic material is one which has different properties in different directions. The material behaviour has to be expressed by a 6x6 stiffness symmetric matrix.

Transverse isotropy also called cross-anisotropy occurs when the properties of the soil are equal in one plane, i.e. in all the directions parallel to this plane, while the properties in the directions perpendicular to this plane are different. The assumption of the transverse isotropy is very often applied to soils, since most of them were deposited vertically and then subjected to horizontal stresses equal in all directions, thus creating a vertical axis of symmetry (Graham and Houlsby, 1983). The plane of anisotropy is mostly considered to be horizontal. The full stiffness matrix for a transversely isotropic material may be expressed according to equation 2.15.

2.3 STIFFNESS ANISOTROPY

$$\begin{bmatrix} \delta\varepsilon_{xx} \\ \delta\varepsilon_{yy} \\ \delta\varepsilon_{zz} \\ \delta\varepsilon_{yz} \\ \delta\varepsilon_{zx} \\ \delta\varepsilon_{xy} \end{bmatrix} = \begin{bmatrix} \frac{1}{E_h} & \frac{-\nu_{hh}}{E_h} & \frac{-\nu_{vh}}{E_v} & 0 & 0 & 0 \\ \frac{-\nu_{hh}}{E_h} & \frac{1}{E_h} & \frac{-\nu_{vh}}{E_v} & 0 & 0 & 0 \\ \frac{-\nu_{hv}}{E_h} & \frac{-\nu_{hv}}{E_h} & \frac{1}{E_v} & 0 & 0 & 0 \\ 0 & 0 & 0 & \frac{1}{G_{hv}} & 0 & 0 \\ 0 & 0 & 0 & 0 & \frac{1}{G_{vh}} & 0 \\ 0 & 0 & 0 & 0 & 0 & \frac{1}{G_{hh}} \end{bmatrix} \begin{bmatrix} \delta\sigma'_{xx} \\ \delta\sigma'_{yy} \\ \delta\sigma'_{zz} \\ \delta\sigma'_{yz} \\ \delta\sigma'_{zx} \\ \delta\sigma'_{xy} \end{bmatrix} \quad (2.15)$$

where E_v and E_h are Young's moduli in vertical and horizontal directions respectively, ν_{vh} and ν_{hh} are Poisson's ratios for horizontal strains from a vertical and horizontal strain respectively, ν_{hv} is Poisson's ratio for vertical strains from a horizontal strain, G_{vh} and G_{hv} are shear moduli in the vertical plane, G_{hh} is shear modulus in the horizontal plane. The existence of the plane of isotropy implies (Masin and Rott, 2014):

$$G_{hh} = \frac{E_h}{2(1 + \nu_{hh})} \quad (2.16)$$

The requirement of symmetry of the matrix leads to:

$$\frac{\nu_{vh}}{E_v} = \frac{\nu_{hv}}{E_h} \quad (2.17)$$

The transverse isotropy model requires:

$$G_{vh} = G_{hv} \quad (2.18)$$

Therefore, a transversely isotropic material may be described by five constants: E_v , E_h , ν_{vh} , ν_{hh} , G_{vh} . Graham and Houlsby (1983) proposed a formulation which uses 3 parameters: E^* , ν^* , α , where E^* is the modified Young's modulus, ν^* the modified Poisson's ratio and α is an anisotropy factor. The parameters are connected to the elastic parameters as follows:

$$\begin{aligned} E_v &= E^* \\ E_h &= \alpha^2 E^* \\ \nu_{vh} &= \frac{\nu^*}{\alpha} \\ \nu_{hh} &= \nu^* \\ 2G_{vh} &= \alpha \frac{E^*}{(1 + \nu^*)} \end{aligned} \quad (2.19)$$

The anisotropy factor describes the ratios of the Young's modulus, Poisson's ratio and shear modulus terms as follows:

$$\alpha = \sqrt{\frac{E_h}{E_v}} = \frac{\nu_{hh}}{\nu_{vh}} = \frac{G_{hh}}{G_{vh}} \quad (2.20)$$

The factor α may be used as a rational measure of soil anisotropy. For $\alpha > 1$ the material is stiffer horizontally than vertically, whereas for $\alpha < 1$ the material is stiffer vertically than horizontally.

2.3.3 Stiffness anisotropy in clays

The clay particles arrangement is illustrated in Figure 2.9. The lacustrine or fresh water clays have relatively porous aggregates and small voids, whereas marine clays have an open and porous structure. The main reason for this is the influence of fresh water which contains low number of ions and as a result the particles of lacustrine clay are oriented in parallel directions during sedimentation (NTNU, 2015).

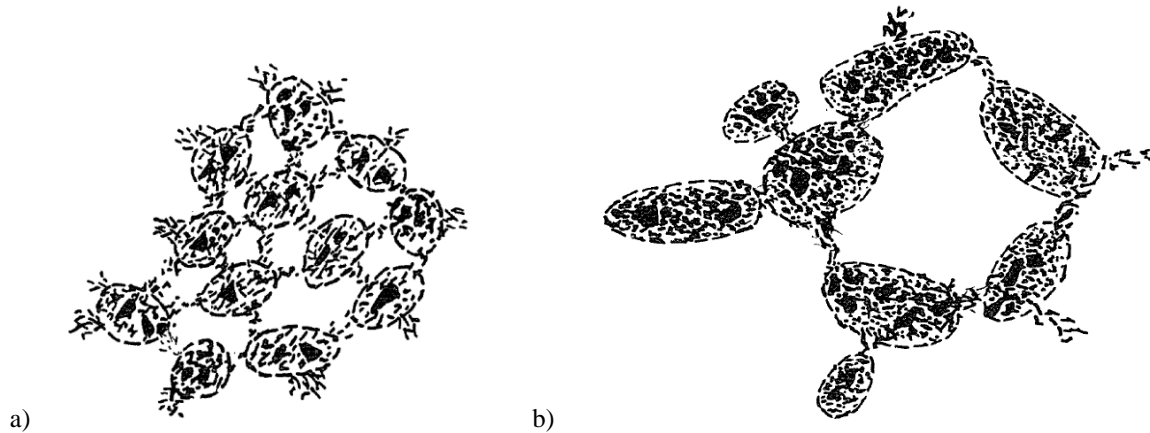


Figure 2.9: Clay particle arrangement: a) clay deposited in fresh water; b) marine clay (Pusch, 1970)

Many naturally deposited clays have one dimensional loading history (Jovicic and Coop, 1998). The deposition process of clays results in inherent anisotropy which tends to induce the horizontal bedding plane in the soil layer. Therefore, stiffness of clays is commonly assumed to be cross-anisotropic and as a result the values of G_{vh} and G_{hv} should be equal. Additionally, the nature of clay minerals is strongly layered. The layered microstructure involves strong bonds within the layers and weaker bonds in between (Sayers and Den Boer, 2016). This contributes to large anisotropy of clay structure. The study by Sayers and Den Boer (2016) showed that the clay minerals may be described as a transversely isotropic medium with the axis of rotational symmetry perpendicular to the clay layers. The study by Hori et al. (2006) showed that the stiffness anisotropy in clays is highly dependent on clay content and mineralogy of the soil. Their findings show that anisotropy increases with increase of clay content.

Wang and Siu (2011) investigated the effects of structure on the mechanical responses of kaolinite with known fabric associations. The experimental results show that the dynamic properties of kaolinite are undeniably related to the soil structure. Stronger interparticle bonds or higher degrees of flocculated structure resulted in higher G_{max} values. Moreover, Wang and Mok (2008) investigated inherent stiffness anisotropy in numerical analysis. They found out that when the fabric changed from isotropic to anisotropic the shear modulus G_{hh} started to become greater than G_{vh} and G_{hv} .

Sully and Campanella (1995) investigated in-situ anisotropy by performing downhole and crosshole shear wave velocity measurements. They investigated the influence of in-situ stresses on measured shear wave velocity. They concluded that the shear wave velocity values in different planes are primarily controlled by the structural anisotropy, whereas the stress-induced factor is almost negligible.

Pennington et al. (1997) studied anisotropy of G_{max} in Gault clay which is a heavily overconsolidated deposit. They used bender elements to measure shear wave velocities in different directions across the samples. Knowing the shear wave velocity values the shear moduli were calculated. The analysis results showed that the

2.3 STIFFNESS ANISOTROPY

shear modulus in the horizontal direction (G_{hh}) is higher than the modulus in vertical direction (G_{vh}) and the ratio is highly dependent on stress state (Figure 2.10). The ratio G_{hh}/G_{vh} ranges between 2 to 2,9. Additionally, the G_{vh}/G_{hv} ratio is approximately equal to 1,4.

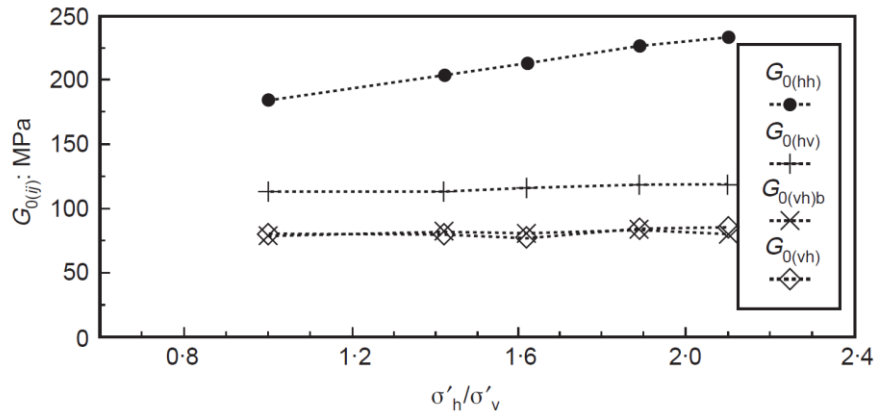


Figure 2.10: Shear moduli values versus σ'_h/σ'_v (OCR>30) (Pennington et al., 1997)

Wongsaroj et al. (2004) examined the anisotropic behaviour of London Clay. Their findings showed that the small strain stiffness is stress dependent. G_{hh} was always larger than G_{vh} and G_{hv} values with the ratio G_{hh}/G_{vh} between 1,5 and 2,0. G_{vh} and G_{hv} values from laboratory measurements show consistency between these 2 values. It is concluded that the assumption of $G_{vh}=G_{hv}$ can be made. They summarised the measurements of the anisotropy ratio on London clay by previous authors (Table 2.2).

Table 2.2: Summary of the G_{hh}/G_{vh} ratios of London Clay (Wongsaroj et al., 2004)

Data Source	Range of G_{hh}/G_{vh}
Simpson et al. (1996)	1,54
Hight et al. (1997)	1,71-1,72
Jovicic and Coop (1998)	1,48-1,61
Yimsiri (2001)	1,6-1,8
Hight et al. (2003)	1,5-2,0

Hori et al. (2006) studied the influence of the size and shape of soil particles on the anisotropy of G_{max} . They investigated five types of sand and three types of clay. The specimens were isotropically consolidated to several levels of confining pressure and measured shear wave velocities in three different directions with bender elements. Their results showed that the stiffness anisotropy in clay is larger than anisotropy in sand. Since anisotropy increased with increasing clay content, this difference may be related to the clay minerals.

Kim and Finno (2012) investigated the evolution of stiffness anisotropy in Chicago clay. Their results showed that the clay is a cross-anisotropic material with the anisotropy ratio of 1 to 1,4, with the average of 1,15 (Figure 2.11).

2.3 STIFFNESS ANISOTROPY

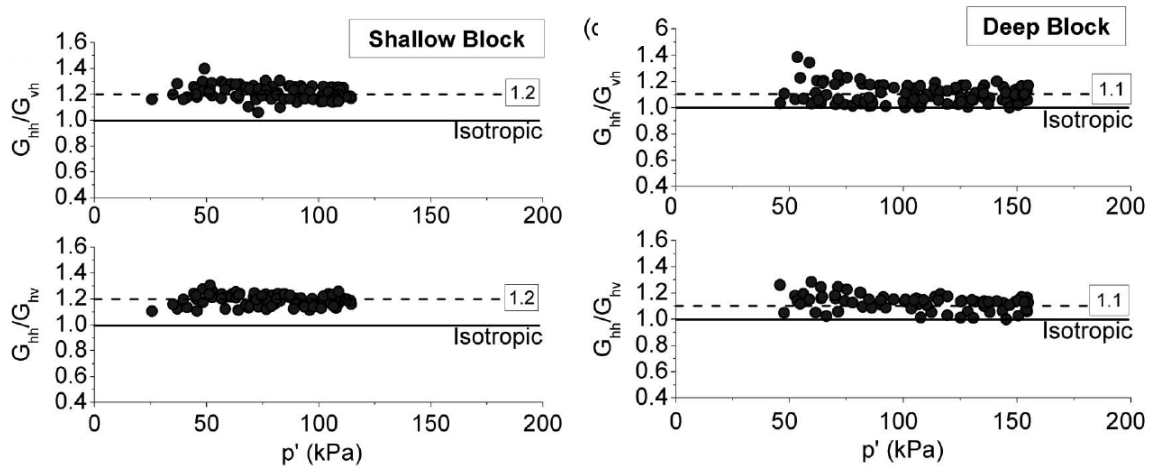


Figure 2.11: Shear moduli ratio for the shallow and deep blocks (Kim i Finno, 2012)

Teng et al. (2014) studied the stiffness anisotropy of soft Taipei clay. They performed shear wave velocity measurements with bender elements both in vertical (V_{vh}) and horizontal directions (V_{hv} , V_{hh}). The tests were conducted in the triaxial apparatus, during both K_0 consolidation and undrained shearing phase. The anisotropic shear moduli G_{hh}/G_{vh} were measured for different samples in different orientations. The test results indicated that G_{hh} was always higher than G_{vh} . At the end of the consolidation all the anisotropy ratios of the shear moduli were greater than unity with the values ranging between 1,15 to 1,44. The findings of Teng et al. (2014) showed that the anisotropy tends to decrease with the increase of the consolidation pressure. What is more, soils with higher OCR tended to have higher anisotropy ratios.

By reviewing a large experimental database, the study by Masin and Rott (2014) identified general trends in stiffness anisotropy both in reconstituted and natural sedimentary clays. The analysis showed that for soft clays the stress-induced anisotropy has a significant influence and it decreases with increasing overconsolidation ratio. However, Lings, Pennington and Nash (2000) emphasized that the cross-anisotropic model may be a too far simplification if the in-situ horizontal stress vary with direction in plan or if there is significant layering in the soil which leads to $G_{vh} \neq G_{hv}$.

Landon and DeGroot (2006) performed vertical and horizontal (V_{vh} , V_{hv} and V_{hh}) shear wave velocity measurements on Boston Blue Clay, Australian Burswood Clay, and Norwegian Ønsoy Clay. The laboratory tests were conducted on the block samples in an unconfined state. Figure 2.12 presents the results plotted with depth. For Boston Blue Clay and Ønsoy Clay V_{hh} shear wave velocities were consequently greater than both V_{vh} and V_{hv} . The average anisotropy ratios for Boston Blue Clay were found: $G_{hv}/G_{vh}=1,20$ and $G_{hh}/G_{vh}=1,68$, and the values were constant with depth. The average ratios for Ønsoy Clay were determined as: $G_{hv}/G_{vh}=0,99$ and $G_{hh}/G_{vh}=1,55$. However, all three shear wave velocities of Burswood Clay were similar to each other. Therefore, it was concluded that the Boston Blue Clay and Ønsoy Clay exhibit stiffness anisotropy. However, V_{vh} and V_{hv} shear wave velocities were not found equal to each other, as is the case in homogenous materials. The discrepancies were attributed to inhomogeneities in these clays, i.e., shells, silts and organics.

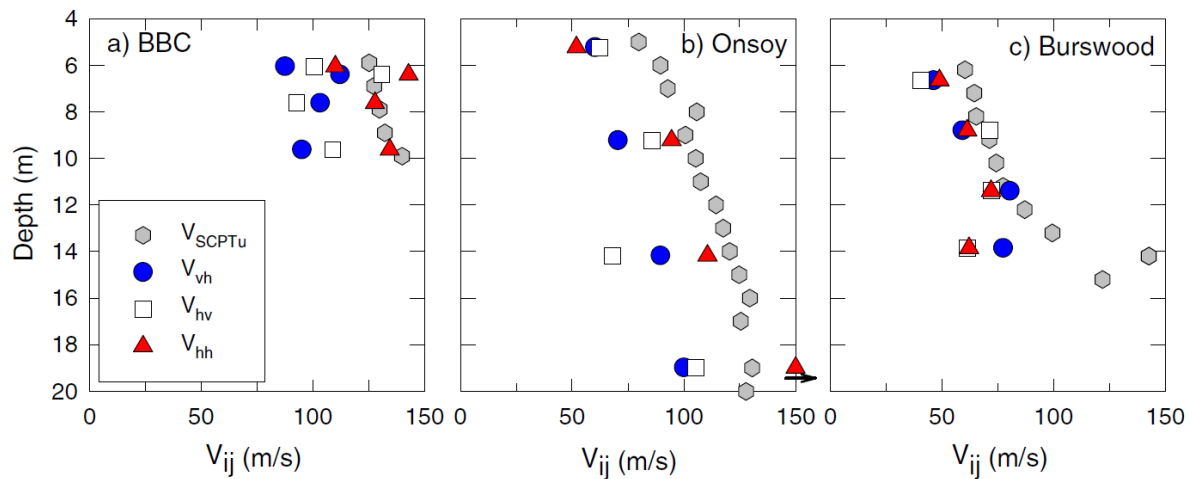


Figure 2.12: Shear wave velocity measurement on Boston Blue Clay, Onsoy Clay and Burswood Clay (Landon and DeGroot, 2006)

2.4 Sampling and sample disturbance

Geotechnical laboratory testing requires extracting the soil samples from the ground. In order to collect reliable test results a sample of sufficient quality has to be obtained. A large number of sampling techniques exist which provide samples of different quality. The choice of the most suitable sampling method and the evaluation of sample quality is crucial in obtaining reliable design parameters of soils.

2.4.1 Sampling methods

The choice of the sampling method is determined by the character of the laboratory investigations, i.e., the importance of the investigations and the parameters which are going to be determined. Sampling may provide samples of three different types: remoulded samples, disturbed samples or undisturbed samples. In order to determine mechanical properties of the soil undisturbed samples are required. For clays several sampling techniques can be used. In Norway piston sampling and block sampling are the most popular ones.

Piston sampling

The most commonly used piston sampler in Norway is $\varnothing 54$ mm Geonor sampler (NTNU, 2015). The sampler consists of a cutting edge, an outer steel cylinder, an inner steel or epoxy cylinder and a core catcher. Piston sampling can be used to obtain undisturbed samples in fine-grained soils, i.e., clays and fine silts. In particularly soft, sensitive clays piston samplers with larger diameters ($\varnothing 95$ mm, $\varnothing 120$ mm) are occasionally used. The zones at the top, bottom and along the walls of the cylinder sample are most susceptible to disturbance. Nevertheless, when following recommended procedures, it is possible to obtain a soil sample of high quality.

Block sampling

Block sample techniques provide samples of highest quality. The sample is cut either from the base or walls of a borehole, using hand-carving methods or a specially designed block sampler. For low plastic soft clays, such as Norwegian clays, block sampling is considered to be the best sampling method (Amundsen et al., 2016).

The Sherbrooke block sampler was introduced in 1979. This technique requires a predrilled borehole fitting the sampler with an outside diameter of 410 mm. The concept uses the cutters together with water pressure

2.4 SAMPLING AND SAMPLE DISTURBANCE

to core out an annulus around the block of the sampled soil. A typical sample's dimensions are: diameter 250 mm and height 350 mm. After extracting the sample from the ground, it is wrapped in several layers of plastic wrap, placed in a PVC tube and stored in a temperature controlled room until the laboratory investigations.

The mini-block sampler was developed at the Geotechnical Division of the Norwegian University of Science and Technology (NTNU) in Trondheim, Norway. The technical drawing of the sampler is shown in Figure 2.13. It is a downsized Sherbrooke block sampler with the diameter of 230 mm, which provides samples with a diameter of up to 160 mm. The operating principles are the same as Sherbrooke sampler procedure.

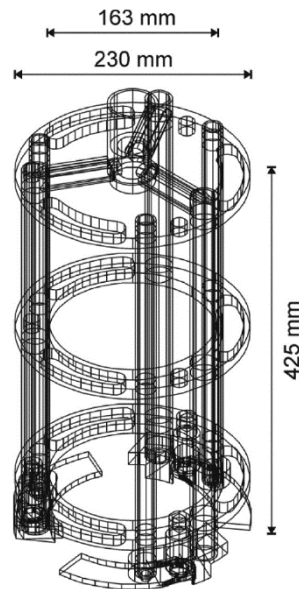


Figure 2.13: Technical drawing of the mini-block sampler (Emdal et al., 2016)

2.4.2 Evaluation of sample quality

Soil samples are exposed to disturbance not only during sampling itself but also during transport, storage, extrusion and preparation for laboratory testing. The most significant effect of sample disturbance on the sample quality is the reduction of measured mechanical parameters values: soil stiffness, preconsolidation stress, undrained shear strength and clay sensitivity (Emdal et al., 2016). Therefore, in order to avoid sample disturbance, during sampling and transport relevant procedures should be followed and the storage time should be minimised. In order to determine the level of reliability of the results obtained in laboratory testing the sample quality is assessed. There are several approaches used to evaluate sample quality, each of them based on different parameters.

Laboratory methods

Sample disturbance may be evaluated by measurement of water expelled from the soil specimen during consolidation. This classification is based on the volumetric strain which is determined using equation 2.21.

$$\varepsilon_{vol} = \frac{\Delta V}{V_0} \quad (-) \quad (2.21)$$

where ε_{vol} is the volumetric strain at in-situ stress level (-), ΔV is the volume change during the consolidation phase (cm^3) and V_0 is the initial specimen volume (cm^3). Large water expulsion may be an indication of significant sample disturbance. Classification of sample quality based on this criterion is presented in Table 2.3.

Table 2.3: Sample quality evaluation based on ε_{vol} (Andresen and Kolstad, 1979)

OCR σ'_c/σ'_{v0} -	Depth m	Perfect quality $\varepsilon_{vol} <$ %	Acceptable quality $< \varepsilon_{vol} <$ %	Disturbed quality $\varepsilon_{vol} >$ %
1-1,2	0-10	3,0	3,0-5,0	5,0
1,2-1,5	0-10	2,0	2,0-4,0	4,0
1,5-2	0-10	1,5	1,5-3,5	3,5
2-3	0-10	1,0	1,0-3,0	3,0
3-8	0-10	0,5	0,5-1,0	1,0

Lunne et al. (2006) suggested to use the ratio $\Delta e/e_0$ to determine sample quality, where Δe is the change in void ratio and e_0 is the initial void ratio. This classification was tested on marine clays with following properties: plasticity index 6-43%, water content 20-67%, OCR 1-4, depth 0-25 m. For clays with parameters out of this range the classification cannot be directly applied. The criteria for evaluation of sample disturbance are given in Table 2.4.

Table 2.4: Sample quality evaluation based on $\Delta e/e_0$ (Lunne et al., 2006)

OCR	$\Delta e/e_0$ Sample quality category			
	Very good to excellent (1)	Good to fair (2)	Poor (3)	Very poor (4)
1-2	<0,04	0,04-0,07	0,07-0,14	>0,14
2-4	<0,03	0,03-0,05	0,05-0,10	>0,10

Sample quality assessment using shear wave velocity

Shear wave velocity and shear modulus may be used to assess sample quality. This technique makes it possible to assess sample quality rapidly, without the need of several days of laboratory testing. Non-destructive sample quality assessment in soft clay soils was studied by Landon et al. (2007). They tested Boston blue clay site in Massachusetts and compared the sample quality determined with both the conventional techniques and the method using shear wave velocity. Several different sampling techniques were used to provide samples of varying quality. The shear wave velocities were measured both in-situ and on unconfined samples. The in-situ V_s was obtained from the seismic piezocone testing (SCPTU). Bender elements were used to measure vertically propagating V_s on unconfined samples, immediately after extracting them from the ground. The shear wave velocities obtained from the in-situ and unconfined measurements were compared to the ratio $\Delta e/e_0$. The findings showed that the quality of the sample measured with the use of shear wave velocity correlates well with the variation in $\Delta e/e_0$ and preconsolidation pressure p_c' . They proposed recommendations for sample quality assessment based on the V_{vh}/V_{SCPTU} ratio. The evaluation is performed according to the classification in Table 2.5.

Table 2.5: Sample quality evaluation using V_{vh}/V_{SCPTU} (Landon et al., 2007)

Sample quality		
Very good to excellent (1)	Poor (3)	Very poor (4)
Fair to good (2)		
$V_{vh}/V_{SCPTU} \geq 0,60$	$0,35 \leq V_{vh}/V_{SCPTU} < 0,60$	$V_{vh}/V_{SCPTU} < 0,35$

2.4 SAMPLING AND SAMPLE DISTURBANCE

Donohue and Long (2010) studied a method of evaluating sample quality in soft clay based on the in-situ and unconfined shear wave velocity (V_s) and soil suction (u_r) measurements. They tested three soft clay sites: Ballinasloe and Bogganfin in Ireland, Onsøy in Norway. To quantify sample disturbance they proposed an empirically derived tentative criterion based on V_s and u_r measurements:

$$L_{vs} = \frac{V_{s \text{ in situ}} - V_{s0}}{V_{s \text{ in situ}} - V_{s \text{ remoulded}}} \quad (2.22)$$

$$L_u = \frac{0,2\sigma'_{v0} - u_r}{0,2\sigma'_{v0}}$$

The classification tested on the investigated sites is presented in Figure 2.14.

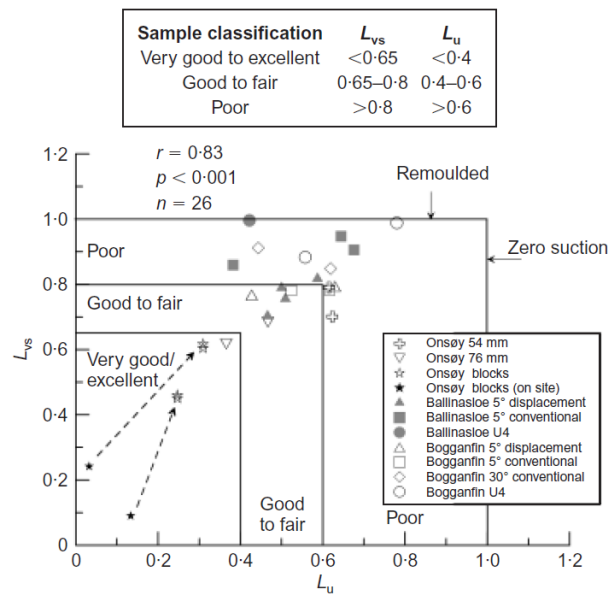


Figure 2.14: Sample quality evaluation based on L_{vs} - L_u criterion (Donohue and Long, 2010)

Chapter 3

Bender elements

This section presents background on bender elements. The main challenges connected with shear wave velocity determination are described. Factors influencing bender elements testing and sources of difficulties in the interpretation of shear waveforms are of interest. Finally, the methodology of anisotropy investigations with bender elements is explained.

3.1 Construction and operating principle

The bender element testing method was first introduced by Shirley and Hampton (1978). It is a popular method for determination of the shear modulus at very small strains by measurements of the shear wave velocity travelling through the soil specimen. Bender elements consist of two piezoceramic elements mounted together, two electrodes on the surface and an inside electrode between the piezoceramic sheets. A piezoelectric material generates electric potential when subjected to mechanical deformation and vice versa, i.e., deforms when the voltage is applied. Wiring of bender elements may be parallel or series (Figure 3.1). In a parallel type connection the direction of polarization of both piezoceramic sheets is identical, whereas in a series type the polarization direction is opposite. Therefore, the parallel version is a better transmitter, since for a given input signal it gives higher amplitude, while series wiring is a better receiver, since for a given displacement the generated voltage is larger (Brignoli et al., 1996). The dimensions of bender elements are approximately: thickness: 0.5-1 mm, width: 10-12 mm, length: 12-20 mm.

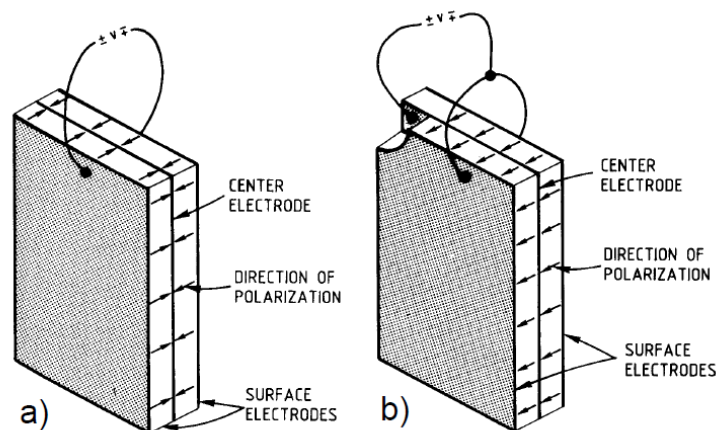


Figure 3.1: Bender elements: a) parallel; b) series (Dyvik and Madshus, 1985)

For the soil investigations bender element testing is usually conducted in the triaxial cell. The typical configuration is presented in Figure 3.2. A voltage pulse is applied to the transmitter element mounted on the base cap of the cell. This causes the elongation of one plate and contraction of the other one and as a result the element

3.2 TRAVEL TIME DETERMINATION

is bended (Figure 3.3). The bending displacement generates the shear wave in the soil. The wave travels through the soil sample and reaches the receiver element which becomes excited and creates an electrical impulse. The signal received by the receiving element is detected and displayed on a digital oscilloscope together with the transmitted signal. Nowadays the sine wave is usually transmitted, since a square wave pulse used during early research was the source of significant distortion of the signal (Blewett et al., 2000).

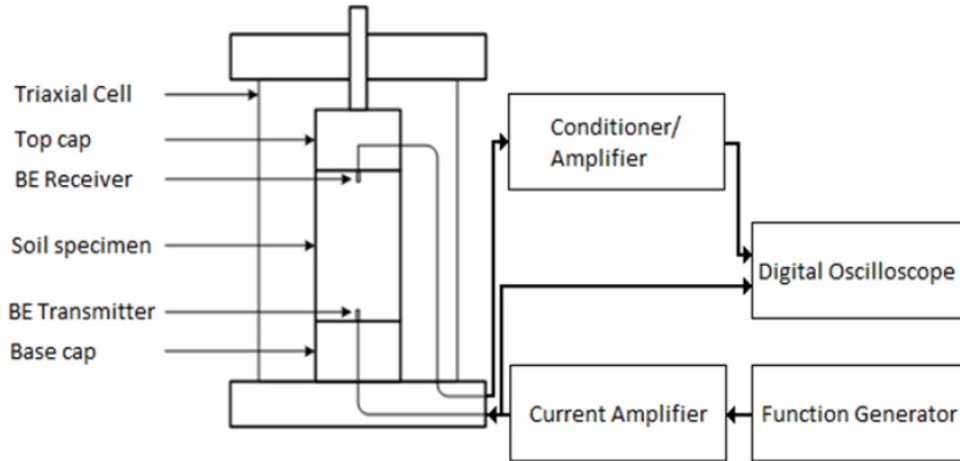


Figure 3.2: Operating principle of BE system (Camacho-Tauta et al., 2012)

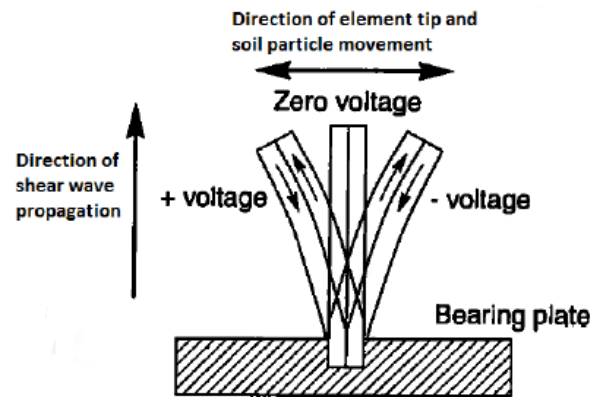


Figure 3.3: Piezoelectric bender element (Kramer, 1996)

Knowing the distance between the two bender elements and the travel time of the wave, the shear wave velocity may be calculated as follows:

$$V_s = \frac{L_{tt}}{t} \quad (3.1)$$

where L_{tt} is the tip-to-tip distance between the bender elements and t is the shear wave travel time.

3.2 Travel time determination

Despite the common use of bender elements to determine the shear wave velocity, there is no accepted procedure, which should be followed. The main difficulty is to evaluate the shear wave travel time. Travel time is the time interval between the initiation of the electrical impulse sent to the transmitter and the initial arrival of the waveform

3.2 TRAVEL TIME DETERMINATION

recorded at the receiver. It may be determined using either time domain techniques (first arrival method, peak-to-peak method, cross correlation) or frequency domain techniques (phase-delay method) (Yamashita et al., 2009).

3.2.1 First Arrival Method

The first arrival method, also called start-to-start method, is based on the time axis, thus this method is known as a time domain technique (Yamashita et al., 2009). The determination of the wave propagation time involves observing the received signal and picking the first deflection point which corresponds to the first arrival of the shear wave. Figure 3.4 presents the identification of the travel time in first arrival method.

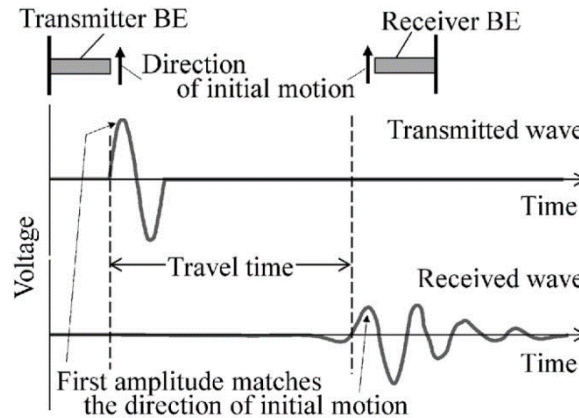


Figure 3.4: Travel time determination in first arrival method (Yamashita et al., 2009)

However, picking of the first arrival point is often ambiguous, as seen in Figure 3.5. This is a result of near-field effect which is a wave dispersion phenomena causing uncertainties in distinguishing the first arrival of the received signal. The near-field effect is further discussed in section 3.4.2. Early studies choose points A or B as the first arrivals of the received signal. Kawaguchi et al. (2001) stated that peak-to-peak travel time determination suggested by Viggiani and Atkinson (1995) is incorrect and recommended to use the point C as the actual first arrival of the received signal. The point C has been also selected by Lee and Santamarina (2005).

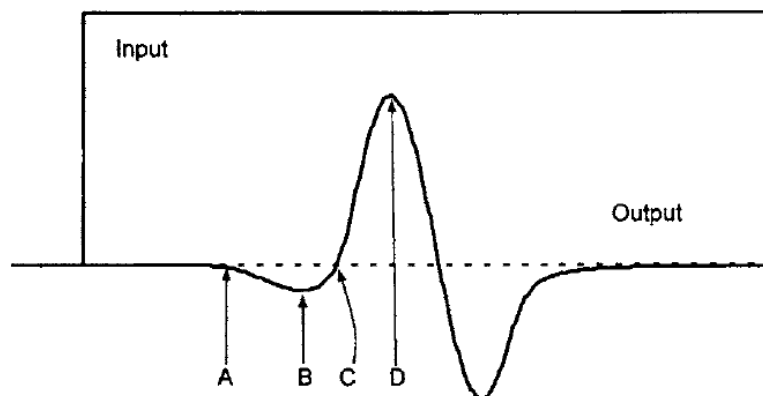


Figure 3.5: Picking of the wave first arrival (Lee and Santamarina, 2005)

3.2.2 Peak-to-peak Method

The principle of the peak-to-peak method is similar to the first arrival method. The travel time is interpreted as the time lag between the first peak of the output signal and the peak position of the input wave. Figure 3.6 illustrates the identification of the travel time in the peak-to-peak method.

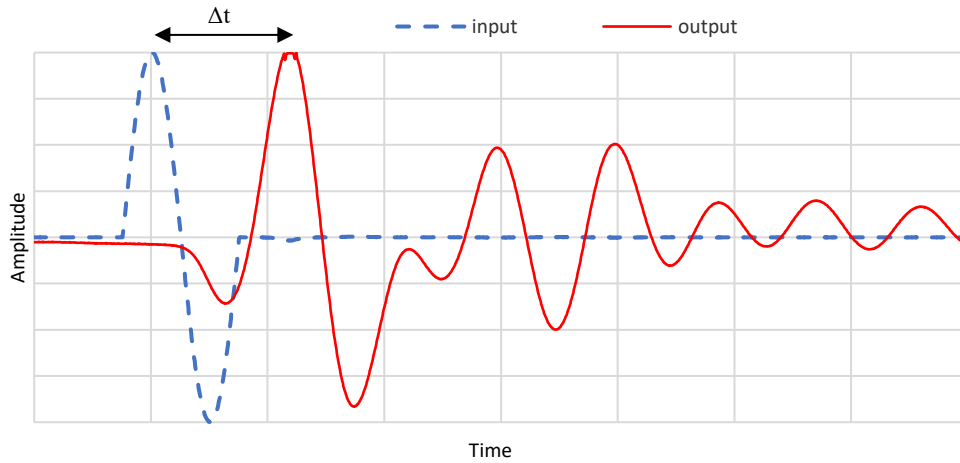


Figure 3.6: Travel time determination in peak-to-peak method

3.2.3 Cross Correlation Method

The cross-correlation function $CR(\tau)$ is a measure of similarity of two signals $x(t)$ and $y(t)$ and is expressed by the integral:

$$CR(\tau) = \int_{-\infty}^{\infty} x(t)y(t + \tau)dt \quad (3.2)$$

where $x(t)$ is time record of the input wave, $y(t)$ is time record of the received wave and τ is the time delay between the two signals (Sanchez-Saliner et al., 1986). The cross correlation CR is a function of the time delay τ . The wave travel time corresponds to the cross-correlation peak. The main principle of the travel time determination in the cross correlation method is illustrated in Figure 3.7.

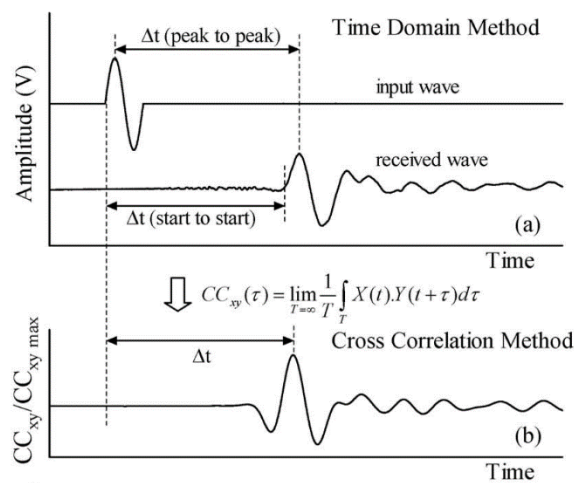


Figure 3.7: Travel time determination in cross correlation method (Yamashita et al., 2009)

3.2.4 Phase Cross Spectrum Method

The Phase Cross Spectrum Method involves calculation of the cross spectrum of the transmitted and received signals. The input and output waves are determined in their frequencies, therefore this method is known as a frequency domain technique. The shear wave propagation time is calculated as follows (Viggiani and Atkinson, 1995a):

$$\Delta t = \frac{\alpha}{2\pi} \quad (3.3)$$

where α is the inclination of the line which relates the absolute phase angle at the cross spectrum and the frequency in the evaluated range. The cross-power spectrum $G_{xy}(f)$ of two signals $X(T)$ and $Y(T)$ is given with the formula:

$$G_{xy}(f) = L_x(f)L_y^*(f) \quad (3.4)$$

where $L_x(f)$ is the linear spectrum of the signal $X(T)$, $L_y(f)$ is the linear spectrum of the signal $Y(T)$ and $L_y^*(f)$ is the complex conjugate of the linear spectrum of $Y(T)$. $L_x(f)$ and $L_y(f)$ are obtained by performing Fourier transformation as follows:

$$L_x(f) = FFT[X(T)] \quad (3.5)$$

$$L_y(f) = FFT[Y(T)] \quad (3.6)$$

An example of the phase cross spectrum method is shown in Figure 3.8.

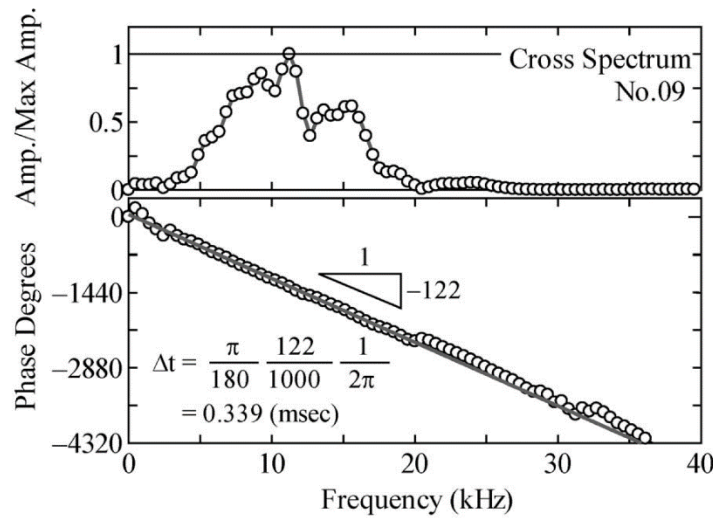


Figure 3.8: Example of phase cross spectrum method (Yamashita et al., 2009)

The study by Yamashita et al. (2009) showed that the travel time interpreted with the use of first arrival, peak-to-peak, cross correlation and phase cross spectrum methods is not always consistent. Even when the cross correlation peak matches with the inclination of the cross spectrum, the time delay obtained from the first arrival method may vary significantly. However, when the frequencies of the input wave and first receiving wave are equal, the travel time should be comparable within the methods.

3.3 Travel distance determination

In order to calculate the shear wave velocity the travel distance of the wave has to be determined. This is commonly believed to be less complex than determination of the travel time. Most of the researchers assume the travel

3.4 FACTORS INFLUENCING BENDER ELEMENT TESTING

distance of the shear wave as the tip-to-tip distance between bender elements. Brignoli et al. (1996) experimentally investigated the assumption of travel distance. They carried out a set of tests using both bender transducers and shear-plate transducer with different penetration length in the soil. The results show that the travel distance should be taken as the least distance between the tips of the transducers (Figure 3.9). This is in agreement with previous findings by Dyvik and Madshus (1985) and Viggiani and Atkinson (1995a). The tip-to-tip distance is used also by Lee and Santamarina (2005) and Kawaguchi et al. (2001).

However, contradictory results were presented by Rio (2006). He tested a large range of samples with different heights and different embedment heights. The investigations of pressure distribution along the transducer's embedded length were carried out. The findings show that the correct travel distance should be measured not between the tips of the transducers but between the centres of dynamic pressure of the transducers, which is approximately 60% of the embedded height.

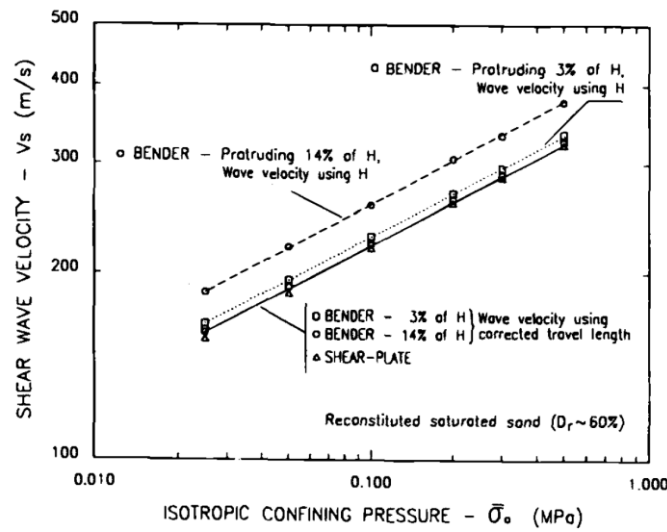


Figure 3.9: Experimental determination of the travel distance (Brignoli et al., 1996)

3.4 Factors influencing bender element testing

The wave propagation in bender element testing has been extensively studied. Both theoretical and experimental analyses have been made by many researchers. Several factors influencing reliability of bender element testing are widely discussed: near-field effect, P-wave propagation and sample geometry. Below, a brief description of each of the factors is presented.

3.4.1 Resonant frequency

The resonant frequency of bender elements is an important parameter. It affects the frequency, travel time determination and the size of the near-field effect (Lee and Santamarina, 2005). A bender element in air may be represented by a cantilever beam with the resonant frequency of (Lee and Santamarina, 2005):

$$f_r = \frac{\omega}{2\pi} = \frac{1}{2\pi} \sqrt{\frac{k_b}{m_b}} = \frac{1}{2\pi} \sqrt{\frac{1,875^4 E_b I}{\bar{m} (\alpha L_b)^4}} \quad (3.7)$$

3.4 FACTORS INFLUENCING BENDER ELEMENT TESTING

where k_b is equivalent spring constant, m_b is cantilever mass, E_b is elastic modulus, I is moment of inertia, \bar{m} is mass per unit length, α is effective length factor affected by the anchor efficiency ($\alpha = 1$ for a perfectly rigid anchor, $\alpha > 1$ for a soft anchor), L_b is cantilever length.

The resonant frequency of the bender element in soil is dependent on bender element and soil properties. Lee and Santamarina (2005) obtained an expression for the resonant frequency of the bender element in soil as follows:

$$f_r = \frac{1}{2\pi} \sqrt{\frac{1,875^4 \frac{E_b I}{(\alpha L_b)^3} + 2\eta V_s^2 \rho_s (1 + \nu) L_b}{\rho_b b h (\alpha L_b) + (\rho_s b^2 L_b) \beta}} \quad (3.8)$$

where $\eta \approx 2$ is mean displacement influence factor at the soil-element interface, V_s is shear wave velocity, ρ_b is bender element mass density, ρ_s is soil mass density, ν is Poisson's ratio, b is BE width, h is BE thickness and β is experimentally determined value.

In the time domain measurements it is recommended to use the input sinusoidal pulse signal of the frequency equal to the resonant frequency of the bender elements since it enhances the response of the receiving bender element (Lee and Santamarina, 2005).

3.4.2 Near-Field Effect

The near-field effect was first introduced by Sanchez-Salinerio et al. (1986) who studied the P- and S- wave propagation in an infinite isotropic elastic medium. In their study the sinusoidal pulses were generated by a point source and received at various distances from the source. They divided the space into near field and far field. They described the near-field effect as coupling between the waves which have the same particle motion but propagate at different velocities and attenuate at different rates.

In order to describe the near field effect in bender element testing the wave radiation caused by a unit impulsive force should be studied (Arroyo et al., 2003). The used notation describes vectors with bold font and scalars with normal font. The assumed vector nomenclature is illustrated in Figure 3.10. The origin of the phenomena is the inhomogeneous isotropic elasto-dynamic equilibrium equation:

$$\rho \ddot{\mathbf{u}} = \mathbf{b} + (\lambda + \mu) \nabla (\nabla \cdot \mathbf{u}) + \mu \nabla^2 \mathbf{u} \quad (3.9)$$

where \mathbf{u} is the displacement vector, \mathbf{b} is the force vector, ρ is the medium's density, λ and μ are Lamé's elastic constants.

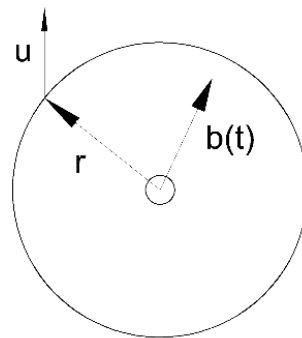


Figure 3.10: Vector nomenclature adapted from (Arroyo et al., 2003)

3.4 FACTORS INFLUENCING BENDER ELEMENT TESTING

Stokes obtained a mathematical fundamental solution providing a transfer function for a unit impulsive force within an infinite elastic medium. This transfer function relates the output displacement vector $\mathbf{u}(t)$ and the input source force vector $\mathbf{b}(t)$ as follows:

$$\mathbf{u} = \mathbf{GR} * \mathbf{b} \quad (3.10)$$

where \mathbf{GR} is the Green's function and $*$ indicates convolution in time. \mathbf{GR} can be expressed as:

$$\begin{aligned} \mathbf{GR} &= N(r, t)[3\mathbf{A} - \mathbf{1}] + F_p(r, t)\mathbf{A} - F_s(r, t)[\mathbf{A} - \mathbf{1}] \\ \mathbf{A} &= \nabla r \otimes \nabla r = \mathbf{r} \otimes \mathbf{r} \\ \|\mathbf{r}\| &= 1 \end{aligned} \quad (3.11)$$

The fundamental solution suggests that the particle oscillation depends only on the distance from the source and time. The coefficients in Green's function are:

- F_p - far-field term travelling at compressive plane wave velocity v_p
- F_s - far-field term travelling at shear plane wave velocity v_s
- N - near-field term travelling at an intermediate velocity

The particle movement \mathbf{u} can be expressed as the movement parallel (\mathbf{u}_p) and perpendicular (\mathbf{u}_s) to the propagation direction:

$$\begin{aligned} \mathbf{u}_p &= (\mathbf{u} \cdot \mathbf{r})\mathbf{r} = (\mathbf{r} \cdot \mathbf{b}) * [2N + F_p]\mathbf{r} \\ \mathbf{u}_s &= \mathbf{u} \wedge \mathbf{r} = (\mathbf{r} \wedge \mathbf{b}) * [F_s - N] \end{aligned} \quad (3.12)$$

The \mathbf{u}_p movement is associated with P-wave propagation, while \mathbf{u}_s movement with the S-wave propagation. Equation (above) shows that when the movement is parallel to the propagation direction, there is no S-like movement because $(\mathbf{r} \wedge \mathbf{b}) = 0$. When the movement is perpendicular to the propagation direction, there is no P-like movement, as $(\mathbf{r} \cdot \mathbf{b}) = 0$. What is more, only when far-field terms F_p, F_s are much larger than the near-field term N , ie. $N / F_i \rightarrow 0$, the P-movement will be associated with P-wave velocity v_p and S movement associated with S-wave velocity v_s .

The coefficients of Green's function are expressed in the time domain as:

$$\begin{aligned} N &= \frac{kt}{r^2} \left[H\left(t - \frac{r}{v_p}\right) - H\left(t - \frac{r}{v_s}\right) \right] \\ F_p &= \frac{k}{v_p^2} \delta\left(t - \frac{r}{v_p}\right) \\ F_s &= \frac{k}{v_s^2} \delta\left(t - \frac{r}{v_s}\right) \\ k &= \frac{1}{4\pi\rho r} \\ r &= \|\mathbf{r}\| \end{aligned} \quad (3.13)$$

These equations indicate what 'near field' and 'far field' mean. The r^2 component in expression for N suggest that attenuation of N is r^{-2} whereas the far field components attenuate with r^{-1} . Therefore, the 'far field' may be understood as a distance from the source where $1/r^2$ component is small enough to assume that $N \rightarrow 0$. When this criterion is not satisfied, then the 'near field' occurs.

The coefficients in frequency domain are given by:

$$N = N_s - N_p \quad (3.14)$$

3.4 FACTORS INFLUENCING BENDER ELEMENT TESTING

$$\begin{aligned}
 N_S &= \frac{k}{v_s^2} \frac{\sqrt{1+n_s^2}}{n_s^2} e^{-i[n_s - \arctan(n_s)]} \\
 N_P &= \frac{k}{v_p^2} \frac{\sqrt{1+n_p^2}}{n_p^2} e^{-i[n_p - \arctan(n_p)]} \\
 F_P &= \frac{k}{v_p^2} e^{-in_p} \\
 F_S &= \frac{k}{v_s^2} e^{-in_s} \\
 k &= \frac{1}{4\pi\rho r}
 \end{aligned}$$

where the two dimensionless ratios n_p, n_s are expressed as:

$$\begin{aligned}
 n_p &= \frac{\omega}{v_p} r = 2\pi \frac{r}{\lambda_p} \\
 n_s &= \frac{\omega}{v_s} r = 2\pi \frac{r}{\lambda_s}
 \end{aligned} \tag{3.15}$$

From equation 3.14 we can observe that the difference between far field and near field terms is dependent only on the ratios n_p, n_s which describe the relation between the distance from the source and the P-wave and S-wave wavelength respectively.

As the shear wave propagation is of interest in this study, using equations 3.14 and 3.15 the solution for the transverse motion may be written as:

$$\begin{aligned}
 S &= F_S - N = F_S - N_S + N_P \\
 S(\omega, r) &= k \left\{ \frac{e^{-in_s}}{v_s^2} - \frac{\sqrt{1+n_s^2}}{v_s^2 n_s^2} e^{-i(n_s - \arctan(n_s))} + \frac{\sqrt{1+n_p^2}}{v_p^2 n_p^2} e^{-i(n_p - \arctan(n_p))} \right\} \\
 k &= \frac{1}{4\pi\rho r}
 \end{aligned} \tag{3.16}$$

The transverse motion of shear wave includes three terms, one far field and two near field. All three terms are related to the transverse motion but they propagate at different velocities. Two of terms: F_S and N_S propagate at shear wave velocity, while N_P at compression wave velocity. In bender element testing, when S-wave motion is examined, the near field term travelling at velocity v_p may reach the receiver before the S-wave and thus causing difficulties with interpretation of the S-wave arrival.

The ratio between the near and far-field terms is thus dependent only on the n_i ratio. To avoid the near-field effect and thus obtain far-field conditions two possible methods may be applied. Increasing the distance between the source and receiver or decreasing the wavelength. As in laboratory bender element testing possibility of increasing the distance is limited, the adjustment of frequency is proposed. This may be expressed by the ratio d/λ :

$$\frac{d}{\lambda} = \frac{d \cdot f}{V_s} \tag{3.17}$$

where d is the travelling distance, f is the frequency and V_s is the shear wave velocity. To minimize the influence of the near-field effect the ratio d/λ should reach a given value (Camacho et al., 2012). That is usually obtained by increasing the frequency. Jovicic et al. (1996) denote the ratio d/λ as R_d . They investigated kaolin samples with R_d ratios from 1.1 to 8.1. Lower R_d values proved to lead to significant near-field effect, while for high R_d values the S-wave arrival was clearly seen. Arroyo et al. proposed the adjustment of frequency as follows:

3.4 FACTORS INFLUENCING BENDER ELEMENT TESTING

$$f_{lim} = \frac{v_s}{\lambda} > \frac{v_s}{1,6 \cdot d} \quad (3.18)$$

Which corresponds to d/λ ratio of 0,625:

$$\begin{aligned} \frac{v_s}{\lambda} &> \frac{v_s}{1,6 \cdot d} \\ \frac{d}{\lambda} &> \frac{1}{1,6} = 0,625 \end{aligned} \quad (3.19)$$

According to Sanchez-Salinero et al. (1986) the ratio $d/\lambda > 2$ is sufficient to avoid the coupling of primary and secondary waves. Arulnathan et al. (1998) showed that the near-field effect disappears when d/λ is greater than 1. Rahman et al. (2015) suggested that the near-field effect may mask the S-wave arrival when the distance between the source and the receiver is less than 4 wavelengths. The very high d/λ values are also not correct. Camacho et al. (2012) suggested the upper d/λ limit of 9.

The near-field effect is therefore a wave dispersion phenomenon stating that the propagating wave consists of four different components: far-field terms travelling at compressive and shear wave velocities and near-field terms travelling at compressive and shear wave velocities. However, Arroyo et al. (2003) suggest that the near-field effect is not the only reason for distortion of the received signal in bender element testing. They claim it does not explain fully the differences between the transmitted and received signal.

3.4.3 P-wave component

Bender elements transmit both P- and S-waves (Sanchez-Salinero et al., 1986). Shear wave measurements performed in oedometers and triaxial cells are significantly influenced by the P-wave component. Figure 3.11 presents the configuration of the wave lobes generated by the bender element. The P-waves reflected from the lateral or end boundaries of the soil sample may interfere with the S-wave arrival. As the P-waves are faster than the S-waves, a P-wave reaches the receiver before the S-wave, thus creating difficulties in the S-wave arrival detection. The ratio between the P- and S-wave velocities is:

$$\frac{v_p}{v_s} = \sqrt{\frac{2(1-\nu)}{1-2\nu}} \quad (3.20)$$

For dry or unsaturated soils $\nu \approx 0,1$ and $\frac{v_p}{v_s} \approx 1,5$. For saturated soils, $\frac{v_p}{v_s}$ is stress dependent and for soils subjected to low effective stresses may exceed 20 (Lee and Santamarina, 2005). The signal interference of P- and S-waves depends on the cell geometry and the $\frac{v_p}{v_s}$ ratio, i.e., saturation and stress conditions (Lee and Santamarina, 2005).

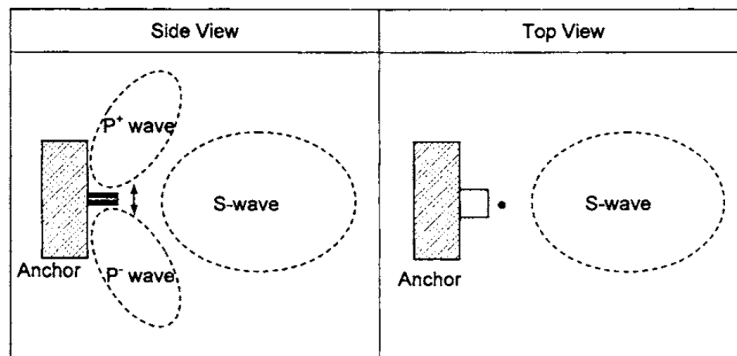


Figure 3.11: Waves generated by a bender element (Lee and Santamarina, 2005)

3.4.4 Sample geometry

In an unbounded elastic soil medium the wave propagation is dependent only on the properties of the medium (Rio, 2006). This assumes no wave reflection and is often made in the cross-hole testing during field investigations. In a bounded medium the wave components are reflected from the boundaries back to the medium, influencing the overall propagating wave. This bounded medium is also known as a waveguide. The wave reflection behaviour is dependent on the nature of the media at the interface and the nature of the incident waves (Rio, 2006).

Rio (2006) studied the influence of sample geometry on the wave propagation in laboratory testing with bender element testing in a triaxial cell. The testing included rubber samples with various parameters and different boundary conditions. The analysis results showed that the geometry of the sample has a great influence on the dynamic behaviour of bender elements. The wave propagation in bulkier samples was observed to be similar to the propagation in an unbounded medium, i.e. with no disturbance from the reflected wave components. Whereas, the propagating wave fronts in slender samples showed influence from the reflected wave components. It was stated that with increasing slenderness of the sample less dispersion due to near-field effect and more dispersion due to wave reflection is expected. Rio (2006) proposed to evaluate the model of sample behaviour with relation to sample geometry as follows:

- $\frac{H^2}{D} < 15 \text{ mm}$ – unbounded medium, dispersion caused by near-field effect only
- $\frac{H^2}{D} > 45 \text{ mm}$ – waveguide

where H is the height and D is the diameter of the sample. For $15 \text{ mm} < (H^2/D) < 45 \text{ mm}$ there is no predominant behaviour of the samples. The proposed classification is presented in Figure 3.12. These limits were established for the tested rubber samples. For actual soil samples subjected to the confining pressure the behaviour limits may be different. Nevertheless, it was concluded that bender elements response is clearly affected by the sample geometry, which is also confirmed by numerical analysis performed by Rio (2006). Therefore, in bender element testing Rio (2006) recommended to first establish the model of sample behaviour and then consider the potential wave dispersion phenomena: near-field effect or/and waveguide dispersion.

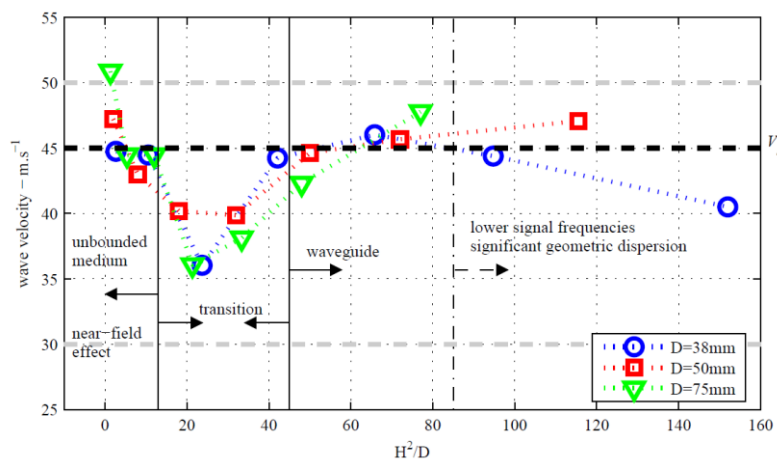


Figure 3.12: Sample behaviour models according to Rio (2006)

3.5 Anisotropy investigations with bender elements

The investigation of anisotropy of small-strain elastic properties of soils may be performed by generating the shear waves in different directions across the sample, with motion polarization in different planes (Sanchez-Salinerio et al., 1986), i.e., V_{ij} where the first subscript i denotes the direction of the S-wave propagation and the second subscript j denotes the plane of the S-wave polarization. Many researchers used bender elements to study the anisotropy of small strain shear modulus. Two different approaches may be distinguished. Figure 3.13 illustrates the main concept of each of these methods.

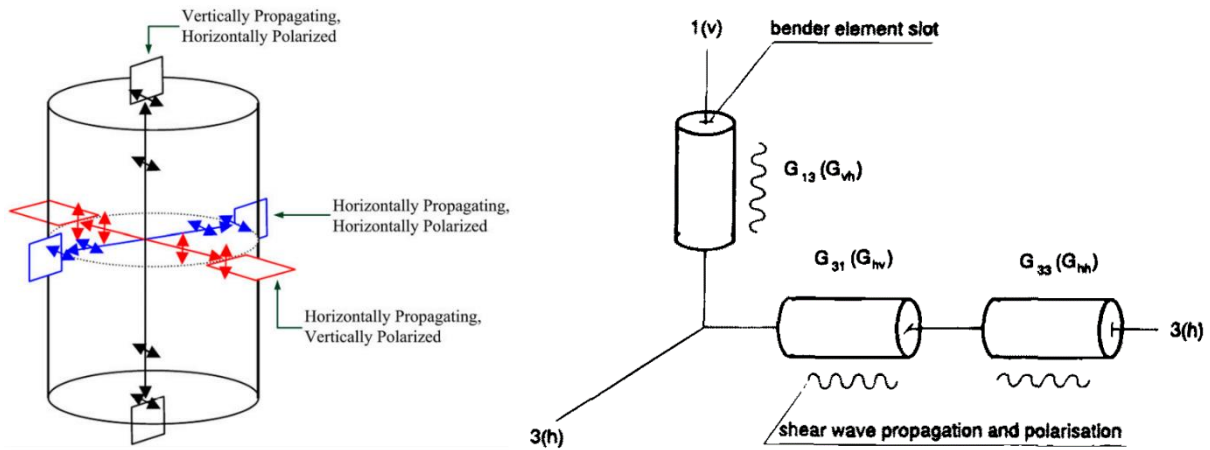


Figure 3.13: Anisotropy investigations with bender elements: a) Teng et al., 2014; b) Jovicic and Coop (1998)

Pennington et al. (1997) and Teng et al. (2014) used multiple pairs of bender elements and incorporated them into the triaxial cell. This setup enabled the measurements of shear wave velocity in different directions and different planes across the sample. In contrast, Jovicic and Coop (1998) used a standard triaxial setup with bender elements located in the top and bottom caps of the cell. Therefore, to study the anisotropy the soil samples were cut not only vertically, but also horizontally, i.e., with the axis in the direction of the minor principle stress. Then the samples were placed in the triaxial apparatus with appropriate bender elements orientation, depending on the desired wave polarization (Figure 3.14).

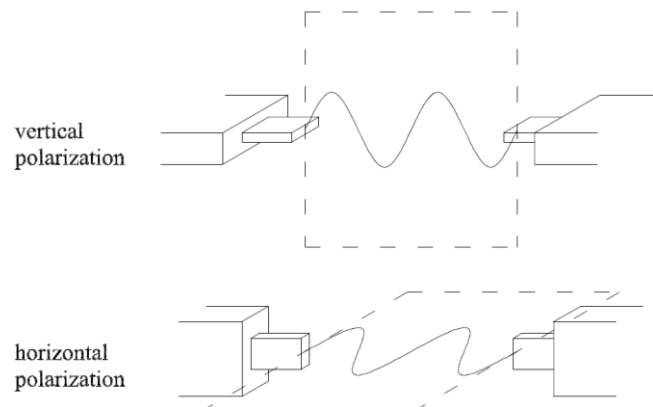


Figure 3.14: Bender elements configuration and consequent wave polarization (Rio, 2006)

Chapter 4

Tiller-Flotten Testing Site

This section presents the Tiller-Flotten Quick Clay Site. The engineering geology with geological setting and stress history of the area is discussed. Lastly, the Tiller-Flotten clay is briefly characterized with special attention to shear wave velocity measurements, and to the clay structure.

4.1 Norwegian Geo-Test Sites

The Norwegian Geo-Test Site is a research project which establishes five test sites in Norway, each of them representing one of the particular soil types: soft clay, quick clay, silt, sand or permafrost. The sites are located near Oslo, Trondheim and Svalbard (Figure 4.1). The project is supported by the Research Council of Norway. The chosen sites are used for geotechnical testing leading to the collection of data necessary in development and testing of new tools and techniques. This study focuses on the Tiller-Flotten Site and quick clay investigations.



Figure 4.1: Location of the NGTS sites (ngi.no)

4.2 Site location

The Tiller-Flotten site is located approximately 10 km south from the city centre of Trondheim in Sør-Trøndelag, Mid Norway. The site has been used for geotechnical research purposes due to the character of the deposit, i.e., its thickness, uniformity, high sensitivity. The site lies within a quick clay hazard zone classified as a ‘high hazard’ zone. In 1816 a major landslide occurred in Tiller area involving 7,000,000 m³ of soil.

4.3 ENGINEERING GEOLOGY

The site is an agricultural area with an adjacent non-cultivated marshy area in the south-west. The area is rather flat, located between 123–125 m a.s.l. To the east the terrain descends to the Nidelva River. The location of the site is shown on the maps in Figure 4.2.

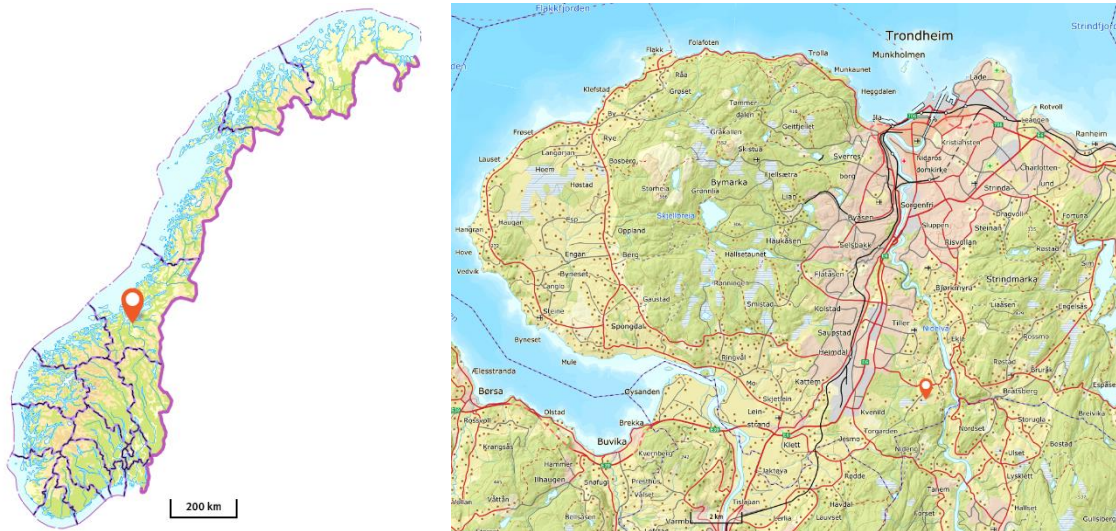


Figure 4.2: NGTS Tiller-Flotten Quick Clay Test Site location (norgeskart.no)

4.3 Engineering geology

4.3.1 Geological setting

The Tiller-Flotten test site is characterized by thick deposits of marine clay. The Nidelva River deposited some alluvial sediments which can be seen to the north and east from the site. The non-cultivated area in the south-western part of the site consists of a 2 m layer of peat deposit above the clay. Minor ravines and slide scars are present in the area. The quaternary geology of Flotten area is presented in Figure 4.3.

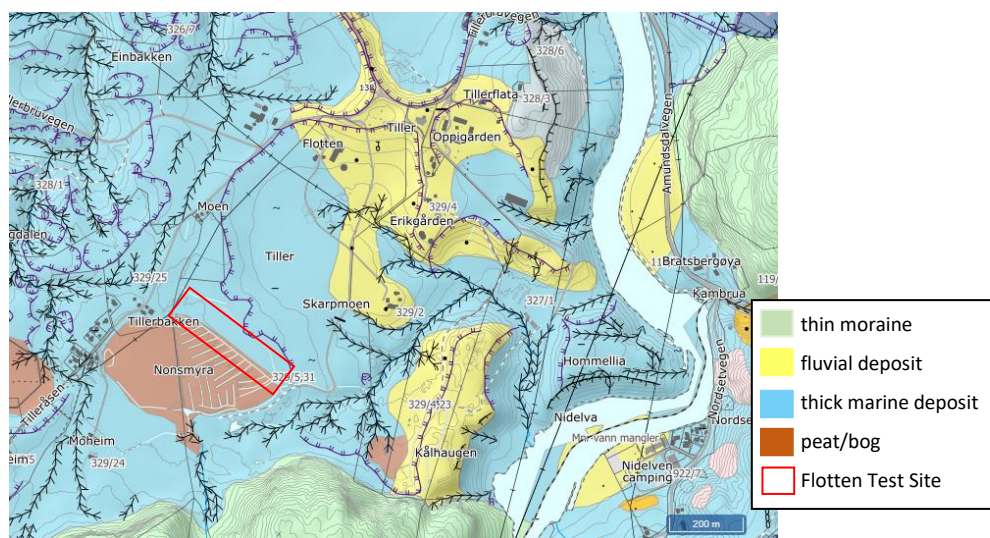


Figure 4.3: NGTS Flotten Quick Clay Test Site quaternary geology (ngu.no)

4.4 STRATIGRAPHY AND INDEX PROPERTIES

The clay deposit started to form after the retreat of the glacier. During the isostatic depression caused by the weight of the ice the material from the glacial erosion was deposited in the surrounding ocean. In the salt water the particles formed a ‘card house structure’ stabilized by van der Waals forces (Gylland et al., 2013). As the ice from the glacier melted, the land masses started to rise. The clay, which was situated under the sea level, now was exposed. The fresh water washed away the salt from the clay and thus the bonds between the particles have been reduced. As a result, the original structure of the soil is maintained but the strength characteristics is drastically changed. When subjected to small mechanical disturbance the clay structure suddenly collapses. Such clay is denoted as ‘quick’.

4.3.2 Stress history

The only major stress changes in Tiller-Flotten area are the glacier influence during the ice age and the Nidelva River sedimentation process. After the retreat of the glacier the stress variation may have been caused by the fluctuations of ground water level. Figure 4.4 presents the ground water distribution and effective stress profile with preconsolidation stresses at Tiller-Flotten site. The pore water pressure measurements indicate that the ground water level is currently located between 1 and 2 m below ground level. The pore pressure distribution is below hydrostatic conditions and between 5 m and 23 m a nearly linear increase can be seen (L'Heureux et al., In press). In the study by L'Heureux et al., (In press) the preconsolidation stress p'_c was determined from the oedometer tests and the overconsolidation ratio (OCR) was estimated. The results show that Flotten clay is slightly overconsolidated. The OCR values were found to be between above 2 in the first 10 m below ground and between 1,5-2,0 from 10 m and below.

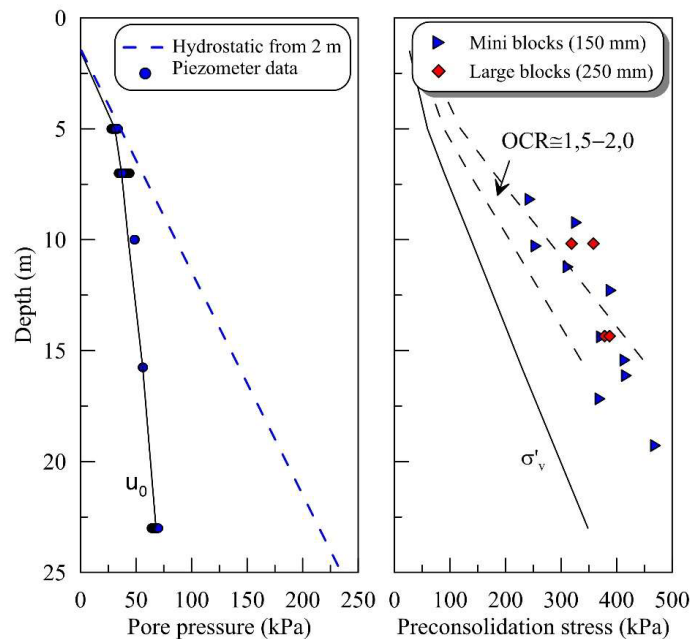


Figure 4.4: In-situ groundwater pressure, effective stress profile and preconsolidation stresses at Tiller-Flotten site (L'Heureux et al., In press)

4.4 Stratigraphy and index properties

The stratigraphy of Tiller-Flotten site is presented in Figure 4.5. The basic soil profile shows that three units may be distinguished. The top unit, between 0 m and 2 m depth, is a dry crust. Between 2 and 20 m depth a deposit of

4.5 SHEAR WAVE VELOCITY MEASUREMENTS

clay can be seen. From 2,0 m to 7,5 m below the ground the clay is of low to medium sensitivity, whereas from 7,5 m and below a very sensitive clay is seen with sensitivity increasing to up to 100. Natural water content ranges between 40-50% from 0 to 5 m depth and decreases to 30-35% at 20 m depth. The water content is below the liquid limit throughout the medium sensitive clay unit, whereas in the very sensitive quick clay unit the water content is higher than the liquid limit. The average bulk density is approximately 18 kN/m³. The clay content ranges between 70% at 8 m depth to 50% at 19 m depth. Salt content values are low, approximately 2 g/l, which suggests that the clay has been leached.

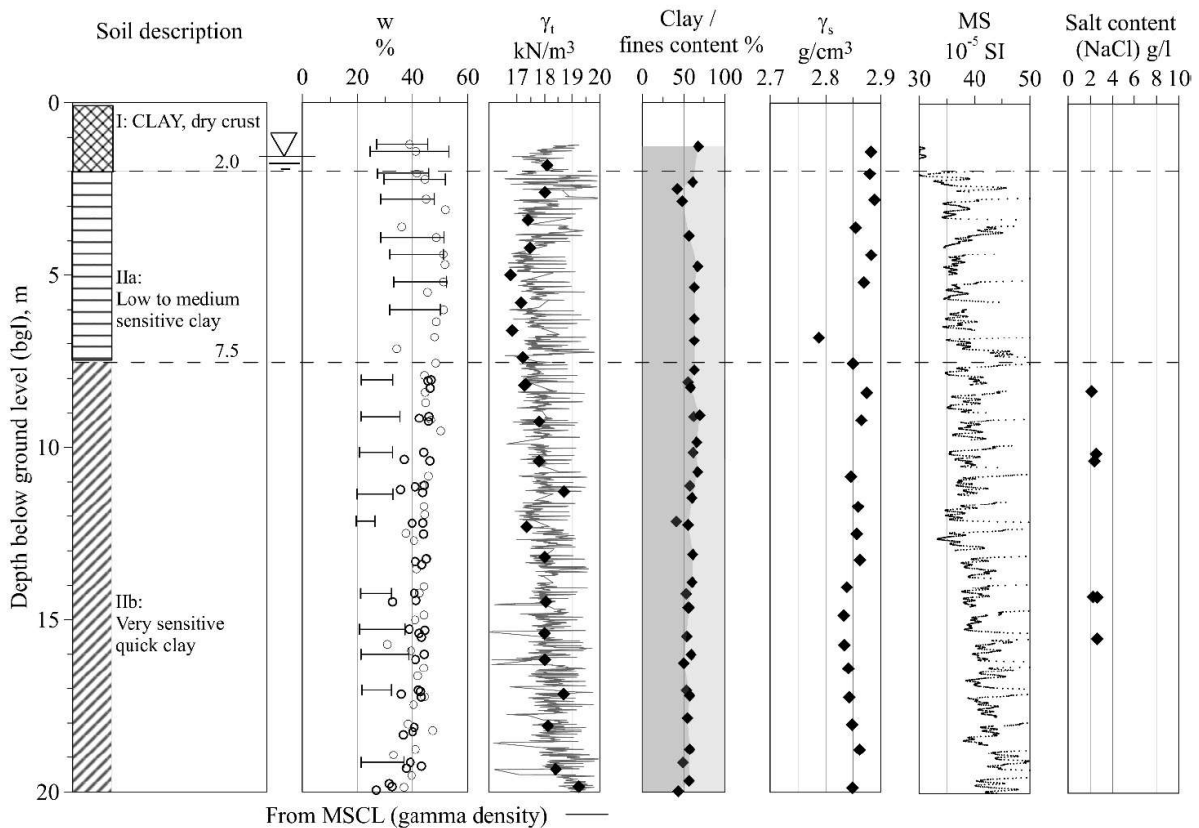


Figure 4.5: Basic soil profile and index properties at Tiller-Flotten site (L’Heureux et al., In press)

4.5 Shear wave velocity measurements

Figure 4.6 presents the shear wave velocity and small strain shear modulus data for Tiller-Flotten site. In-situ shear wave velocity was measured using several techniques: seismic cone penetration test (SCPTU), seismic dilatometer (SDMT) and multichannel analysis of surface waves (MASW). Laboratory testing was performed on high quality block samples using bender elements. The measurements were performed both on unconfined samples ($V_{s,0}$) and on samples reconsolidated to in-situ stresses ($V_{s,1}$). The results show shear wave velocity values from approximately 120 m/s at 3 m depth to 225 m/s at 20 m below ground level. These values are characteristic for Norwegian soft marine clays (L’Heureux et al., In press). Small strain shear modulus increases from approximately 30 MPa below the dry crust to 100 MPa at 20 m below ground level. Laboratory determined values are reported to be consistently lower than the in-situ measured ones.

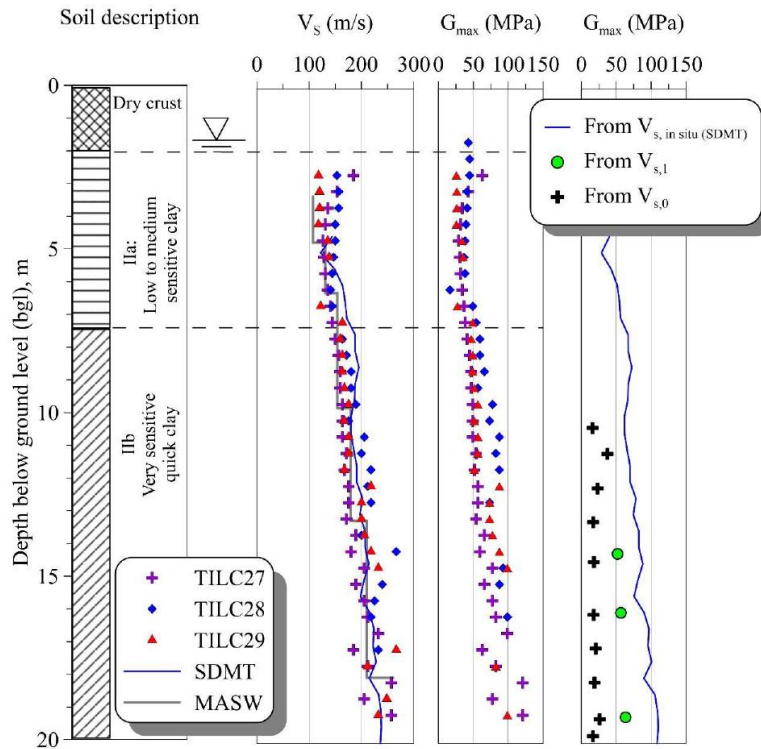


Figure 4.6: Shear wave velocity (V_s) and small strain shear modulus (G_{max}) with depth at Tiller-Flotten Site (L'Heureux et al., In press)

4.6 Clay mineralogy and structure

The mineralogy and structure of Tiller-Flotten clay was investigated using X-ray analyses. The clay fraction was found to be dominated by phyllosilicates such as illite and chlorite, whereas the coarser fraction consists of quartz and feldspars (Gylland et al., 2013). Phyllosilicates were found to have a preferred horizontal orientation (Gylland et al., 2013).

The structure of Tiller-Flotten clay was found to be varved and laminated, with lighter and darker intervals (L'Heureux et al., In press). An example of a split core section with visible layering is illustrated in Figure 4.7. The clay structure developed during variations in sedimentation process in marine environment, i.e., changing sediment load and speed of meltwater flow. This affected the deposition environment and resulted in seasonal varves. The lighter layers consist of coarser material which deposited under higher stress conditions. On the other hand, the darker layers most likely formed during winter when the sediment suspension was reduced due to ice cover.



Figure 4.7: Split core section with visible varves at Tiller-Flotten site (L'Heureux et al., In press)

Chapter 5

Laboratory Investigations

This chapter treats the performed laboratory investigations which were carried out at the geotechnical laboratory at NTNU. The following laboratory tests were carried out:

- Index testing.
- Preliminary bender elements testing on an unconfined specimen.
- Bender elements testing on unconfined and consolidated samples in the triaxial cell on triaxial samples cut from the mini-block samples in different orientations.

The description of the equipment used for tests, sample preparation procedure and the overview of the tests performed are included in the section below.

5.1 Bender element equipment

Figure 5.1 presents the testing system used during this study. The system consists of: bender elements, power supply, data acquisition (DAQ) device, triaxial cell with cell pressure controller, and computer with control software. The bender element test setup is incorporated in the triaxial cell. The sender element is situated at the base cap while the receiver element is located in the top cap of the cell. The schematic work of the bender element system is illustrated in Figure 5.2.

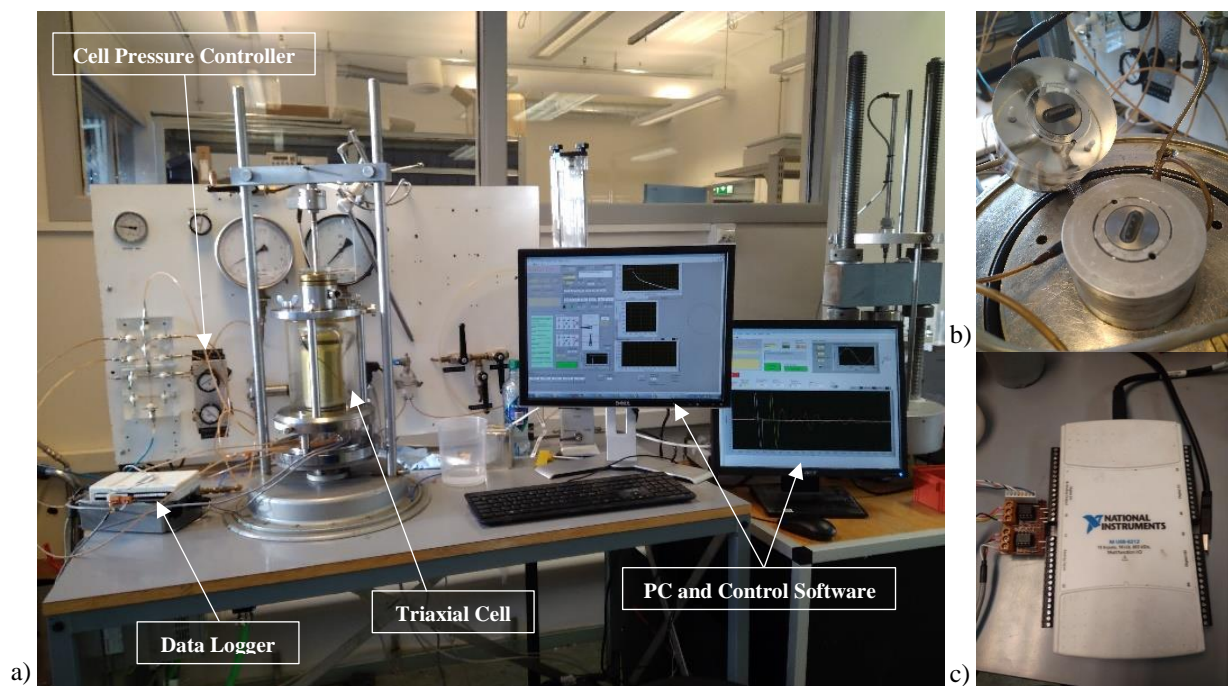


Figure 5.1: Bender element testing system at the geotechnical laboratory at NTNU: a) full view of the testing system; b) bender elements; c) data acquisition device

5.1 BENDER ELEMENT EQUIPMENT

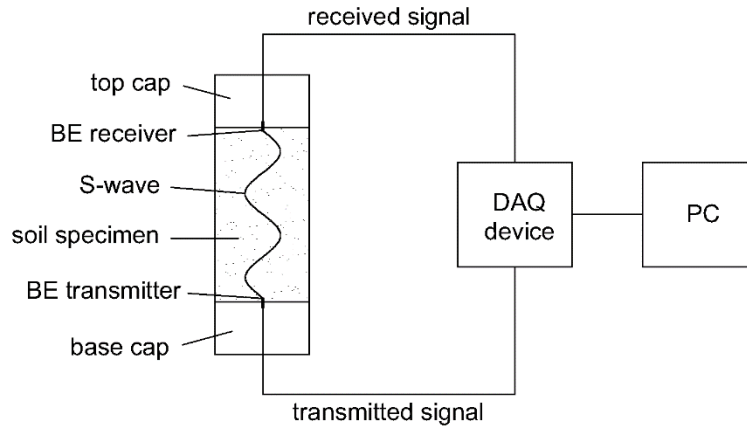


Figure 5.2: Schematic work of the bender element system

The data acquisition device is used to send and receive the signal. The sampling rate of the system is 200 kHz; meaning the data is recorded every 5 μ s. Bender element transmitter is set up to generate an S-wave input signal. A sinusoidal pulse with a maximum voltage of ± 5 V can be generated. The transmission of the signal is controlled manually for the measurements on the unconfined samples, whereas for the specimens subjected to consolidation pressure the program is run automatically at a user specified time interval. The received signal is recorded continuously in both cases. To visualise the signals the LabVIEW software is used. An example of the output from the LabVIEW program is presented in Figure 5.3.

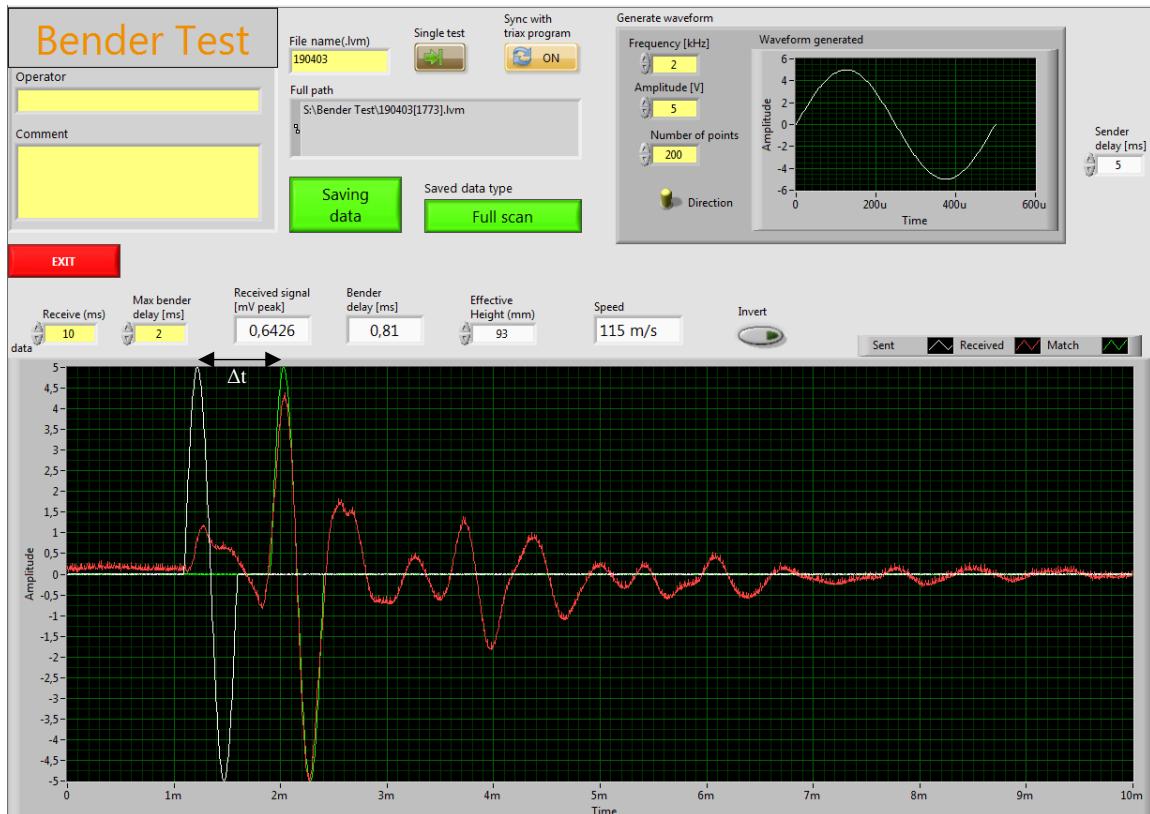


Figure 5.3: Example of the output from the LabVIEW program

The input values are: frequency (kHz), amplitude (V), number of points, receive time (ms), sender delay (ms). The output values are: received signal (mV peak), bender delay (ms), effective height (mm), velocity (m/s).

5.1 BENDER ELEMENT EQUIPMENT

The software presents the results in the form of a graph where the white is the sent signal, red is the received signal and green is the match signal. To analyse the results the bender elements test data may also be exported to Microsoft Excel. In order to match the shape of the received signal with the input signal, the method of least squares is used. The matching process is shown in Figure 5.4. The travel time of the S-wave is determined using the peak-to-peak method, i.e., the bender delay is determined as the time difference between the peaks of the sent and match signal. The bender elements are embedded into the sample at 2,5 mm depth at each end. The resultant effective height is thereby calculated as the sample height reduced by 5 mm. The bender element program calculates shear wave velocity using the following formula:

$$V_s = \frac{d}{t} \quad (5.1)$$

where d is the effective height (mm) and t is the bender delay (ms).

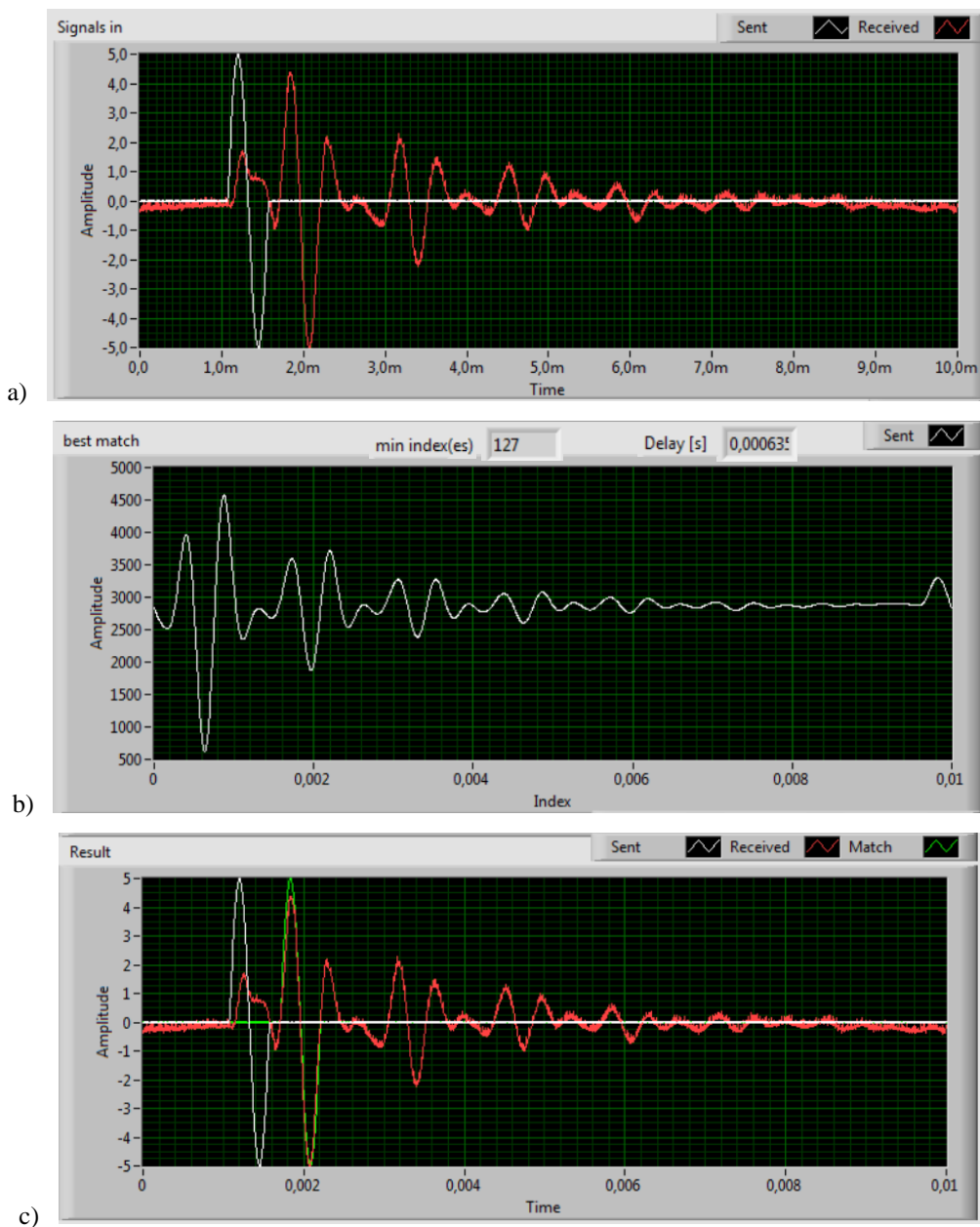


Figure 5.4: Example of the matching process: a) sent and received signals b) least squares, best match c) result of matching

5.2 Soil specimens

The investigations were conducted on mini-block samples from Flotten NGTS Quick Clay Test Site. The samples were collected in November 2017, therefore they had been stored for 1 year and 5 to 6 months prior to the laboratory testing. On the day of sampling, the samples were wrapped in several layers of plastic film to minimise moisture loss. Prior to transport, individual samples were placed in PVC tubes. The gaps between the sample and the tube were filled with styrofoam spheres (Figure 5.5). Until the laboratory testing the samples were stored in a temperature controlled room. During this study four mini-block samples were utilized. Two of them had the height of 35 cm and the other two a reduced height to 25 cm.

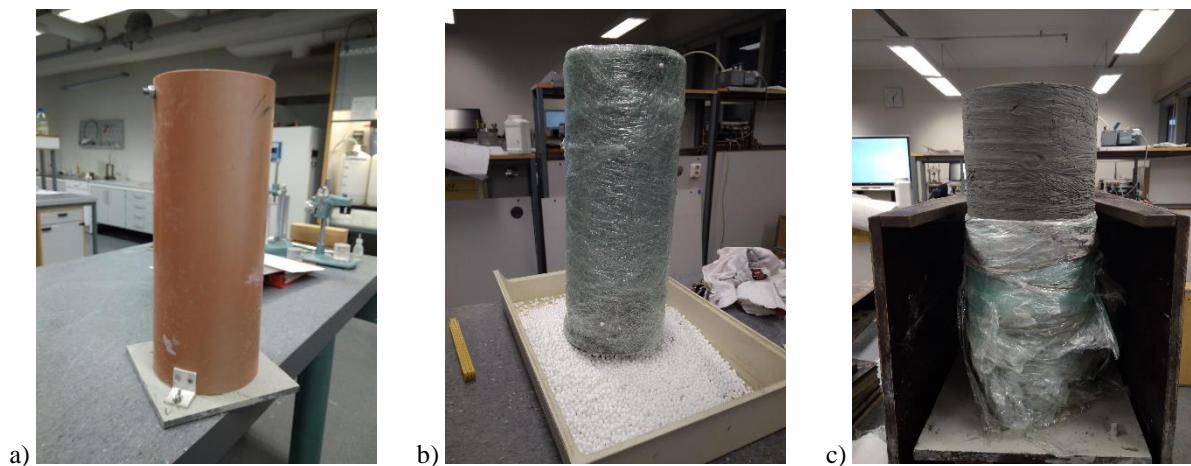


Figure 5.5: Mini-block 9,75-10,10 m depth: a) sample in a PVC tube; b) sample after opening the tube; c) mini-block prepared for cutting

5.2.1 Division of the samples

The mini-blocks were unwrapped and first visually investigated. In each of the samples, a dry section near the edges of the block was identified, 1,5 to 2 cm thick, dependent on the sample. This was treated as soil of high disturbance, therefore these parts were avoided during the investigations. An example of this disturbance is illustrated in Figure 5.6.

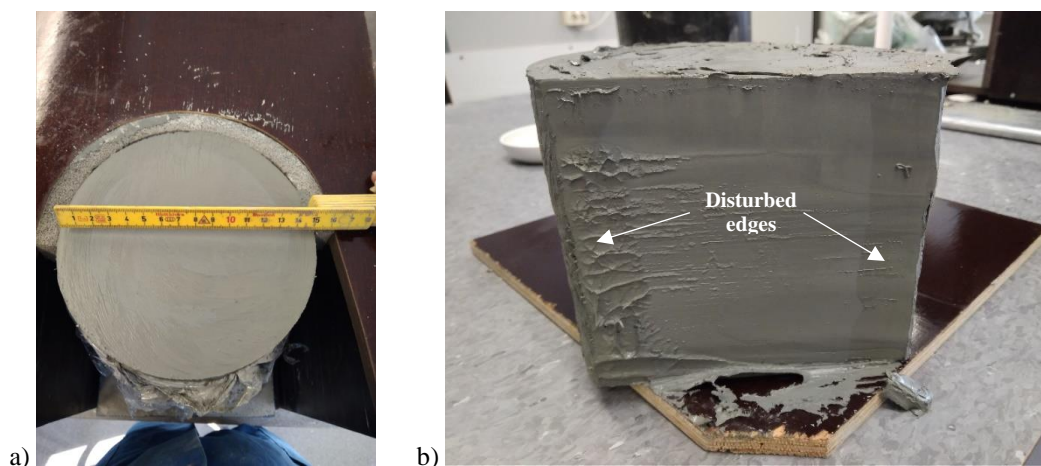


Figure 5.6: Example of the disturbance near the edge of the mini-block sample: a) view from the top; b) cross-section

5.2 SOIL SPECIMENS

Prior to laboratory testing, the sample division was planned. The mini-blocks were divided as presented in Figure 5.8. Since this study focuses on investigations of anisotropy, the aim was to obtain at least one vertically-cut and two horizontally-cut samples from each mini-block. Firstly, the vertical samples were cut and afterwards the horizontal ones for measurement of V_{hv} and V_{hh} . Unfortunately, some mistakes were made during preparation and testing. Therefore, the first horizontal samples from the mini-blocks 9,75-10,10 m and 10,80-11,05 m depths could not provide relevant results and were not included in this report. As a result, mini-blocks taken from 9,75-10,10 m and 10,80-11,05 m resulted in only two samples. Consequently, these samples could only produce the measurements of V_{vh} and V_{hv} . On the other hand, mini-blocks 12,80-13,15 m and 19,45-19,70 m depth were able to provide measurements for all three different shear wave velocities: V_{vh} , V_{hv} and V_{hh} . An additional vertical sample was cut from the mini-block 12,80-13,15 m. It was used to test the effects of a longer consolidation time. Since the edges were disturbed, the area of the sample of good quality was limited.

Cutting procedure involved first cutting larger slices of the soil from the mini-block and then trimming them to the desired dimensions. Cutting was performed with a wire saw. The clay was found to be varved and laminated. Several darker intervals in the homogenous clay were encountered during cutting of the samples (Figure 5.7). After cutting each of the large slices, the remaining part of the mini-block was wrapped in several layers of plastic film and placed in the storage room to prevent the sample from drying. The top and bottom parts of the sample and the central cut-offs were utilised for index testing.

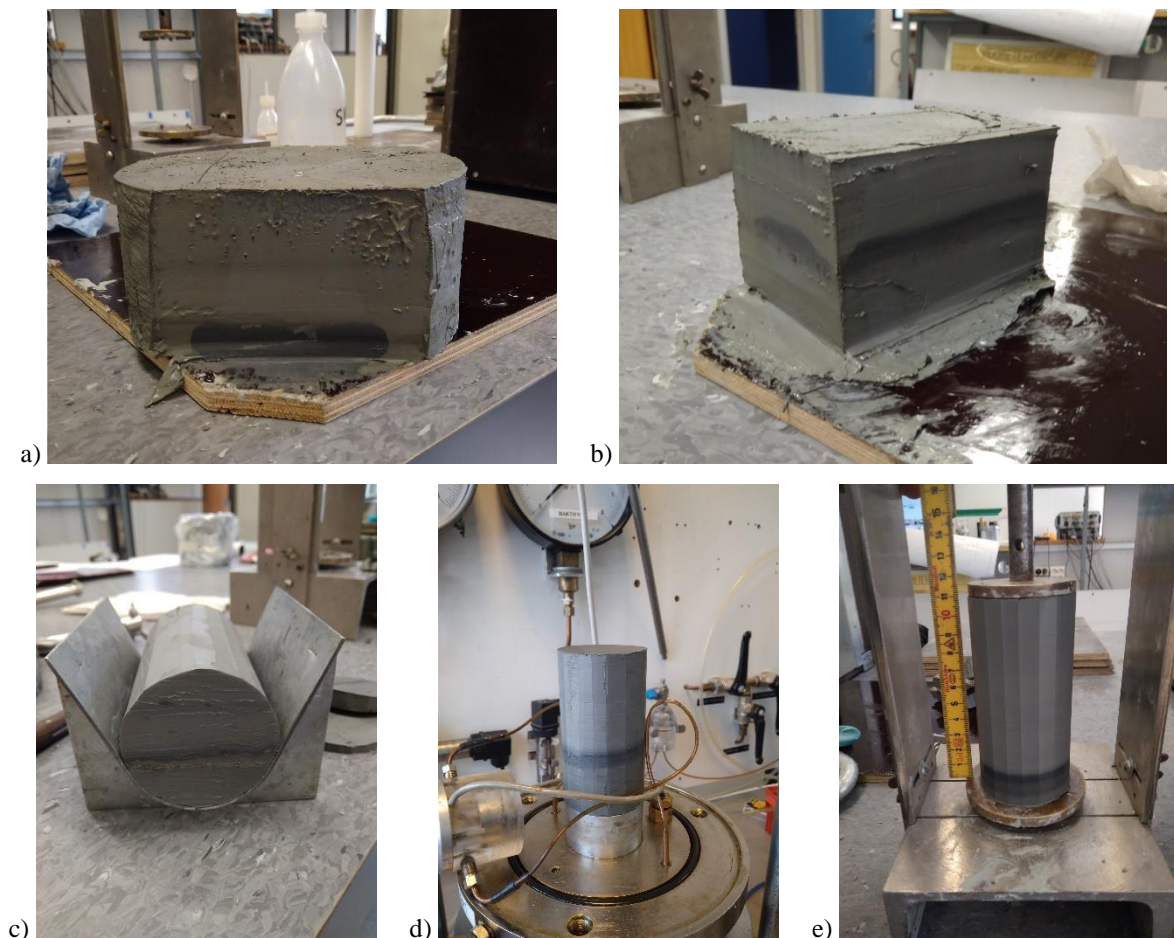


Figure 5.7: Visible varves and layering in clay: a) Sample 2hv; b) Sample 1vh; c) Sample 4hv; d) Sample 4vh; e) Sample 3vh

5.2 SOIL SPECIMENS

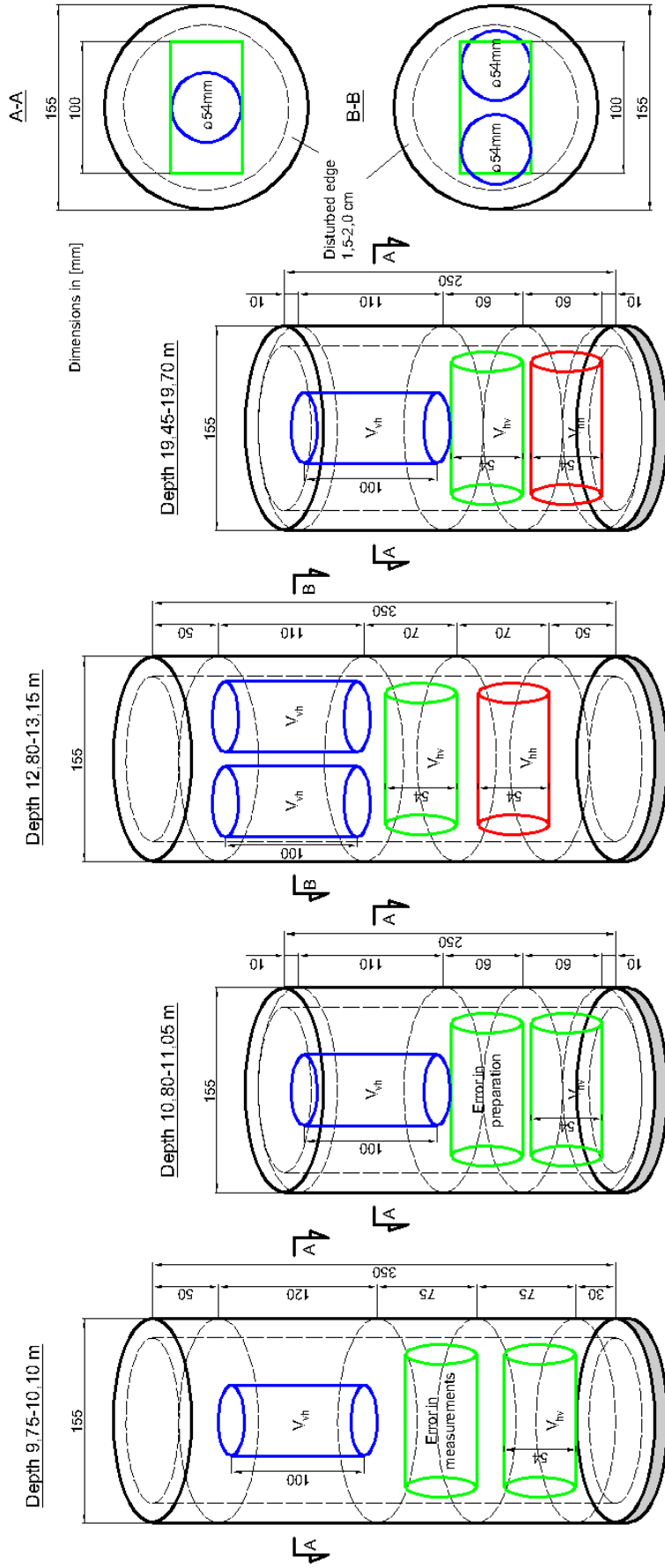


Figure 5.8: Division of the mini-block samples

5.2.2 Preparation for testing

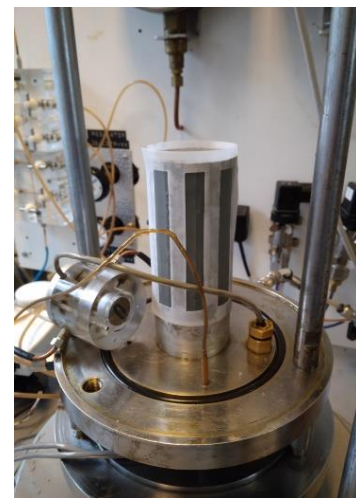
Figure 5.9 presents the steps in preparation of the soil specimens for the bender elements testing in the triaxial cell. The pre-cut specimens from the mini-block samples were trimmed to the diameter of 54 mm and height of 100 mm; which are standard dimensions of triaxial samples in Norway. Then the samples were placed in the triaxial apparatus as soon as possible. The specimens were placed on the bottom transmitter element in the correct orientation. Filter paper was wrapped around the specimens and placed on both the bottom and top of the samples. By this, water extorted from the specimen could flow radially and be transported to the ends of the specimens to the pore water tubes. To separate the specimens from the cell fluid, rubber membrane was placed around the specimens. While placing the top cap with the receiver element the alignment of the bender element transducers was maintained. Then the outside cylinder was mounted, cell filled with water and the consolidation was started.



a) Trimming of the sample



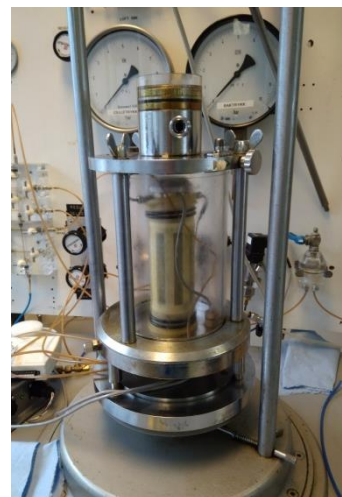
b) Cutting to 100 mm height



c) Filter paper



d) Rubber membrane



e) Sample in the triaxial cell

Figure 5.9: Preparation of the specimen for bender elements testing in the triaxial cell

5.3 Index testing

Index testing is an important part of geotechnical investigations. The aim of the tests is to classify the soil and to be able to correlate the mechanical properties with the soil properties from index tests. The following index tests were performed:

- Water content,
- Density,
- Atterberg limits,
- Salinity,
- Fall cone,
- Grain size distribution.

A brief summary of the testing procedures is given below.

5.3.1 Water content

The water content was determined according to the standard ISO 17892-1 (ISO, 2014a). Specimens of clay were dried to a constant mass in the oven in the temperature of 105°C. The water content was calculated using equation 5.2.

$$w = \frac{m_1 - m_2}{m_2 - m_c} \cdot 100 = \frac{m_w}{m_d} \cdot 100 \quad (\%) \quad (5.2)$$

where w is the water content (%), m_1 is the mass of the cup and wet sample (g), m_2 is the mass of the cup and dry sample (g), m_c is the mass of the cup (g), m_w is the mass of water (g) and m_d is the mass of dry specimen (g).

5.3.2 Density

Bulk density was determined according to the standard ISO 17892-2 (ISO, 2014b). A small calibrated cylindrical ring with known mass and volume was pushed into a prepared sample. The weight of the sample was determined and the density was calculated as follows:

$$\rho = \frac{m}{V} \quad \left(\frac{g}{cm^3} \right) \quad (5.3)$$

where ρ is the density (g/cm³), m is mass of the sample (g) and V is the volume of the sample (cm³).

The unit weight was defined accordingly:

$$\gamma = \frac{m \cdot g}{V} \quad \left(\frac{kN}{m^3} \right) \quad (5.4)$$

where γ is the unit weight (kN/m³) and $g = 9,81 \text{ m/s}^2$.

After trimming to the triaxial test dimensions the average cylinder density of the specimens was determined. Knowing the weight and the volume of the samples the density was calculated using equation 5.3.

For determination of the grain density a calibrated pycnometer with known weight and volume was used. The test was conducted in accordance with ISO 17892-3 (ISO, 2015). The density of solids was calculated as follows:

$$\rho_s = \frac{m_d \cdot \rho_w}{m_{wp} + m_d - m_{wps}} \quad \left(\frac{g}{cm^3} \right) \quad (5.5)$$

5.3 INDEX TESTING

Where m_d is the mass of dry sample (g), ρ_w is the density of water (g/cm^3), m_{wp} is the mass of waterfilled pycnometer (g), and m_{wps} is the mass of waterfilled pycnometer and the sample (g).

5.3.3 Atterberg limits

The Atterberg limits were determined according to ISO 17892-12 (ISO, 2018b). The liquid limit and plastic limit were determined. The liquid limit was determined by the Casagrande method.

Plasticity index:

$$I_p = w_L - w_P \quad (\%) \quad (5.6)$$

Liquidity index:

$$I_L = \frac{w - w_P}{w_L - w_P} \quad (-) \quad (5.7)$$

5.3.4 Salinity

A clay sample was put in the centrifuge in order to expel the water from the sample. Then the electric conductivity of the pore water was measured and the salt content was obtained.

5.3.5 Fall cone

The fall cone test was performed to measure the shear strength of the clay, both for undisturbed (s_u) and remoulded (s_r) samples. The procedure according to ISO 17892-6 (ISO, 2017) was followed.

Sensitivity was calculated using equation 5.8.

$$S_t = \frac{s_u}{s_r} \quad (-) \quad (5.8)$$

5.3.6 Grain size distribution

In order to determine the grain size distribution of the clay the hydrometer analysis was carried out. A calibrated hydrometer was used. After predetermined time intervals it was lowered into the suspension and the reading was performed. The measurement in accordance with ISO 17892-4 (ISO, 2016) was followed.

5.3.7 Degree of saturation, porosity and void ratio

The degree of saturation was calculated as follows:

$$S_r = \frac{V_w}{V_p} = \frac{w \cdot \gamma}{\gamma_w \left(1 + w - \frac{\gamma}{\gamma_s}\right)} \quad (-) \quad (5.9)$$

where V_w is the volume of water (m^3), V_p is the volume of voids (m^3), γ_w is the unit weight of water (kN/m^3).

The porosity was determined using the equation 5.10.

$$n = \frac{V_p}{V} = \left(1 - \frac{\gamma}{\gamma_s(1 + w)}\right) \cdot 100 \quad (\%) \quad (5.10)$$

The void ratio was calculated using equation 5.11.

$$e = \frac{V_p}{V_s} = \frac{\gamma_s(1 + w)}{\gamma} - 1 \quad (-) \quad (5.11)$$

5.4 Bender elements testing

5.4.1 Methodology

After installing the samples in the triaxial cell the bender elements tests on unconfined specimens were performed. Then the cell was filled with water and the consolidation phase was started. The pressure was increased to the desired value and pore water tubes were open. The samples were isotropically consolidated to the effective stress equal to the horizontal effective stress at the given depth. The primary consolidation was considered finished when the volume change was less than 0,1% of the specimen volume per hour or $0,1 \text{ cm}^3/\text{hour}$, whichever was greater (ISO, 2018a). The majority of samples were left consolidating for 24 hours with the cell pressure kept constant. Sample 3vh2 was left consolidating for 77 hours. Longer consolidation was carried out in order to evaluate the long-term time effect on small strain shear modulus. The triaxial test program recorded: deformation (mm), cell pressure (kPa) and the amount of expelled water from the sample (ml). The data was saved every 10 s. Bender element tests were simultaneously conducted alongside the consolidation process. Every 10 s the electric signal was transmitted and the received signal was recorded. During consolidation the frequency of the input signal was manually adjusted so that the frequencies of both the sent and received signals were equal to each other. This adjustment also allowed the strength of the output signal to be optimised. The used frequencies varied between 0,7 and 3 kHz. The amplitude of 5 V was maintained for all the tests. The output data from bender elements tests was obtained as described in section 5.1. Three different measurements of the shear wave velocity were performed:

- V_{vh} - shear wave propagating vertically with horizontal polarization,
- V_{hv} - shear wave propagating horizontally with vertical polarization,
- V_{hh} - shear wave propagating horizontally with horizontal polarization.

In order to measure V_{hv} and V_{hh} the samples were cut in the direction of the minor principle stress and the bender elements were oriented so that the polarization of the shear wave was in the vertical and horizontal plane respectively. Figure 5.10 illustrates the orientation of the samples and the arrangement of bender elements.

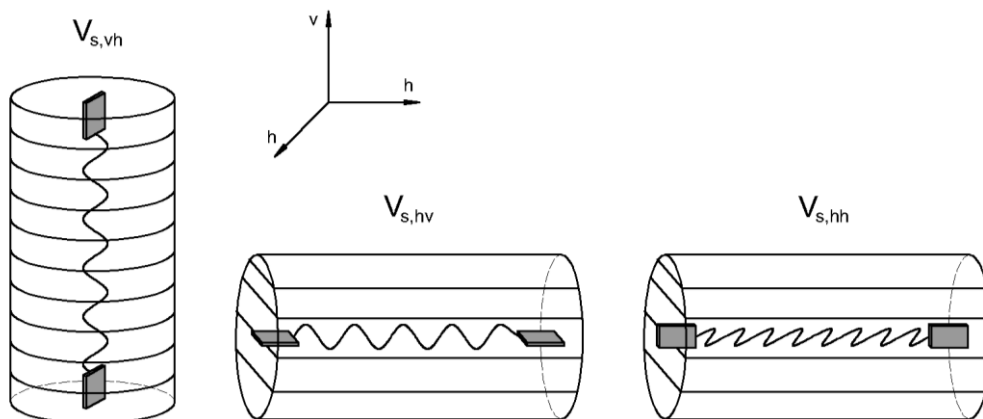


Figure 5.10: Arrangement of samples and bender elements for measurements of shear wave velocities in different planes

5.4.2 Overview of tests performed

Firstly, the examination of the bender element system was carried out. This involved performing a series of bender elements tests on an unconfined specimen. The sample from the Tiller-Flotten Test Site with the dimensions: diameter 54 mm, height 100 mm, obtained with the use of piston sampling was used. The depth in which this sample was taken was noted. The aim of these preliminary measurements was to: evaluate the accuracy of the bender elements system, provide the information about the possible frequency and amplitude range, and to provide the basis for the procedure followed in the main testing in the triaxial apparatus. The soil specimen during the tests is shown in Figure 5.11.



Figure 5.11: Preliminary bender element tests on the unconfined specimen

The main bender elements tests were carried out on mini-block samples. Four samples were investigated, each of them from different depth from 9,75 m to 19,7 m below ground level. Index testing was carried out on three of the samples. The pore pressure distribution shown in section 4.3.2 was not known in the beginning of the study. The in-situ effective stresses were calculated assuming ground water at 1,5 m below ground level with hydrostatic pore pressure distribution. Since the pore pressure distribution present in-situ is below hydrostatic, the in-situ effective stresses were underestimated. Therefore, the used notations σ_{v0}' , σ_{h0}' represent the calculated stresses which are not actual in-situ stresses. The coefficient of earth pressure at rest, K_0 of 0,6 for sample 1 and of 0,7 for the other three samples was used. Unit weight was assumed according to bulk density from cylinder as index tests results were not available at the start of the consolidation. The consolidation was ended after the end of primary consolidation for the first block sample, whereas the next three samples were consolidated for 24 hours. Additional consolidation time was applied to specimen 3vh2. In Table 5.1, the tests carried out in this study are listed with their test conditions.

5.4 BENDER ELEMENTS TESTING

Table 5.1: Summary of performed bender element tests

Specimen no.	Depth	Sampling date	Index testing	Shear wave velocity	Ground water level	Unit weight γ	σ_{v0}'	K_0	σ_{h0}' =effective confining pressure	consolidation time
-	m	-	-	-	m	kN/m ³	kPa	-	kPa	h
1vh	9,75-10,10	2.11.2017	no	vh	-1,5	18	93,9	0,6	56,4	3 h 46 mins
1hv				hv			95,3		57,2	3 h 42 mins
2vh	10,8-11,05	7.11.2017	yes	vh		18,5	107,2	0,7	75	24 h
2hv				hv						
3vh1	12,8-13,15	8.11.2017	yes	vh		18,5	125,1	0,7	87,6	77 h
3vh2				vh						
3hv				hv						
3hh				hh						
4vh	19,45-19,7	10.11.2017	yes	vh		19	192,8	0,7	134,9	24 h
4hv				hv						
4hh				hh						

Chapter 6

Overview of results

This section presents the summary of the test results. Detailed discussion of the results is included in Chapter 7.

6.1 Index testing results

Index testing results are summarised in Table 6.1. Grain size distribution curves are presented in Appendix C.

Table 6.1: Index testing results

Specimen no	-	2	3	4
Depth	m	10,80-11,05	12,80-13,15	19,45-19,70
Density, ρ	g/cm^3	1,82	1,82	1,85
Density of solids, ρ_s	g/cm^3	2,93	2,76	2,87
Water content, w	%	43,4	43,1	36,6
Degree of saturation, S_r	-	0,97	1,00	0,94
Porosity, n	%	56,6	53,8	52,8
Void ratio, e	-	1,30	1,20	1,12
Liquid limit, w_L	%	30,0	32,0	28,2
Plastic limit, w_P	%	22,5	24	23,8
Plasticity index, I_P	%	7,5	8,0	4,4
Liquidity index, I_L	-	2,8	2,4	3,1
Salinity, S	g/l	1,8	1,5	1,8
Undrained shear strength, s_u	kPa	46,9	41,5	58,4
Remoulded shear strength, s_r	kPa	0,8	1,1	3,0
Sensitivity, S_t	-	57,4	39,2	19,2

6.2 Bender elements testing results

6.2.1 Preliminary testing on the unconfined specimen

Figure 6.1 shows measured input and output signals obtained in preliminary bender element tests on unconfined specimen. The input signal was generated with different input frequencies from 0,5 kHz to 5 kHz.

6.2 BENDER ELEMENTS TESTING RESULTS

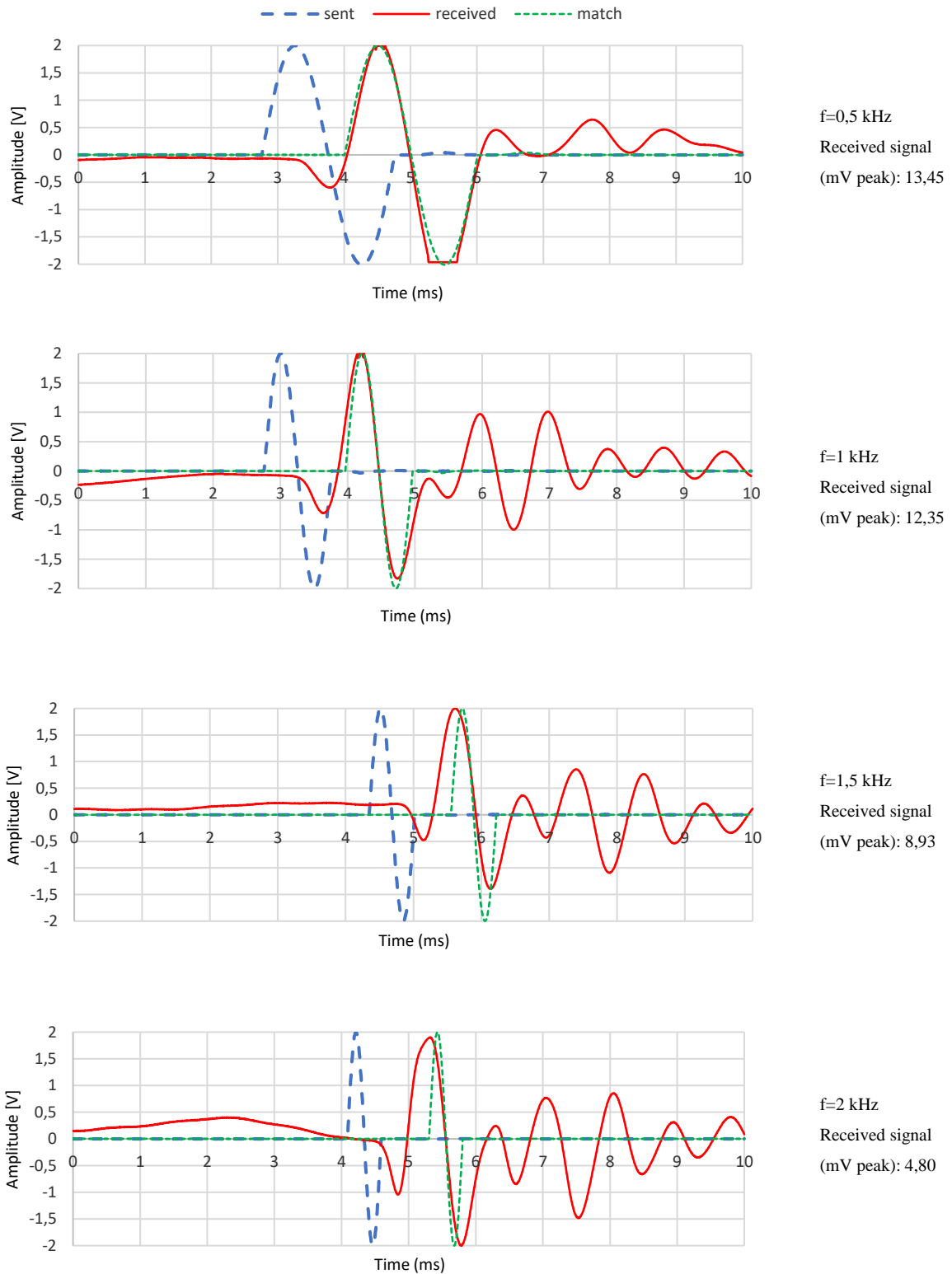
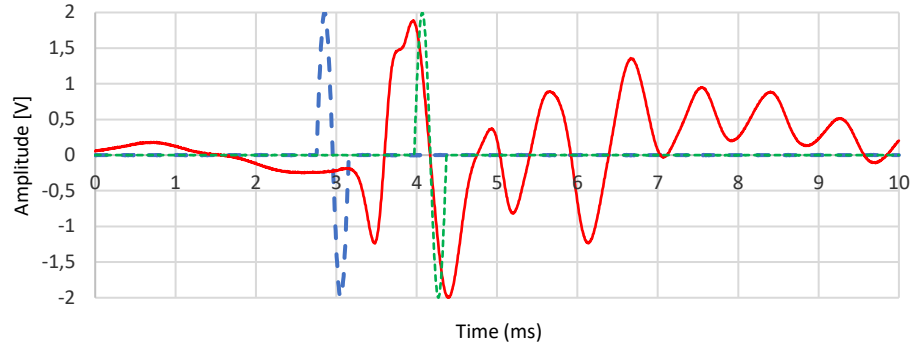
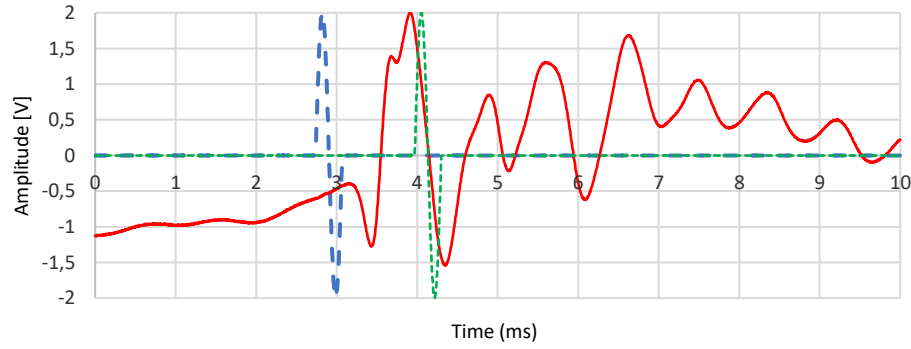


Figure 6.1: Effects of input signal frequency on output signals for the preliminary tests on unconfined specimen

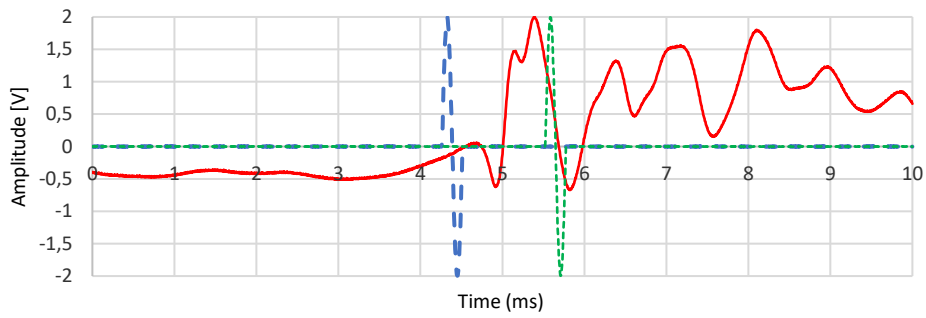
6.2 BENDER ELEMENTS TESTING RESULTS



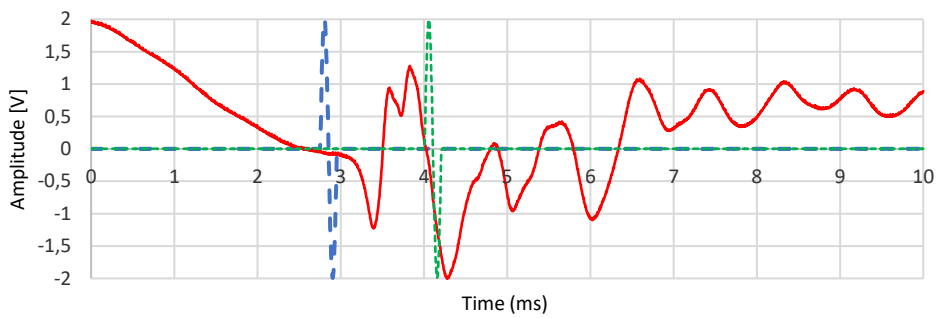
f=2,5 kHz
Received signal
(mV peak): 3,31



f=3 kHz
Received signal
(mV peak): 2,58



f=4 kHz
Received signal
(mV peak): 2,12



f=5 kHz
Received signal
(mV peak): 1,28

Figure 6.1 (Continued.)

6.2.2 Main tests

The data from bender element tests was exported to Microsoft Excel. The axial deformation recorded during the consolidation allowed for the correction of the height of the sample and thus the calculation of the changing travel distance of the wave. The shear wave velocity was calculated using equation 6.1.

$$V_s = \frac{L_{tt,0} - \delta}{t} \left(\frac{m}{s} \right) \quad (6.1)$$

where $L_{tt,0} = 95$ is the initial tip-to-tip distance between bender elements (mm), δ is axial deformation during consolidation (mm) and t is bender delay (ms).

The small strain shear moduli were calculated using measured propagation velocities:

$$G_{vh} = \rho \cdot V_{vh}^2; \quad G_{hv} = \rho \cdot V_{hv}^2; \quad G_{hh} = \rho \cdot V_{hh}^2 \quad (MPa) \quad (6.2)$$

Where ρ is the bulk density from the index testing (g/cm^3). Since for specimen 1 the index testing was not performed, the bulk density $\rho = 1,82 g/cm^3$ for calculation of G_{max} was assumed.

Table 6.2 summarises obtained shear wave velocity values and calculated small strain shear moduli for 3 stages:

- Unconfined specimen,
- At the end of primary consolidation (EOPC),
- After 24 hours from the beginning of consolidation.

The bender element tests data with the triaxial data for each specimen is presented in Table 6.3. Full results from triaxial and bender elements tests are included in Appendix D. The results obtained during bender elements testing are plotted against time and presented in Figures 6.2-6.5. For each depth and each sample orientation the plotted values are:

- Expelled water (cm^3),
- Shear wave velocity (m/s),
- Frequency (kHz).

Table 6.2: Summary of V_s and G_{max} values obtained in bender element testing

No	Depth (m)	V_s	V_s (m/s)			G_{max} (MPa)		
			Unconfined	EOPC*	After 24 h consolidation	Unconfined	EOPC*	After 24 h consolidation
1vh 1hv	9,75-10,10	vh	67	95	-	8,2	16,4	-
		hv	71	97,2	-	9,2	17,2	-
2vh 2hv	10,80-11,05	vh	61	101	107,6	6,8	18,6	21,1
		hv	63	105,6	109,9	7,2	20,3	22,0
3vh1 3vh2 3hv 3hh	12,80-13,15	vh1	66	114,2	120,7	7,9	23,7	26,5
		vh2	63	114,5	118,0 (121,8)	7,2	23,9	25,3 (27)
		hv	66	115,5	119,8	7,9	24,3	26,1
		hh	67	136,2	142,5	8,2	33,8	37,0
4vh 4hv 4hh	19,45-19,70	vh	68	139,6	146	8,6	36,1	39,4
		hv	67	152	157	8,3	42,7	45,6
		hh	74	181	188,2	10,1	60,6	65,5

*EOPC: end of primary consolidation
() – value after 77 h consolidation

6.2 BENDER ELEMENTS TESTING RESULTS

Table 6.3: Bender element testing results

Depth m	V _s	Cons. stage	Time, t		Deformation mm	Expelled water ml	Axial strain, ε _a %	Volumetric strain, ε _{vol} %	Frequency, f kHz	Bender delay ms	Effective height, d mm	Shear wave velocity, V _s m/s	G _{max} MPa	λ=v/f mm	d/λ
			min	h											
9,75-10,1	vh	unconfined	0	0	-	-	-	-	1.0	1,418	95,00	67,0	8,2	67,00	1,42
		EOPC	-	-	-	-	-	-	-	-	-	-	-	-	-
	after 3,78 h	227	3,78	-	-	-	-	-	2,0	0,990	93,87	94,8	16,4	47,41	1,98
	unconfined	0	0	-	-	-	-	-	0,8	1,338	95,00	71,0	9,2	88,75	1,07
hv	vh	EOPC	94	1,56	1,164	3,13	1,164	1,37	1,8	0,965	93,84	97,2	17,2	54,02	1,74
		after 3,71 h	222	3,71	1,170	3,09	1,170	1,35	2,0	0,945	93,83	99,3	17,9	49,65	1,89
	unconfined	0	0	-	-	-	-	-	0,7	1,557	95,00	61,0	6,8	87,14	1,09
	EOPC	104	1,74	1,331	4,18	1,331	1,83	1,8	0,927	93,67	101,0	18,6	56,11	1,67	
10,8-11,05	vh	after 24 h	1440	24	1,412	4,21	1,412	1,84	2,0	0,870	93,59	107,6	21,1	53,79	1,74
		unconfined	0	0	-	-	-	-	0,9	1,508	95,00	63,0	7,2	70,00	1,36
	EOPC	158	2,63	1,524	4,98	1,524	2,17	2,0	0,885	93,48	105,6	20,3	52,81	1,77	
	after 24 h	1440	24	1,567	5,34	1,567	2,33	2,0	0,850	93,43	109,9	22,0	54,96	1,70	
12,8-13,15	vh1	unconfined	0	0	-	-	-	-	0,8	1,439	95,00	66,0	7,9	82,50	1,15
		EOPC	109	1,82	0,799	4,51	0,799	1,97	1,8	0,825	94,20	114,2	23,7	63,44	1,49
	after 24 h	1440	24	0,866	4,77	0,866	2,08	2,0	0,780	94,13	120,7	26,5	60,34	1,56	
	unconfined	0	0	-	-	-	-	-	0,7	1,508	95,00	63,0	7,2	90,00	1,06
19,45-19,7	vh2	EOPC	228	3,8	1,135	4,89	1,135	2,13	2,0	0,820	93,87	114,5	23,8	57,23	1,64
		after 24 h	1440	24	1,168	5,358	1,168	2,34	2,0	0,795	93,83	118,0	25,4	59,01	1,59
	unconfined	0	0	-	-	-	-	-	0,7	1,439	95,00	66,0	7,9	94,29	1,01
	EOPC	258	4,31	0,314	4,90	0,314	2,14	2,14	1,8	0,820	94,69	115,5	24,3	64,15	1,48
hh	hv	after 24 h	1440	24	0,336	6,13	0,336	2,67	2,0	0,790	94,66	119,8	26,1	59,91	1,58
		unconfined	0	0	-	-	-	-	0,7	1,418	95,00	67,0	8,2	95,71	0,99
	EOPC	92	1,53	3,773	5,06	3,773	2,21	2,21	2,8	0,670	91,23	136,2	33,7	48,63	1,88
	after 24 h	1440	24	3,797	7,60	3,797	3,32	3,0	0,640	91,20	142,5	37,0	47,50	1,92	
hh	vh	unconfined	0	0	-	-	-	-	0,7	1,397	95,00	68,0	8,6	97,14	0,98
		EOPC	91	1,52	2,177	4,19	2,177	1,83	1,83	1,8	0,665	92,82	139,6	36,0	77,55
	after 24 h	1440	24	2,262	4,24	2,262	1,85	2,2	0,635	92,74	146,0	39,5	66,38	1,40	
	unconfined	0	0	-	-	-	-	-	0,6	1,418	95,00	67,0	8,3	111,67	0,85
hh	hv	EOPC	211	3,51	0,786	4,58	0,786	2,00	2,2	0,620	94,21	152,0	42,7	69,07	1,36
		after 24 h	1440	24	0,780	6,40	0,780	2,80	2,2	0,600	94,22	157,0	45,6	71,38	1,32
	unconfined	0	0	-	-	-	-	-	0,7	1,284	95,00	74,0	10,1	105,71	0,90
	EOPC	162	2,70	1,774	4,56	1,774	1,99	1,99	2,5	0,515	93,23	181,0	60,6	72,41	1,29
hh	hh	after 24 h	1440	24	1,824	5,65	1,824	2,47	2,5	0,495	93,18	188,2	65,5	75,29	1,24
		unconfined	0	0	-	-	-	-	-	-	-	-	-	-	-

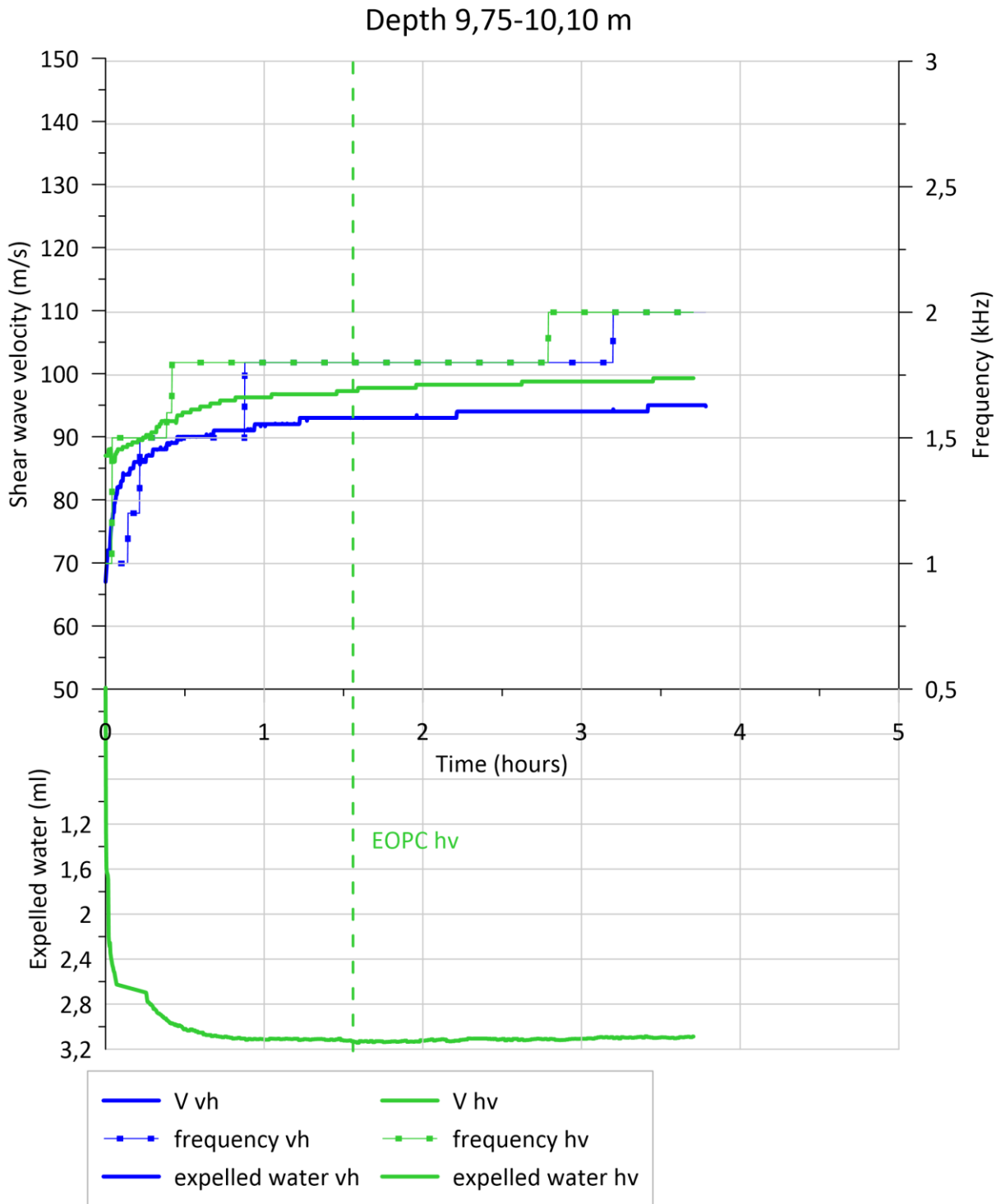


Figure 6.2: Shear wave velocity, frequency, expelled water data during consolidation for samples at 9,75-10,10 m depth

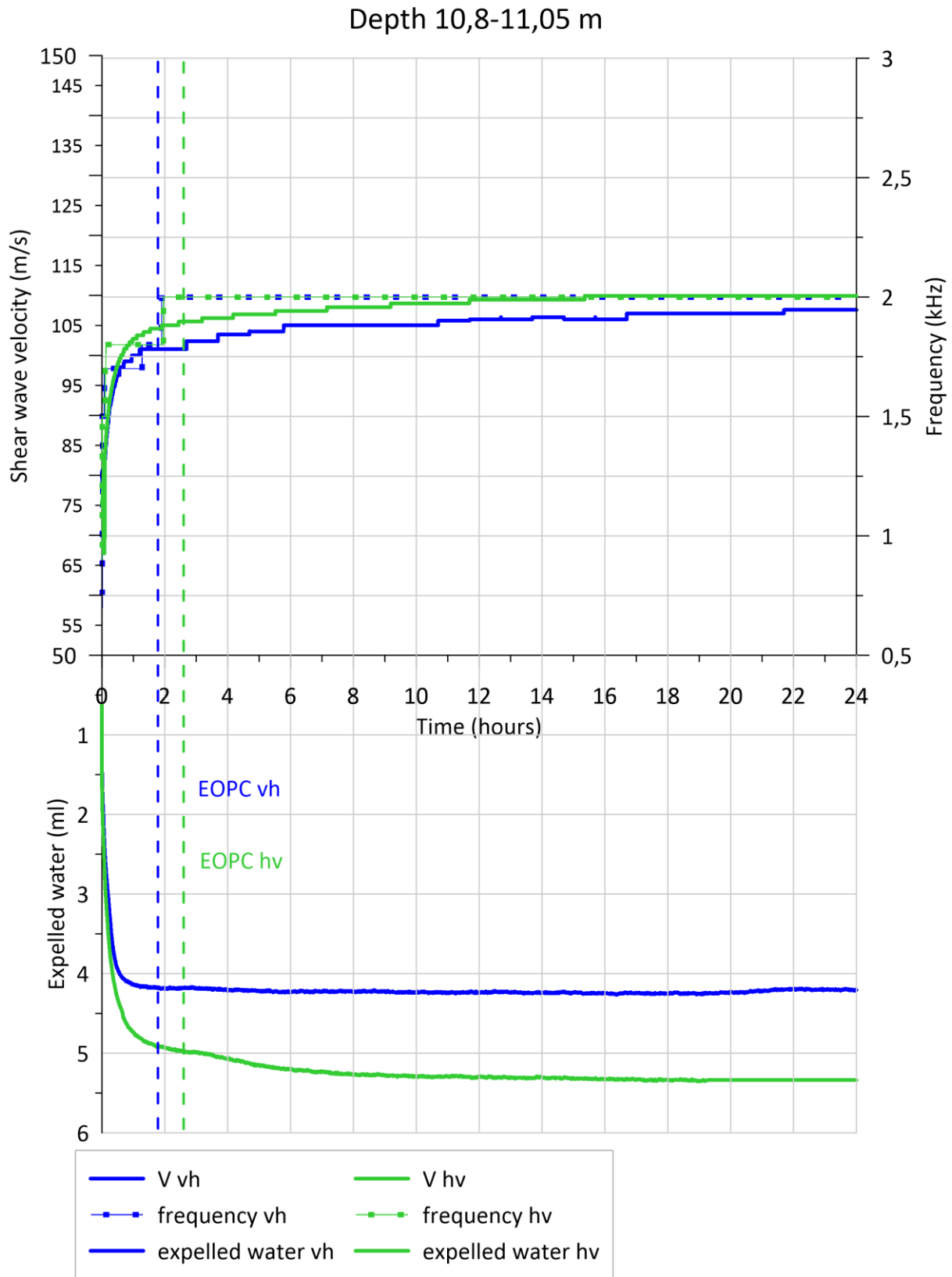


Figure 6.3: Shear wave velocity, frequency, expelled water data during consolidation for samples at 10,80-11,05 m depth

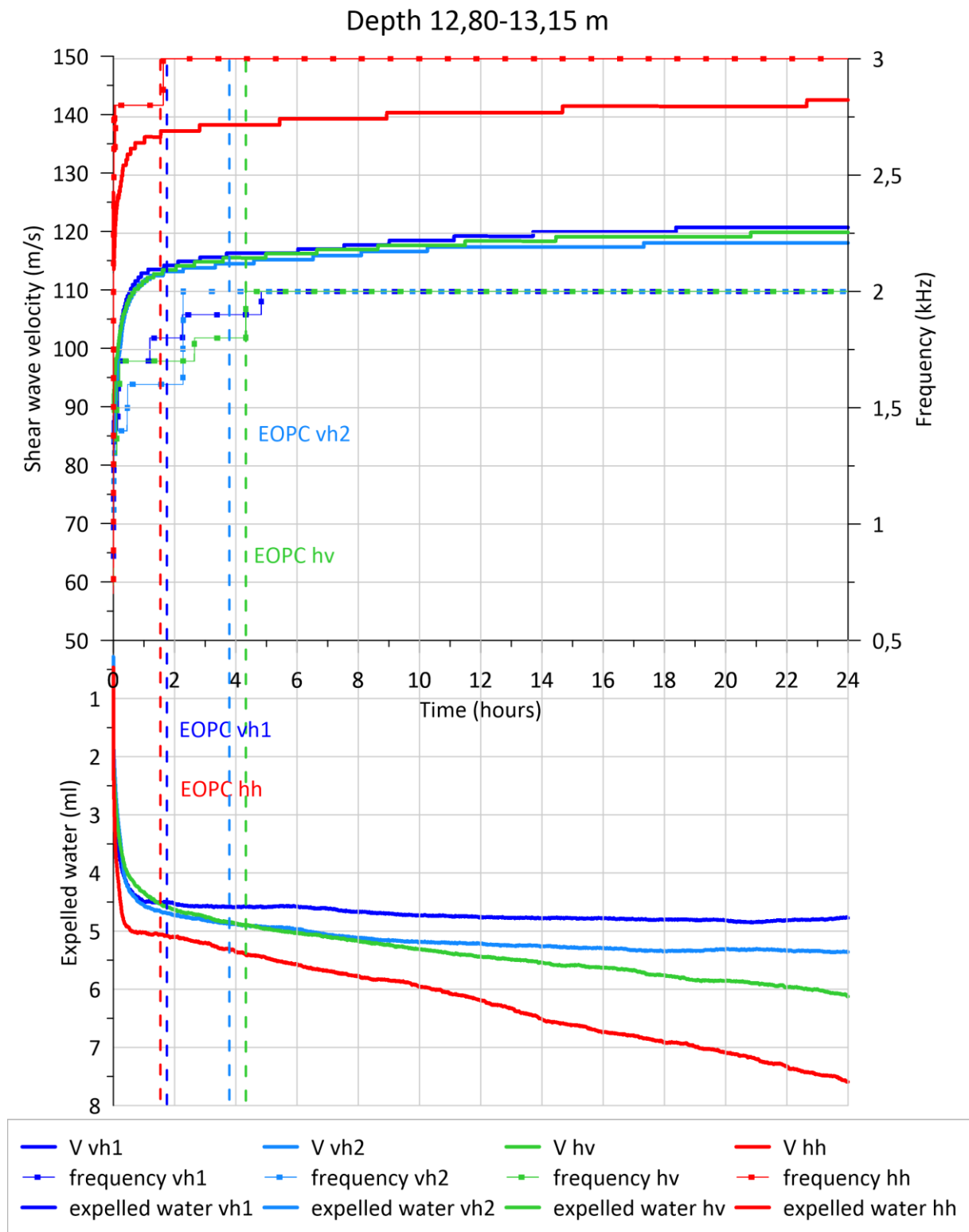


Figure 6.4: Shear wave velocity, frequency, expelled water data during consolidation for samples at 12,80-13,15 m depth

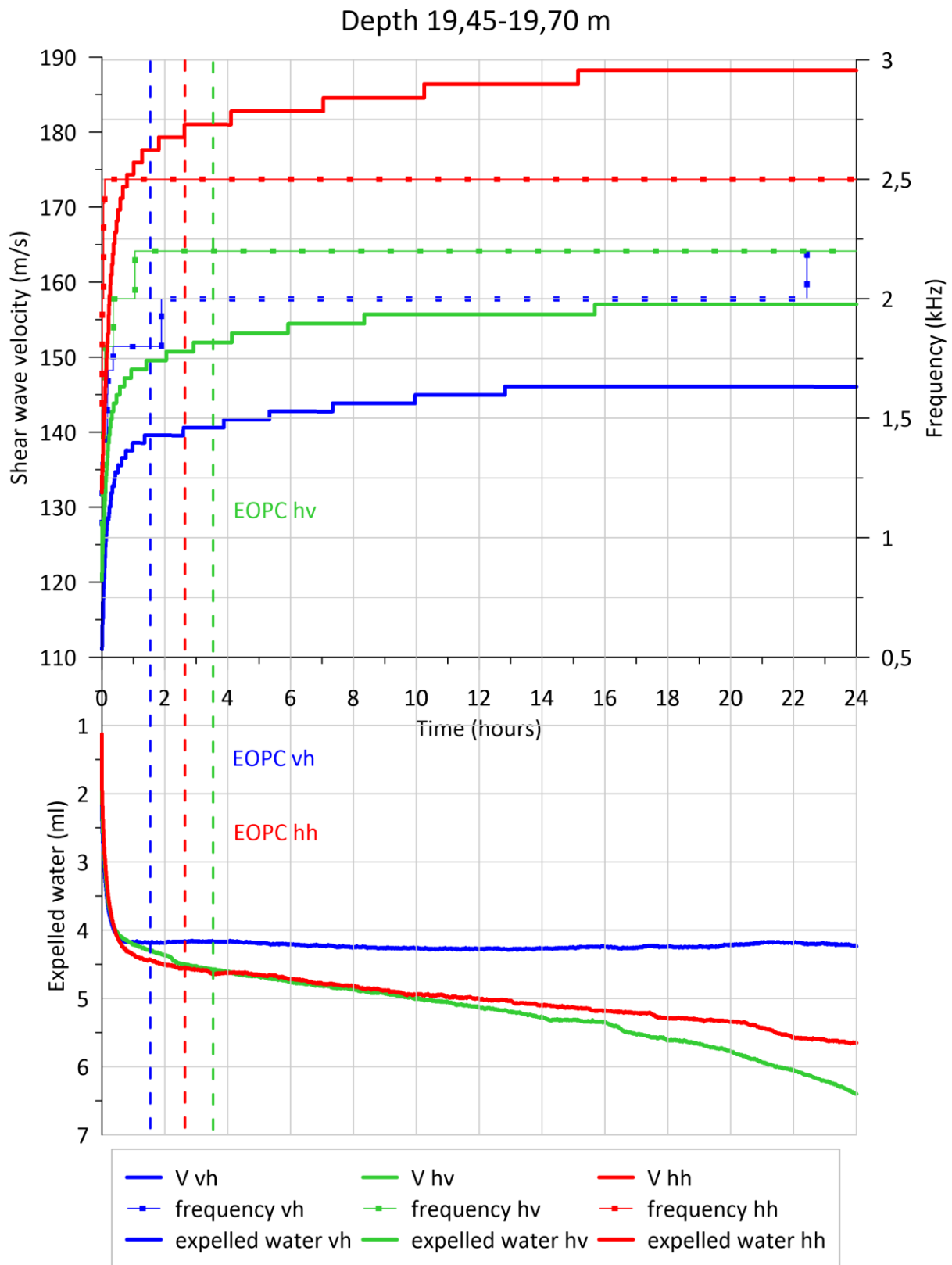


Figure 6.5: Shear wave velocity, frequency, expelled water data during consolidation for samples at 19,45-19,70 m depth

6.2 BENDER ELEMENTS TESTING RESULTS

Figures 6.6 and 6.7 plot the shear wave velocity and small strain shear modulus values against depth. In Figure 6.8 variation of G_{max} during consolidation is presented.

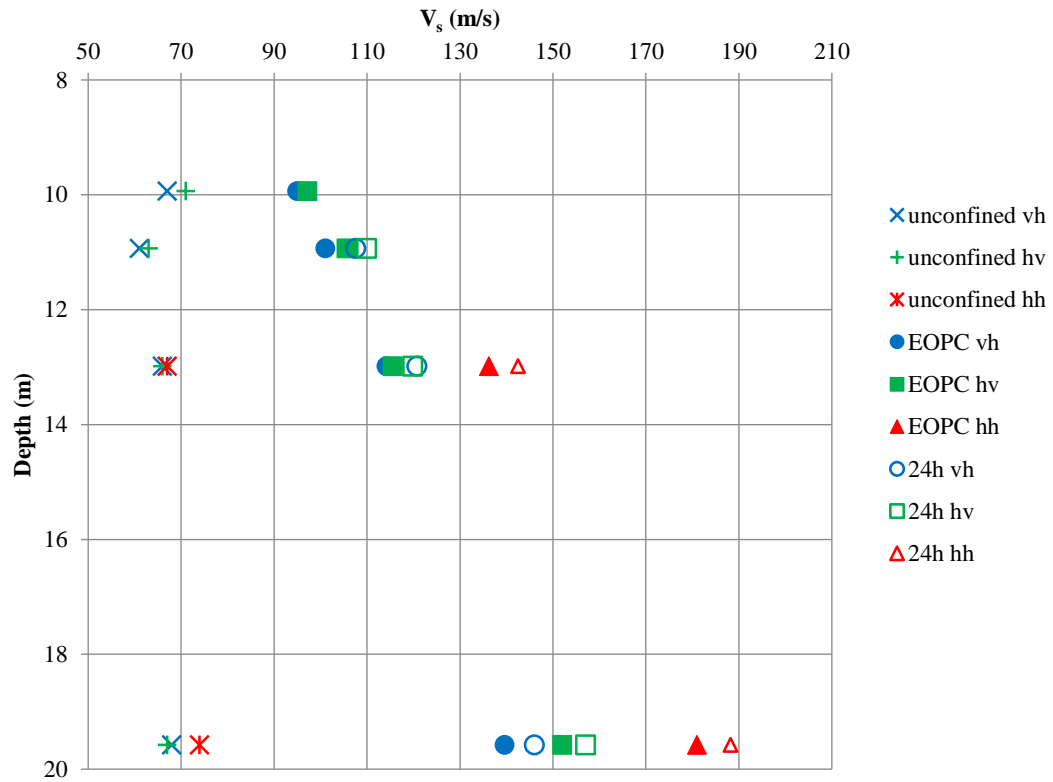


Figure 6.6: Shear wave velocity (V_s) with depth

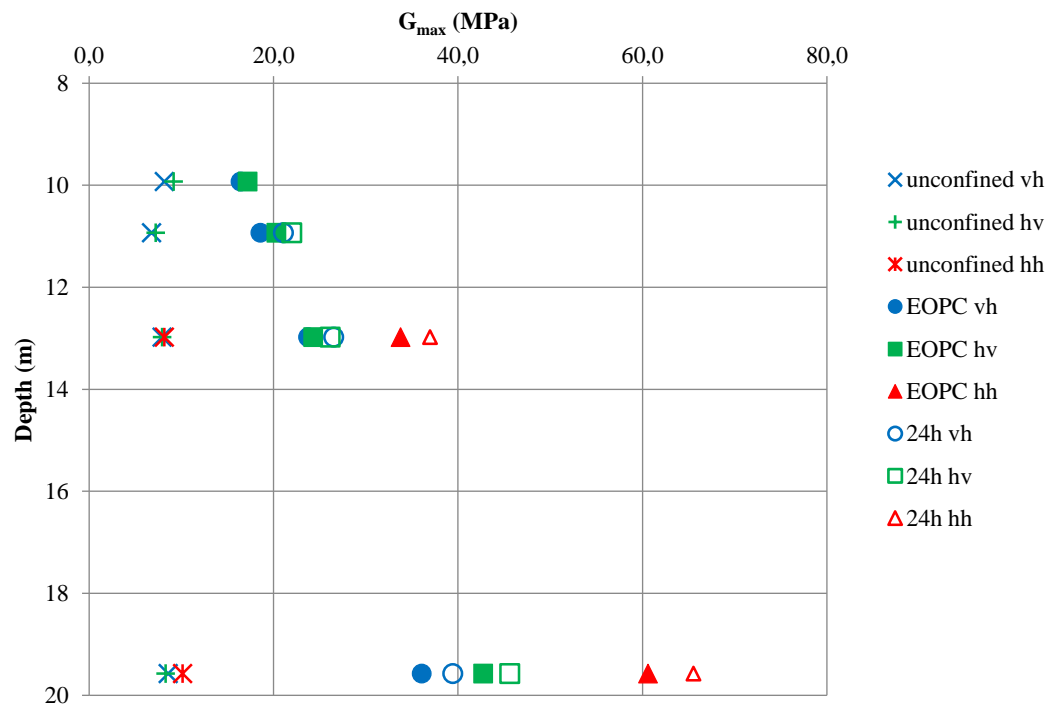


Figure 6.7: Small strain shear modulus (G_{max}) with depth

6.2 BENDER ELEMENTS TESTING RESULTS

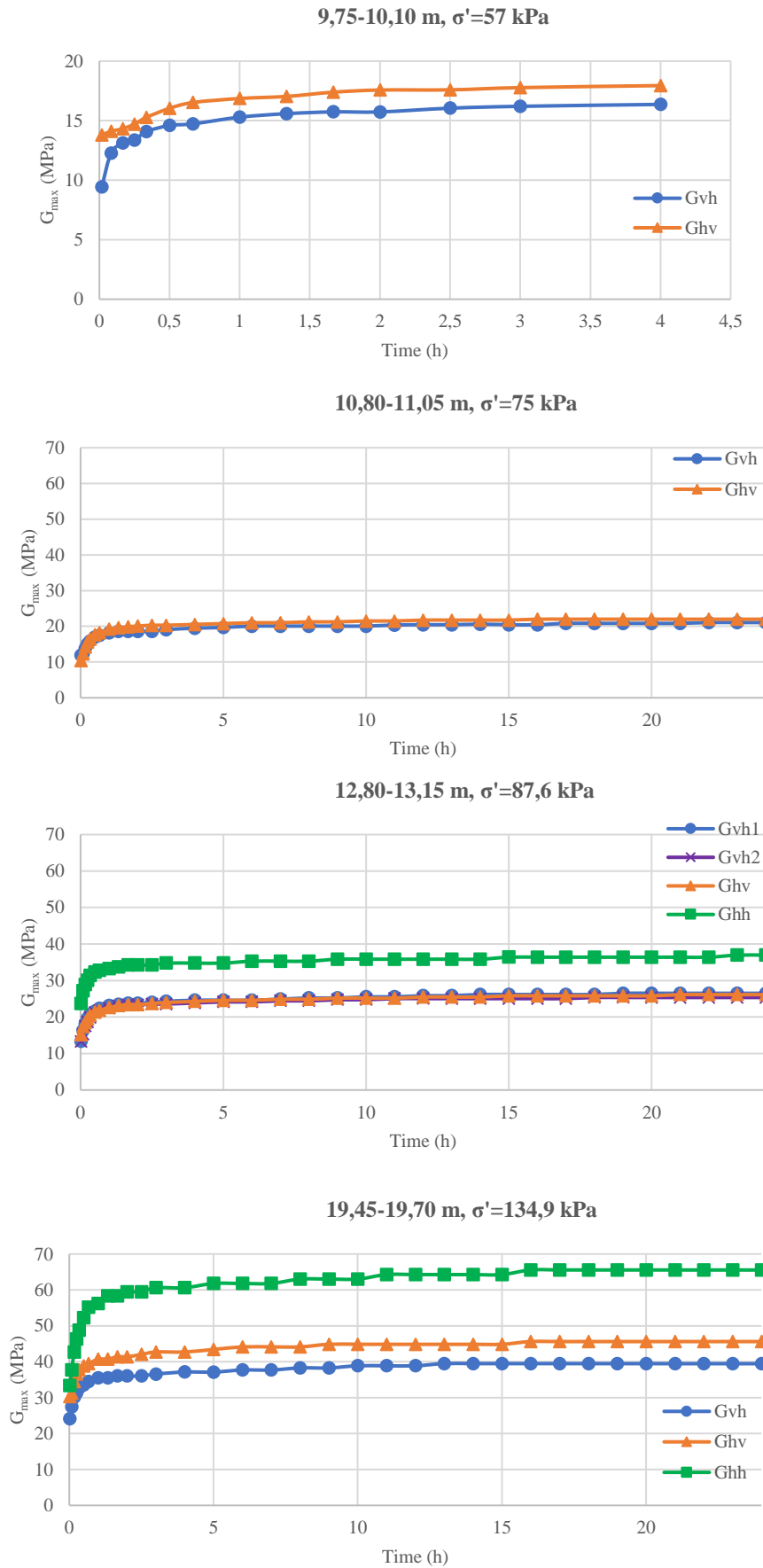


Figure 6.8: Variations in G_{max} with time of consolidation

6.3 Sample quality

Table 6.4 summarises sample quality assessment. Sample quality was determined at the end of primary consolidation. The classifications, based on both volumetric strain and the change in void ratio, were considered. OCR of 2 was assumed for sample 1, and 1,5-2 for samples 2, 3 and 4. The measurements on unconfined samples were not performed immediately after extracting the samples from the ground and thus, the classification using shear wave velocity could not be taken into consideration. Based on the volumetric strain, the quality of every sample was evaluated as being acceptable. With considerations to the change in void ratio, the samples were classified as being between good to fair, and very good to excellent.

Table 6.4: Sample quality assessment

Depth m	Shear wave velocity	ε_{vol} %	Quality	$\Delta e/e_0$	Quality
9,75-10,10	vh	-	-	-	-
	hv	1,37	acceptable	-	-
10,80-11,05	vh	1,83	acceptable	0,032	very good to excellent
	hv	2,18	acceptable	0,038	very good to excellent
12,80-13,15	vh1	1,97	acceptable	0,035	very good to excellent
	vh2	2,13	acceptable	0,039	very good to excellent
	hv	2,14	acceptable	0,039	very good to excellent
	hh	2,21	acceptable	0,043	good to fair
19,45-19,70	vh	1,83	acceptable	0,032	very good to excellent
	hv	2,00	acceptable	0,033	very good to excellent
	hh	1,99	acceptable	0,032	very good to excellent

Chapter 7

Discussion

In this section the experimental findings from the bender elements tests are discussed. The analysis of obtained waveforms in bender elements testing is carried out. The performance of bender elements system is assessed and the near-field effect is examined. The changes in shear wave velocity and small strain shear stiffness with time of consolidation are analyzed. The interpretation of results in terms of stiffness anisotropy is performed. Shear wave velocity and small strain shear modulus results obtained in the laboratory investigations are compared to in-situ measured values.

7.1 Waveform analysis

7.1.1 Preliminary testing

The test results show that the bender element system is capable of transmitting the waves in low frequency ranges. Above frequency of 5 kHz, the signal could not be detected. In the frequency range 0,5-1 kHz the received signal was the least distorted and was of frequency similar to the frequency of the input signal. When the input frequency was higher than 1,5 kHz, the frequency of the received signal significantly differed from the frequency of the input signal. According to Rio (2006) when excited by a pulse signal, the transmitter bender element cannot vibrate at frequencies higher than its own natural frequency. The maximum frequency of the received signal which could be obtained is 1 kHz, therefore, it is inferred that the natural frequency of the bender element crystal is approximately 1 kHz.

Furthermore, the frequency changes of the input signal affected the voltage of the received signal. The maximum response of 12-13,5 mV was obtained for the frequencies 0,5-1 kHz and it decreased with increasing frequency. According to Lee and Santamarina (2005) 'the bender element response is enhanced when the frequency approaches the resonant frequency of the bender element-soil system'. Therefore, since the maximum response was found to be in the frequency range 0,5-1 kHz, it is suggested that the resonant frequency lies within this range. According to Camacho (2012), provided that the characteristic points in the output signal can be identified, the voltage of the output signal is not critical for interpretation of the waveforms.

Moreover, after the input signal was no longer acting on the transducer, all the responses were similar to each other. It was a vibration of approximately constant frequency, regardless of the frequency of the input signal. Figure 7.1 analyses the vibration of three chosen signals with frequencies 1 kHz, 2 kHz and 3 kHz. It is clear that the vibration frequency is in the range 0,8-1 kHz. In ideal case this frequency should be equal to the resonant frequency of bender elements (Rio, 2006).

7.1 WAVEFORM ANALYSIS

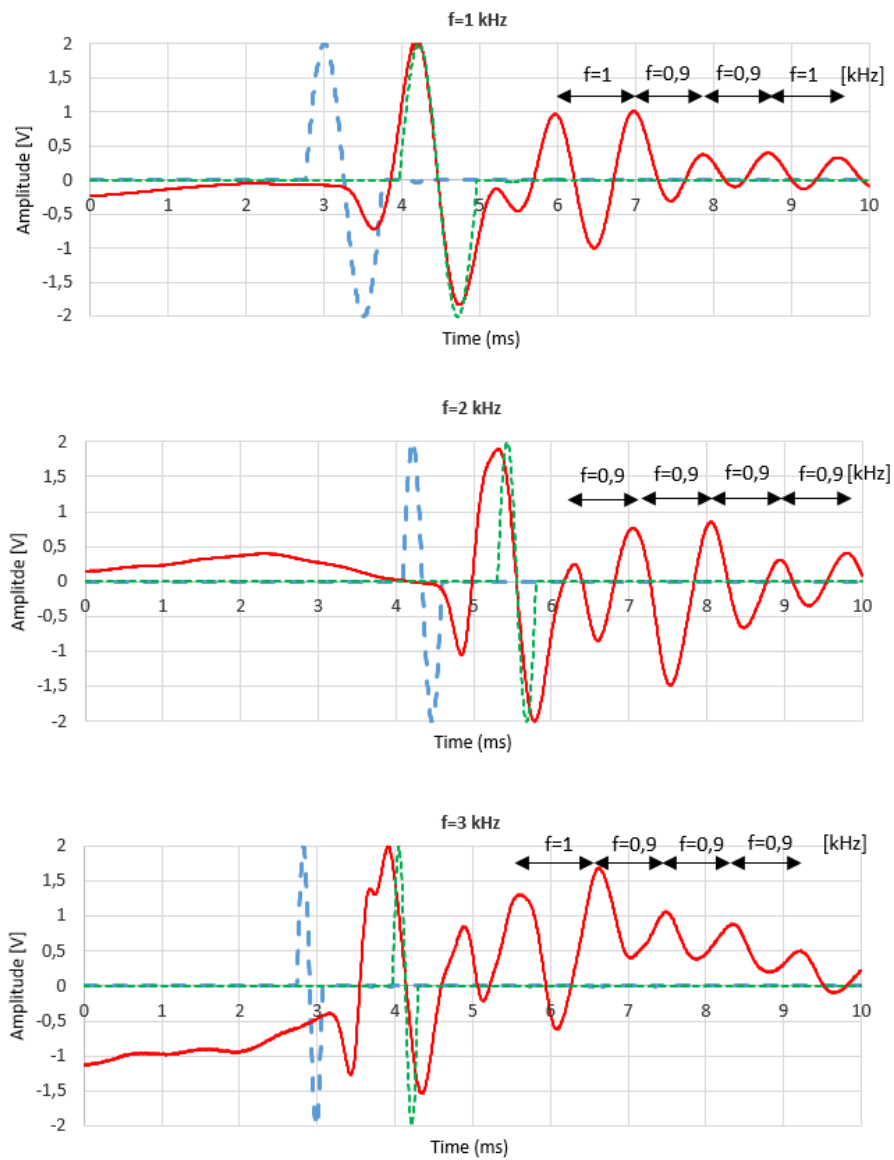


Figure 7.1: Analysis of the received signal, unconfined specimen; frequencies 1 kHz, 2 kHz, 3 kHz

7.1.2 Frequency changes

The measurements were performed with different frequencies of the input signal. The frequency differed with the consolidation pressure, time of consolidation and sample orientation.

The input signal for the measurements on unconfined samples was in the range 0,6-1 kHz. With increasing cell pressure and consolidation time the frequency of the input signal for all the samples increased to up to 3 kHz for the sample 3hh. Figure 7.2 presents an example of different input signal frequencies for the sample 3vh. For unconfined measurements the frequency of 0,8 kHz was used. After 30 minutes of consolidation under the confining pressure of 87,6 kPa the frequency of 1,7 kHz was the most suitable. After 5 hours of consolidation the frequency was increased to 2,0 kHz and this value was maintained until the end of the test.

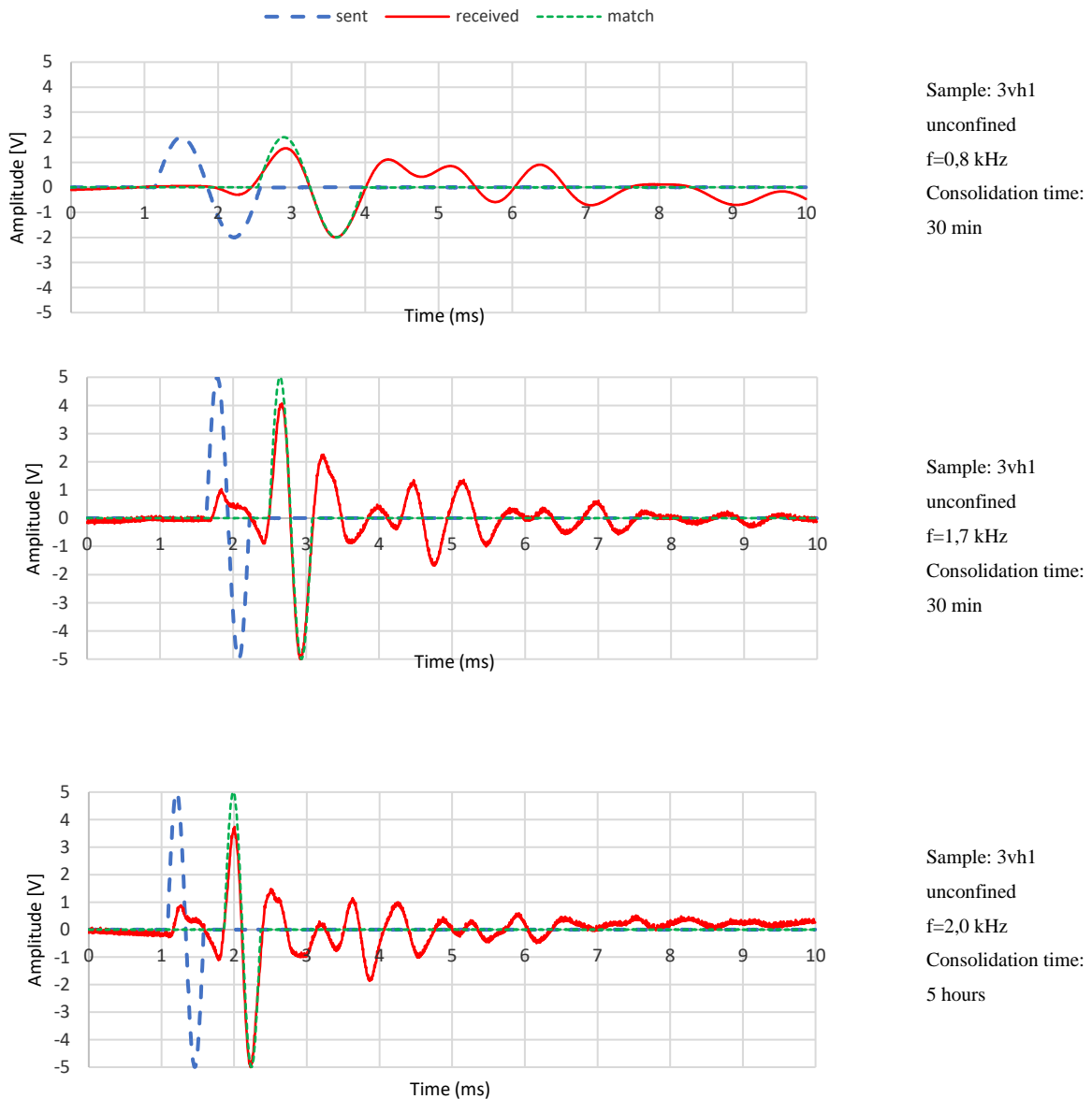


Figure 7.2: Illustration of changes in frequency of the input signal before and during consolidation for sample 3vh

7.1 WAVEFORM ANALYSIS

Figure 7.3 shows the variation in the frequency of the input signal with changing shear wave velocity including all the samples at three stages: unconfined measurement, at the end of primary consolidation and after consolidating for 24 hours. The frequency of the input signal clearly increases with increasing shear wave velocity. According to Lee and Santamarina (2005) the resonant frequency of an anchored bender element buried in a soil mass is dependent not only on bender element mechanical properties but also on the soil properties, i.e., density and stiffness. Increase of the frequency of the input signal with increasing consolidation time is therefore inferred to be the result of increasing soil stiffness represented by increasing shear wave velocity. The maximum frequency used during consolidation stage was 3 kHz.

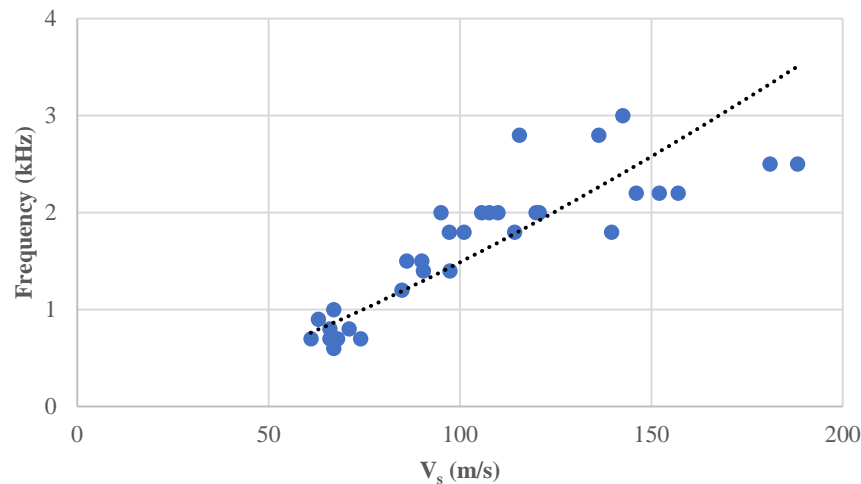


Figure 7.3: Effect of shear wave velocity on the frequency

7.1.3 Signal distortion and near-field effect

Near-field effect is known to influence the shear wave arrival determination. According to the literature, near-field effect is dependent on the ratio between the wave travel distance and the wavelength (d/λ). Additionally, it was found to be dependent on the confining pressure level (Kawaguchi et al., 2001).

The signal distortion was found to be present in all the obtained waveforms. A difference in distortion could be seen between the unconfined samples and samples subjected to the cell pressure. Figure 7.4 shows the comparison of transmitted, received and match signals for vertically cut samples subjected to different consolidation stresses. Shear wave arrival was identified with the first major positively polarized up rise of the received signal. For unconfined measurements a small negative deflection before the major positive peak can be seen for all the samples. In the case of consolidated samples however, a small positively polarized peak occurs initially. Following this, recordings indicate a negative dip, before the major positive peak. The first positive deflection occurs approximately 0,5-0,9 ms before the major positive peak and is dependent on the used frequency. The amplitude of this distortion is approximately constant for all the applied pressures. This signal distortion is believed to result from the near-field effect and the interference from the P-wave propagation. Kawaguchi et al. (2001) investigated the influence of the pressure level on the near field effect. They discovered that the near-field effect is more significant when the samples are subjected to low pressure and that it disappears with increasing pressure. However, in this study no correlation between the signal distortion and the cell pressure was found.

7.1 WAVEFORM ANALYSIS

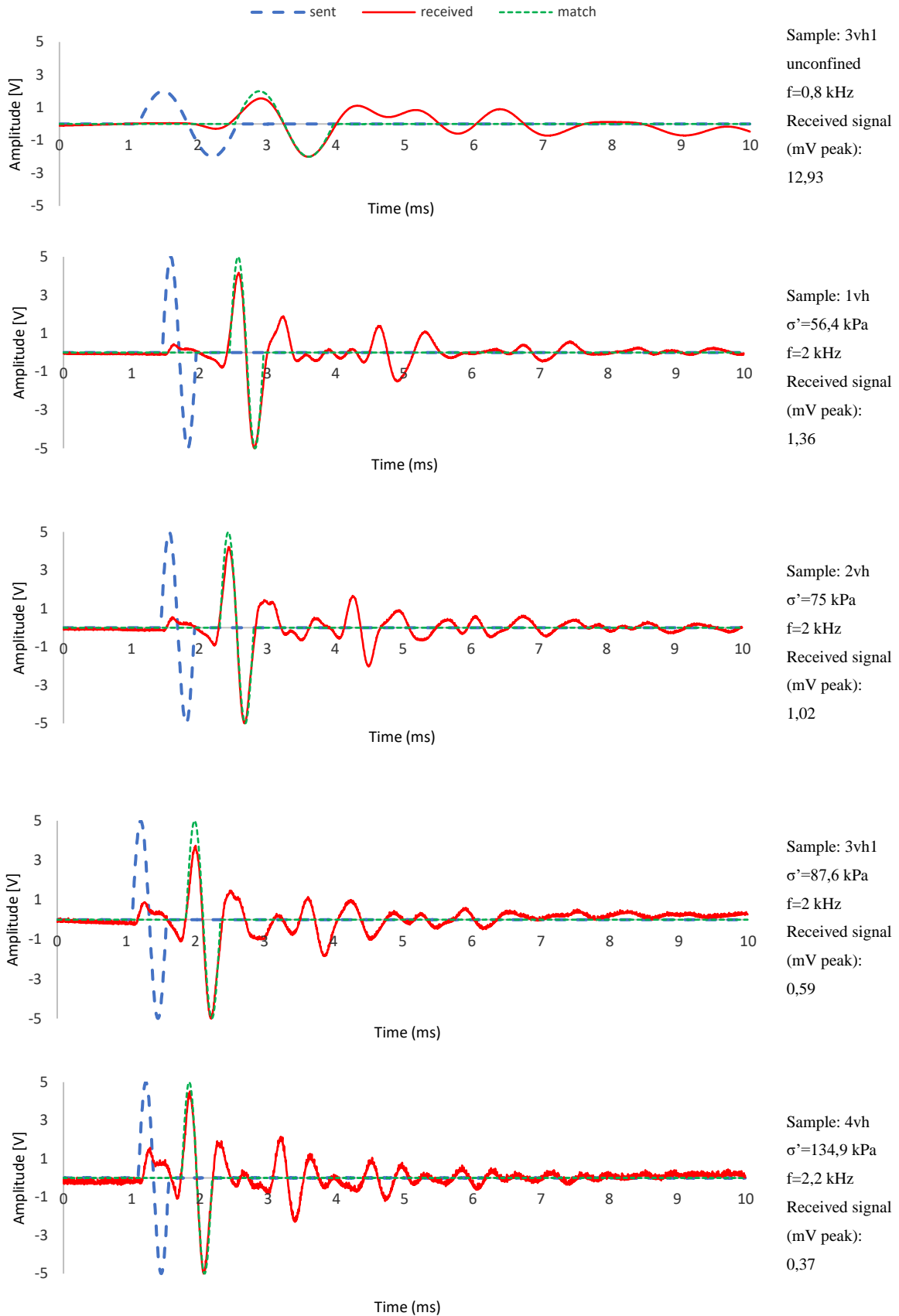


Figure 7.4: Variation in received signal for different consolidation stresses

7.1 WAVEFORM ANALYSIS

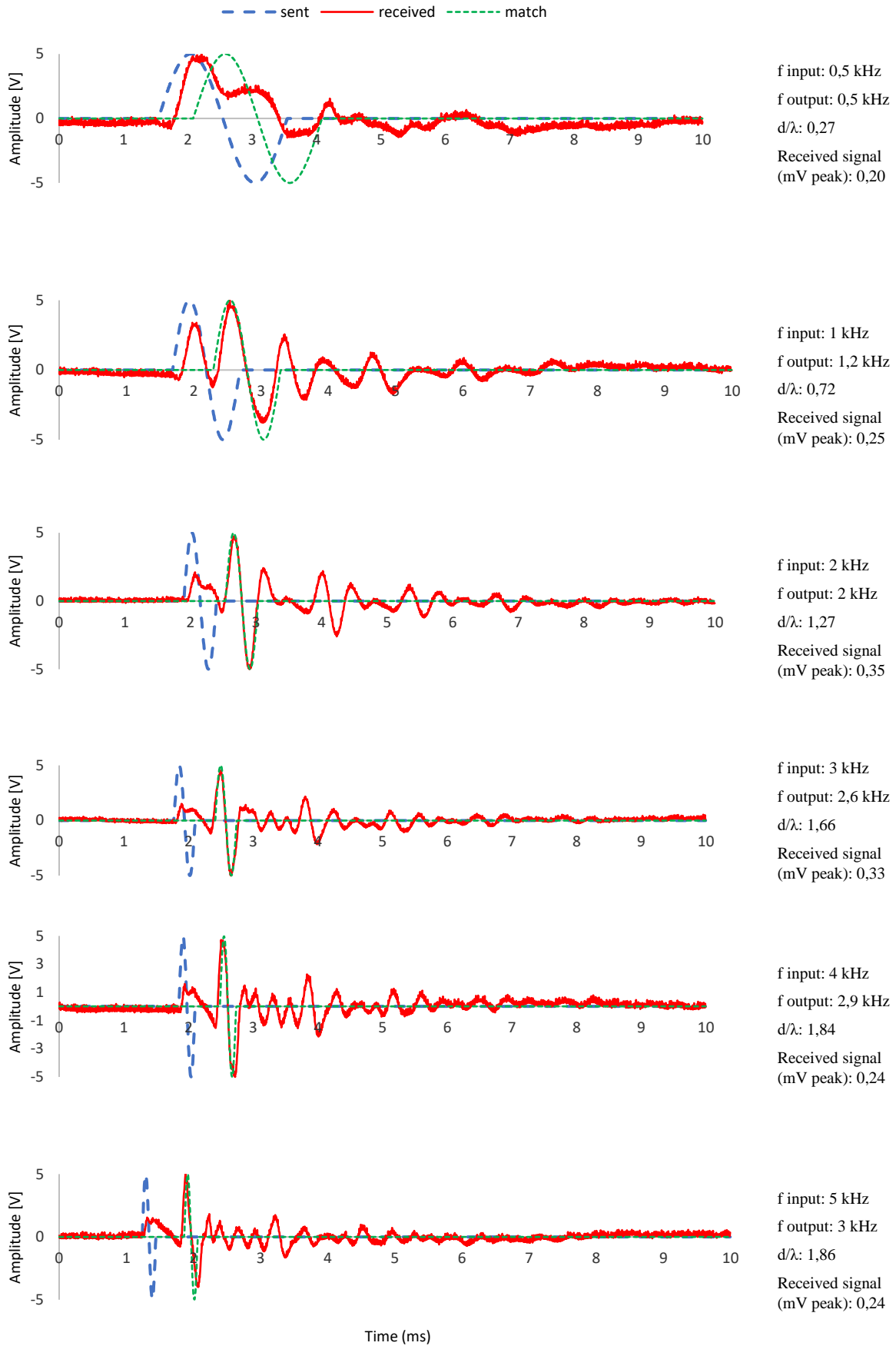


Figure 7.5: Examination of near-field effect for sample 4vh, $\sigma' = 134$ kPa

7.1 WAVEFORM ANALYSIS

To evaluate the near-field effect the ratio between the travel distance and the wavelength (d/λ) is usually used. As seen in Table 6.3, the d/λ ratio values for the unconfined samples were between 0,85-1,42. With increasing consolidation time the utilized frequency increased and in consequence the ratio d/λ increased. During consolidation the measurements were performed with d/λ between 1-2,14. The highest value of 2,14 was found for sample 3hh in the beginning of consolidation. However, after stabilization of the signal it decreased to 1,88 at the end of primary consolidation and increased again to 1,92 after 24 hours of consolidation. The average d/λ ratio for all the measurements was found to be 1,55.

To better identify the effect of frequency on near-field effect bender elements tests with excitation frequencies ranging from 0,5 kHz to 5 kHz were performed. Figure 7.5 shows the recorded waveforms. Measurements were performed on the sample 4vh after 24 hours of consolidation under the confining pressure of 134,9 kPa. The following data is listed near each of the waveforms: input excitation frequency (kHz), predominate frequency of the output signal identified with the frequency of the first cycle of the recorded signal, which is considered to be the S-wave arrival and ratio d/λ . The d/λ ratio was found to be the lowest for the frequency 0,5 kHz and was equal to 0,27. With increasing input frequency the ratio increased to up to 1,86. For d/λ lower than 1, the distortion of the received signal was significant. For frequencies 2-5 kHz, the distortion of the received signal before the first major positively polarized peak was of the pattern seen in Figure 7.4 and did not change with varying d/λ ratio.

For frequencies greater than 2 kHz, the predominant signal frequency at the receiver seems to be lower than the input signal frequency. For these cases the d/λ ratio was determined using the output frequency. According to Brignoli et al. (1996) this is the result of the energy absorbing soil behavior and the dynamic interaction soil-transducer. Rio (2006) also found that the frequency of the response was lower than the input frequency while exciting with frequencies higher than the resonant frequency. He stated that this fact is due to the transient state of vibration when applying a pulse signal. The pulse signals are not sufficient to obtain a steady-state of vibration where the response of the receiver transducer reaches the frequency of the input signal. Therefore, behaviour of the receiver bender element to the pulse signal is highly influenced by its own dynamic properties and it is the resonant frequency of the bender element-soil system which characterizes the response. Thus, in this case, the resonant frequency of the soil-transducer system illustrated with the signals in Figure 7.5 is inferred to be 2 kHz.

Figure 7.6 illustrates the relationship between the shear wave velocity and the travel distance to wavelength ratio for the waveforms presented in Figure 7.5. The shear wave velocity tends to decrease with increasing d/λ . When d/λ is between 1,0 and 1,8 the shear wave velocity values are stabilized and are approximately 140-145 m/s. Therefore, in order to obtain relevant wave travel times it is suggested that the measurements should be performed within this range of d/λ . This is consistent with the recorded waveforms presented in Figure 7.5, which show that frequencies of 2 kHz or more give the least significant near-field effect.

7.2 SHEAR WAVE VELOCITY

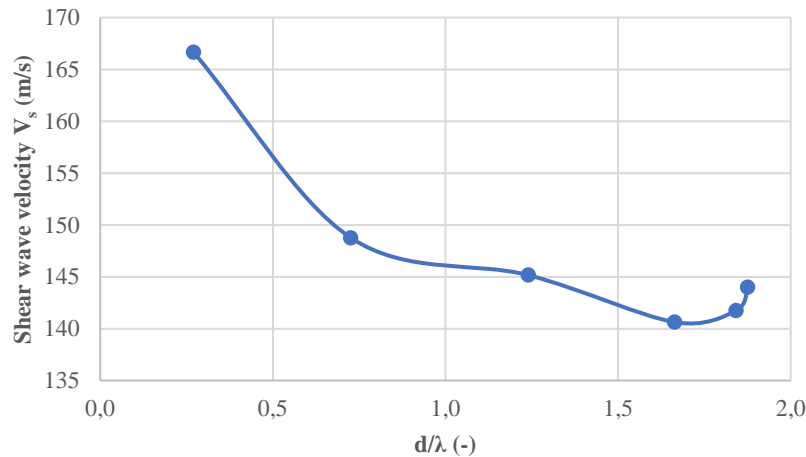


Figure 7.6: Relationship between shear wave velocity and d/λ for the tests on sample 4vh, $\sigma'_v=134$ kPa

The near-field effect can be reduced by increasing d/λ , which is increasing with the excitation frequency. However, as was also seen during the measurements on unconfined samples, the system is not capable of generating the signal with frequency greater than 5 kHz. Therefore, d/λ cannot be increased to the value sufficient to reduce the near-field effect. It is inferred that since the maximum frequency is 5 kHz, the elimination of the dispersion from the received pulse signal is not possible to achieve. However, the measurements with excitation frequencies equal to the resonant frequency of the transducer-soil system are deemed appropriate. The resulting d/λ ratio greater than unity is believed to give results of sufficient reliability.

7.2 Shear wave velocity

7.2.1 Shear wave velocity with depth

Measured shear wave velocities were plotted with depth and presented in Figure 6.6. No visible pattern was found for the shear wave velocities on unconfined samples. The values are rather constant with depth. V_s on samples subjected to the confining stress visibly tend to increase with depth of the sample. As inferred from the results, this trend is approximately linear and it is valid for all three shear wave velocities separately: v_h , v_v and h_h . Comparison of laboratory determined shear wave velocities with the in-situ measured ones is performed in section 7.3.4.

7.2.2 Shear wave velocity with time of consolidation

As seen in Table 6.2 for unconfined samples shear wave velocity is between 60-75 m/s. After applying confining pressure, V_s significantly increased. The greatest increase can be seen during primary consolidation. At the end of primary consolidation V_s increased to 91-181 m/s, dependent on the depth of the sample. The primary consolidation ceased after 1,5-5 hours from the start of consolidation. Although the primary consolidation was completed, V_s kept gradually increasing with time. After 24 hours of isotropic confining pressure V_s values are 3-7% greater than V_s at the end of primary consolidation. Towhata (2008) suggested that this increase is the effect of the aging process connected with rearrangement of clay particles during time, leading to stronger bonding between the particles and greater shear rigidity of the clay.

7.3 Small strain shear modulus

7.3.1 Effect of effective stress on shear modulus

Figure 7.7 plots the shear modulus calculated for the end of the primary consolidation versus the average confining pressure. A clear dependency of G_{\max} on the effective stress can be seen. Shear moduli in vertical and horizontal directions increase with increase of the consolidation stress. Additionally, anisotropy tends to increase with average effective confining stress.

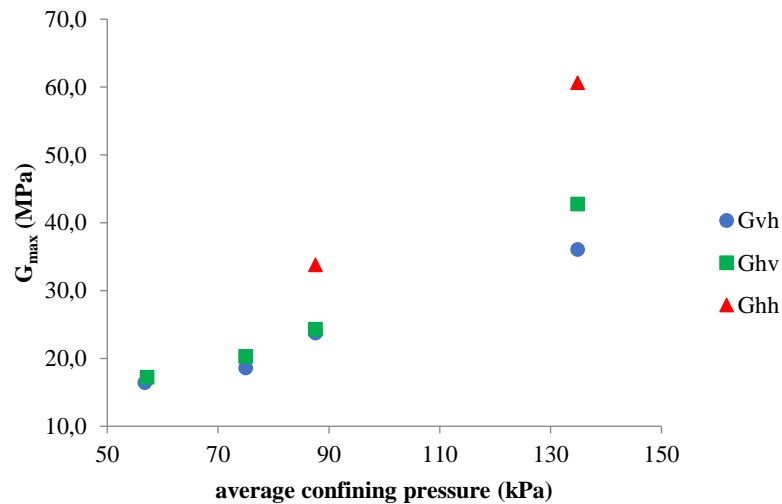


Figure 7.7: Shear modulus versus average effective confining pressure

7.3.2 Development of G_{\max} with consolidation time

The values of G_{\max} for unconfined samples are between 8-10 MPa and do not differ significantly with depth. Clear increase of shear modulus with time of consolidation was found (Figure 6.8). The samples 2, 3 and 4 were subjected to the confining pressure for 24 hours. To assess the effect of longer secondary compression, sample 3vh2 was consolidated for 77 hours.

In order to evaluate the long-term effect of confining pressure on the small strain shear modulus the variation in G_{\max} was plotted as a function of the logarithm of time (Figures 7.8 to 7.11). As shown in graphs below, during the initial phase of primary consolidation shear modulus is either constant or increases slightly linearly. Then G_{\max} increases rapidly until it starts to stabilise. The values at the end of primary consolidation are 0,8 up to 5 times greater than the unconfined ones and are in the range 16-61 MPa, dependent on depth.

After primary consolidation is completed, the further increase in shear modulus is observed, but at a smaller rate. On the logarithmic scale of time the secondary rate of increase in G_{\max} is observed to be close to linear. This slight nonlinearity is attributed to the fact that the shear modulus is determined from the square of the velocity (Anderson and Stokoe, 1978). However, this variation is small and the G_{\max} -time relationship after primary consolidation can be assumed linear. It is suggested that G_{\max} changes during primary consolidation phase are due to void ratio changes, whereas the increase in second phase is believed to result from structure forming process connected with strengthening of bonds in clay (Anderson and Stokoe, 1978). This is consistent with Towhata (2008) stating that the cementation and bonding between clay particles develop gradually with time and

7.3 SMALL STRAIN SHEAR MODULUS

in consequence, the shear rigidity and strength of the clay increase with time. G_{\max} values after 24 hours of isotropic confinement fall between 21 and 66 MPa.

After 77 hours of consolidation of sample 3vh2 G_{\max} value reaches 27 MPa, which is 7% greater than the value at the end of primary consolidation for this sample. Additionally, G_{\max} for sample 3vh1 after 24 hours of consolidation is 26,5 MPa. Therefore, the results after 24 and 77 hours do not differ significantly. Thus, it is suggested that the isotropic confinement of 24 hours gave reliable G_{\max} values for evaluation of long-term consolidation.

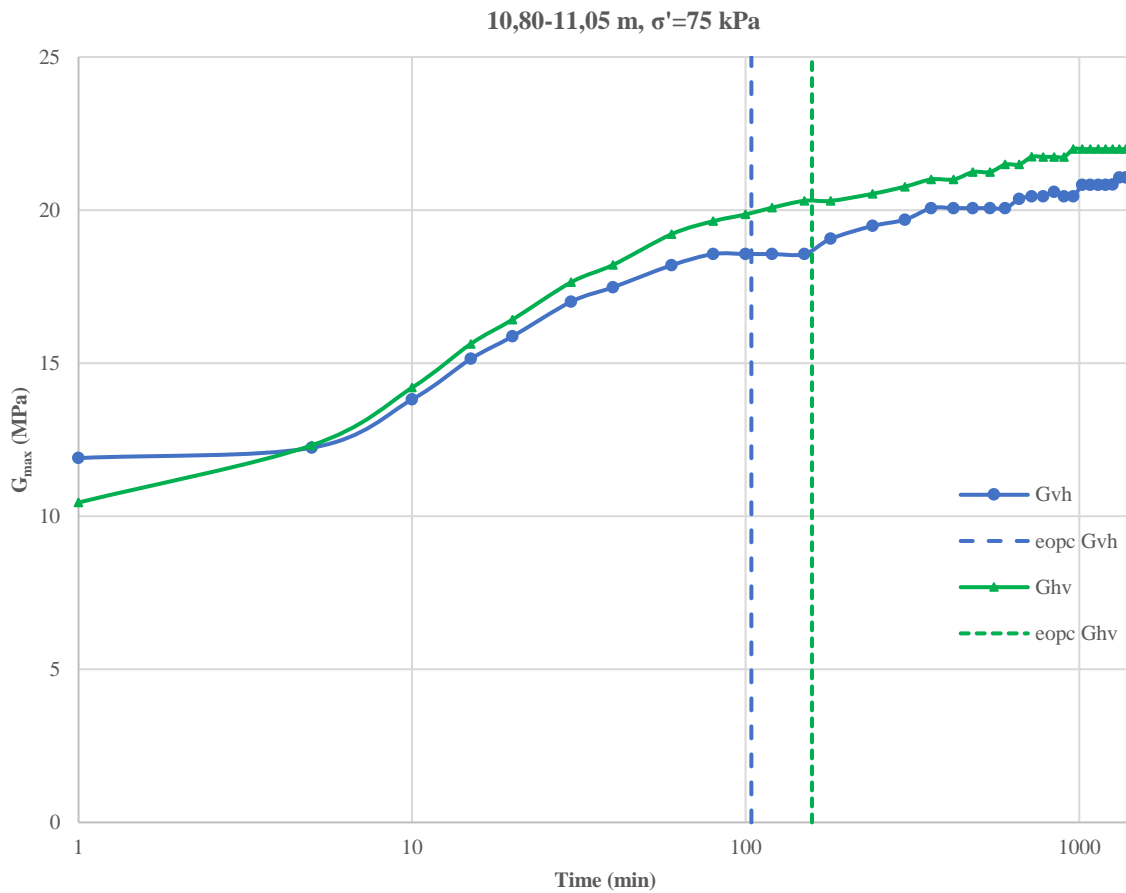


Figure 7.8: Shear modulus changes with time of consolidation for Sample 2

7.3 SMALL STRAIN SHEAR MODULUS

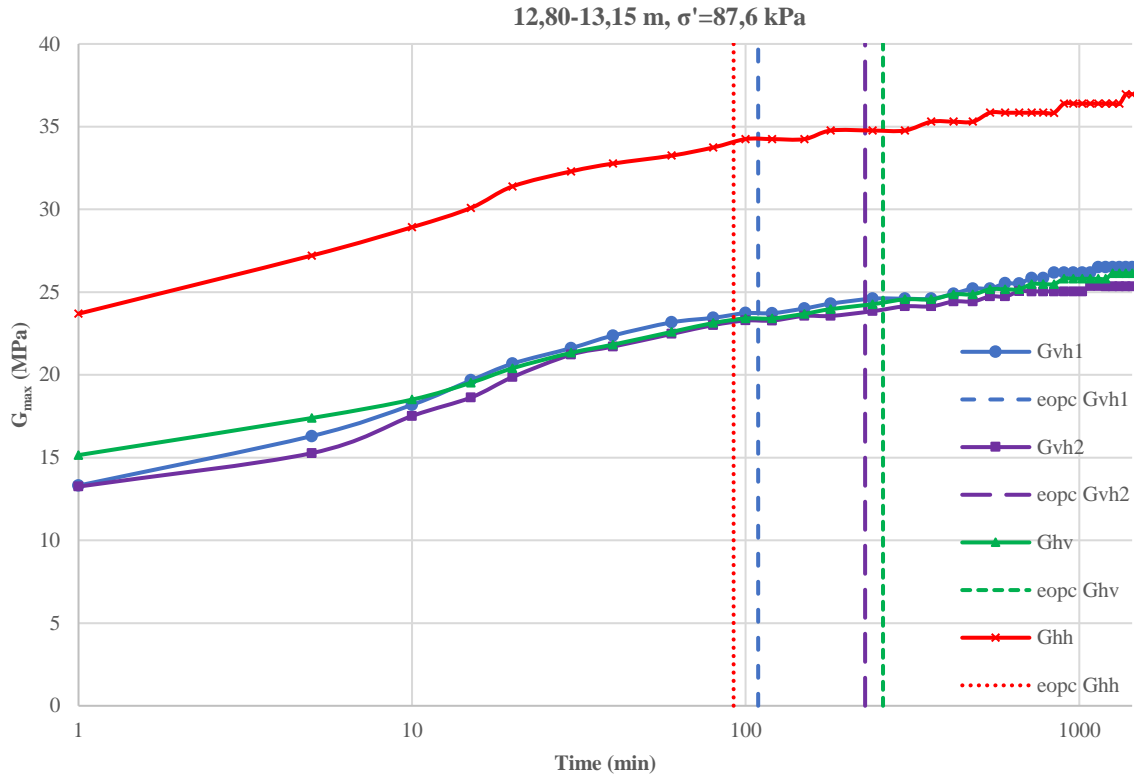


Figure 7.9: Shear modulus changes with time of consolidation for Sample 3

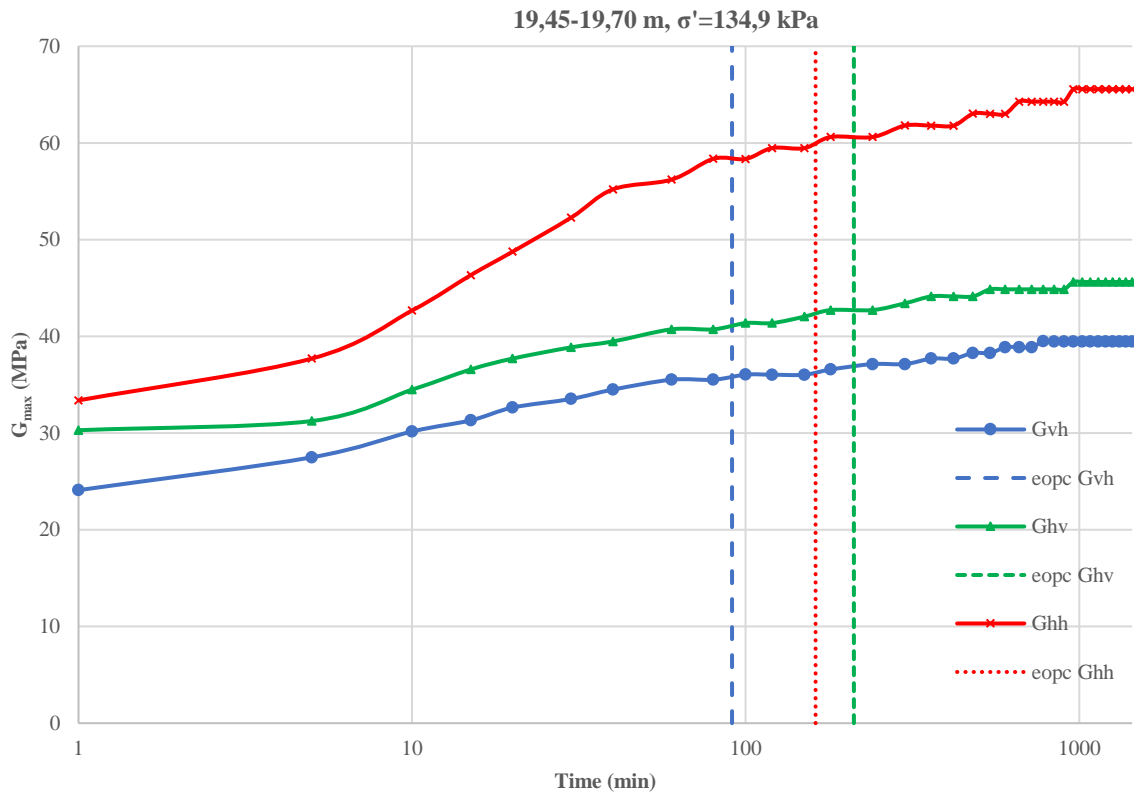


Figure 7.10: Shear modulus changes with time of consolidation for Sample 4

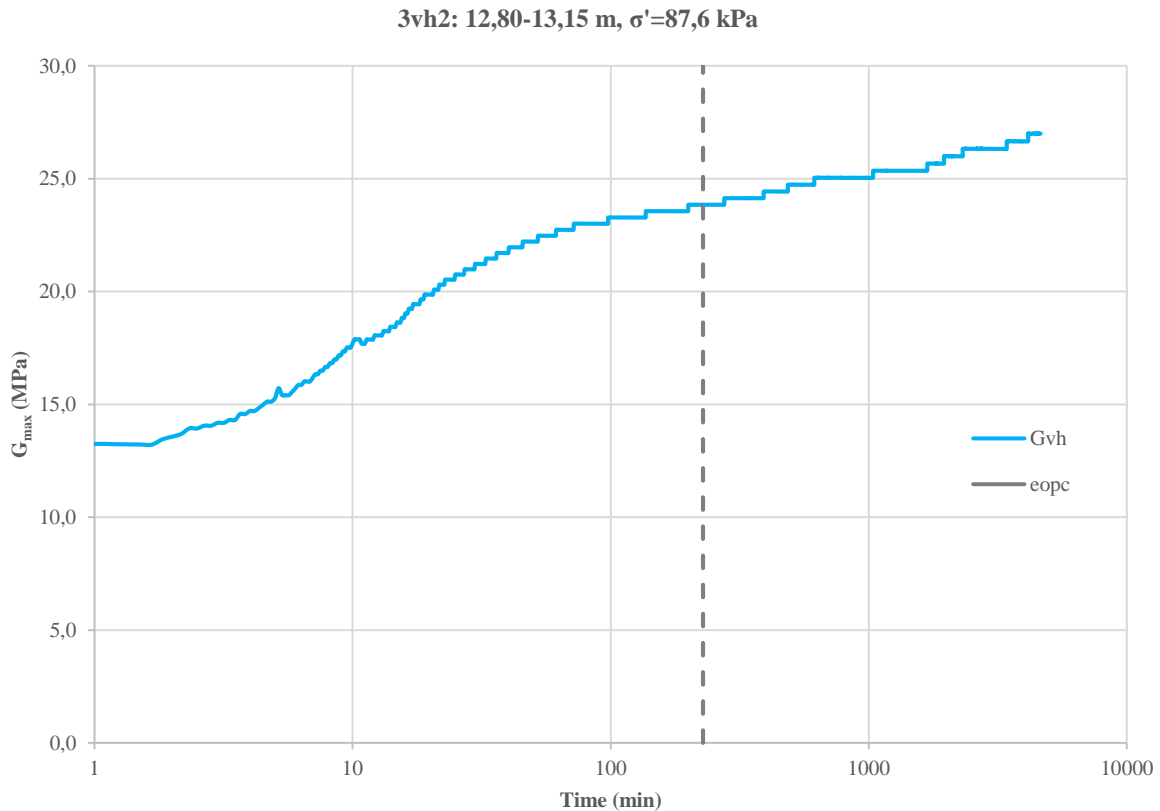


Figure 7.11: Shear modulus changes with time of consolidation for Sample 3vh2

In order to quantify the effect of long-term consolidation, two parameters were calculated for each sample: the coefficient of shear modulus increase with time, I_G , and the normalized shear modulus increase with time, N_G . The parameters were calculated using the following formulas given by Anderson and Stokoe (1978) in equations 2.9 and 2.10. Additionally, the rate of secondary modulus increase was compared to the relationship given by Kokusho et al. (1982), who proposed to relate it to the plasticity index. The formula given in equation 2.11 was used. This normalization was performed so that the samples subjected to different confining pressures could be compared. Table 7.1 summarises the obtained results.

The coefficient I_G ranges between 1,9 to 5,5 and tends to increase with depth of the sample. No relationship between normalized modulus N_G and depth of the sample was found. This is consistent with Kokusho et al. (1982) who showed independence of the secondary modulus increase rate on the effective stress level. The resulting values are between 6 and 11% and fall in the range for natural cohesive soils (Anderson and Stokoe, 1978). Prolonged secondary compression for 77 hours resulted in values consistent with results for sample 3vh1 consolidating for 24 hours. The estimations of $\Delta G/G_{1000}$, performed according to Kokusho et al. (1982), give generally lower values than the direct calculations. The differences are within 20-35%, therefore it is suggested that the formula can be used as a rough approximation, however it cannot be treated as fully reliable estimation of the shear modulus increase rate.

7.3 SMALL STRAIN SHEAR MODULUS

Table 7.1: Coefficient of shear modulus increase with time (I_G) and normalized shear modulus increase with time (N_G) for the evaluation of the long-term effect

Depth m	Anderson and Stokoe (1978)						Kokusho et al. (1982)
	vh		hv		hh		-
	I_G MPa	N_G %	I_G MPa	N_G %	I_G MPa	N_G %	N_G %
10,80-11,05	2,3	11,1	1,9	8,5	-	-	7,4
12,80-13,15	2,6 (2,5)*	9,8 (9,8)*	2,3	8,9	2,3	6,4	7,6
19,45-19,70	2,9	7,5	3,7	8,2	5,5	8,3	5,7

(*)values for sample 3vh2

Figure 7.12 illustrates the variation in normalized shear modulus with time, N_G , with respect to void ratio. It can be seen that the values of N_G tend to increase with increasing void ratio. This finding is consistent with Anderson and Stokoe (1978).

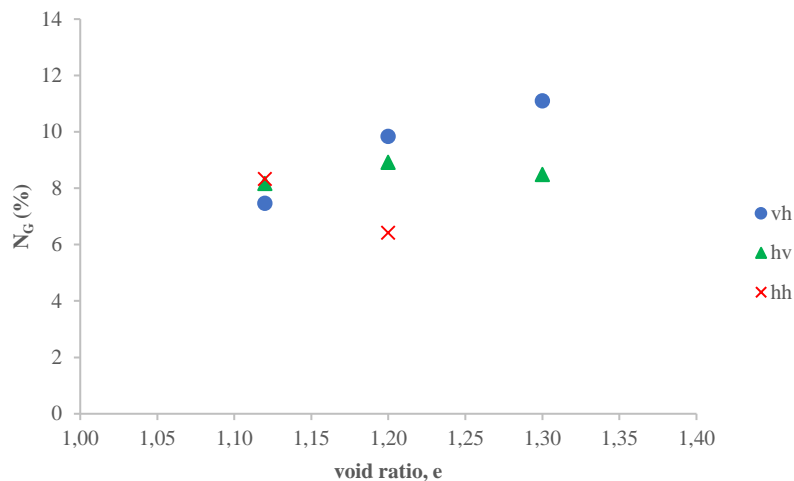


Figure 7.12: Relationship between normalized shear modulus increase with time (N_G) and void ratio (e)

7.3.3 Correlations between G_{max} and index parameters

G_{max} versus water content

Figure 7.13 presents the relationship between shear modulus and water content. There is a clear trend of decreasing G_{max} with increasing water content. In Norwegian practice shear modulus is normalized with respect to the sum of mean consolidation stress and attraction and is expressed with equation 7.1:

$$g_{max} = \frac{G_{max}}{\sigma'_m + a} \quad (7.1)$$

The study by Langø (1991) showed clear dependency of g_{max} on water content. In Figure 7.14 g_{max} is plotted versus water content for clays from several sites in Norway. It can be seen that the normalized shear modulus decreases with increasing water content. The trend shown in Figure 7.13 is therefore consistent with findings of Langø (1991).

7.3 SMALL STRAIN SHEAR MODULUS

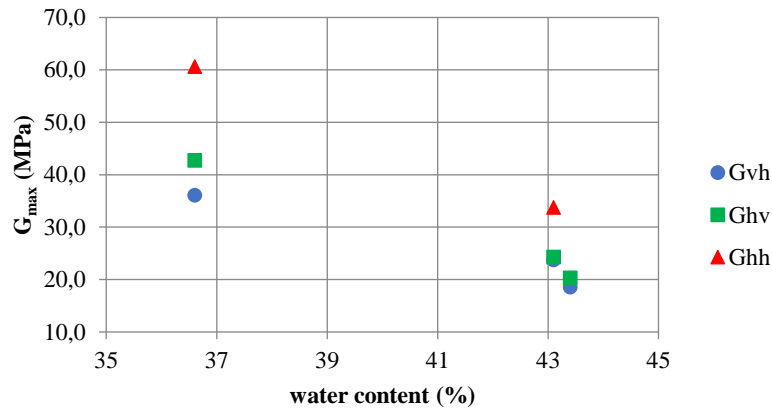


Figure 7.13: Relationship between G_{max} and water content

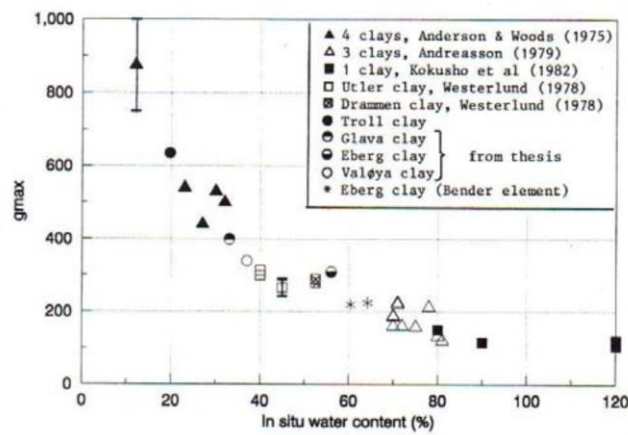


Figure 7.14: Normalized shear modulus g_{max} versus water content (Langø, 1991)

G_{max} versus void ratio

Void ratio is one of the main parameters affecting shear modulus. Figure 7.15 presents the relationship between G_{max} and void ratio. It can be seen that there is a tendency of decreasing G_{max} with increasing void ratio, as would be expected.

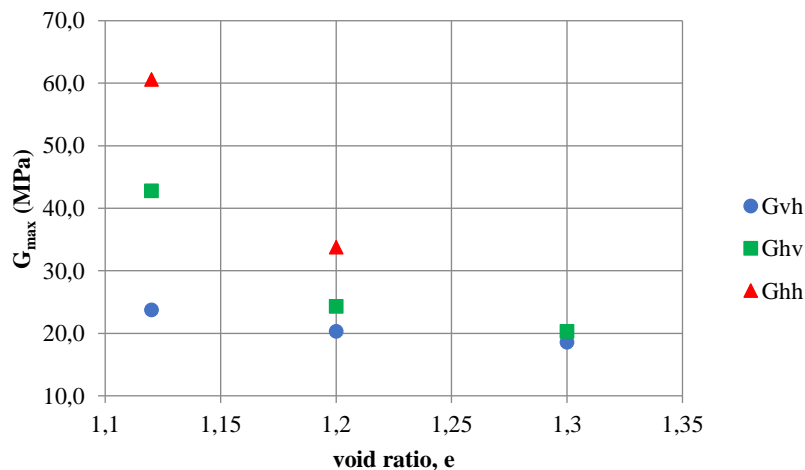


Figure 7.15 Shear modulus versus void ratio

7.3 SMALL STRAIN SHEAR MODULUS

In Figure 7.16 the data have been normalized as suggested by Leroueil and Hight (2003) (equation 2.4). A line corresponding to $S = 400, F(e) = 1/e^{1.8}, K_0 = 0,7, n = 0,25$ was plotted together with normalized values of shear modulus in the vertical direction G_{vh} . Additionally, the best fit lines used by Long and Donohue (2007) and Long and Donohue (2010) for Norwegian marine clays are plotted. As can be seen, the chosen coefficients differ from those used in both studies by Long and Donohue. This is most likely because shear wave velocity measurements used by Long and Donohue were performed in-situ and not in the laboratory, as in this study. Therefore, G_{max} values obtained in this study are lower and in order to normalise the values of G_{max} , different coefficient had to be used. Moreover, the number of G_{vh} data points is too low to deem the final result reliable. Nevertheless, Figure 7.16 shows that the relationship by Leroueil and Hight (2003) is of relevance and with more data it is possible to obtain a good fit.

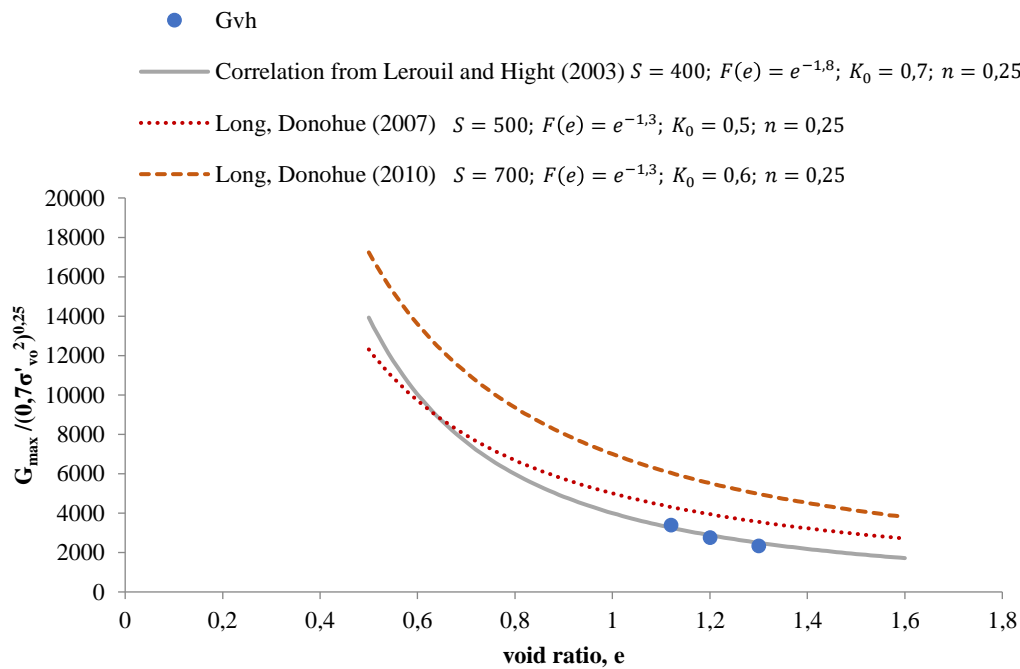


Figure 7.16: Relationship between G_{max} according to Leroueil and Hight (2003) and e

G_{max} versus plasticity index

Figure 7.17 illustrates the variation of G_{max} with plasticity index. It shows the trend of decreasing G_{max} with increasing plasticity index. Hardin (1978) indicated that the plasticity index influence on G_{max} is related to OCR. According to Vucetic and Dobry (1991), for clays with overconsolidation ratio greater than 1, G_{max} increases with plasticity index. However, other researches showed negligible effect of plasticity index on G_{max} . Due to lack of data about exact OCR values for samples in this study and due to limited number of data points, it is therefore not possible to confirm the relationship presented in Figure 7.17.

7.3 SMALL STRAIN SHEAR MODULUS

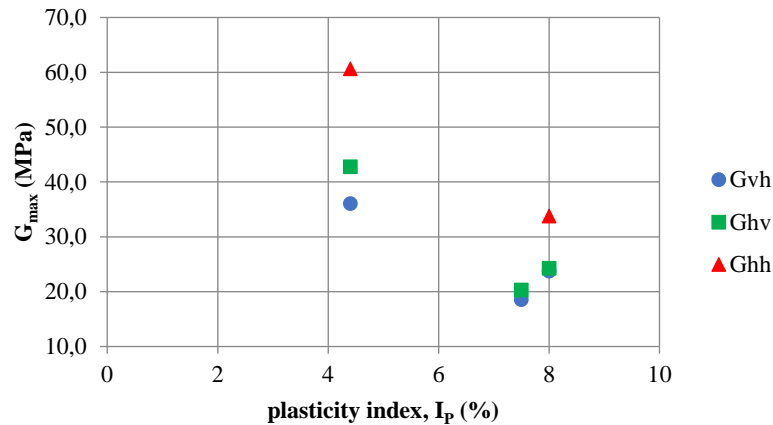


Figure 7.17: Shear modulus versus plasticity index

7.3.4 Comparison of V_s and G_{max} between in-situ and laboratory tests

Figure 7.18 presents shear wave velocity values and estimated small strain shear modulus from in-situ measurements using different techniques. The values obtained in laboratory testing on vertically cut samples in this study have also been plotted for respective depths. Both unconfined (vh,0) and subjected to the confining stress (vh,1) values were included. The shear wave velocities measured in the laboratory are consistently lower than the ones measured in-situ. The shear wave velocity values obtained in the laboratory are 35-45% lower than the in-situ ones. The laboratory values of G_{max} are 58-70% lower than the in-situ ones. Lower V_s values obtained in bender element testing than with in-situ measurements at Tiller-Flotten site were also reported by other authors (L'Heureux et al., In press).

Several reasons for lower V_s and G_{max} values determined in laboratory testing comparing to the in-situ measurements can be found. The isotropic consolidation which was performed does not resemble the in-situ conditions very well since the in-situ stress conditions are anisotropic. The applied vertical stress was lower than the in-situ one and therefore, the measured shear wave velocity was lower, as the shear wave velocity depends on the effective applied stress. Additionally, the applied isotropic confining stress was calculated taking into consideration hydrostatic ground water pressure. However, the current piezometric profile in Tiller-Flotten site shows that the groundwater pressure is below hydrostatic, thus the calculated effective stresses were lower than the actual in-situ one. As a result, the applied consolidation stress was lower than the intended effective horizontal stress and that contributed to lower V_s values.

Moreover, Tan et al. (2002) attributed the differences between in-situ and laboratory measurements to the sampling process, which results both in stress relief and loss of structure. Stress relief is defined as the change from the in-situ anisotropic stress state to the isotropic sampling effective stress. Their study showed that reconsolidation to the in-situ stresses can recover effective stress but cannot fully recover G_{max} . The results showed consistently lower of about 10% laboratory values than the in-situ seismic cone tests. Their analysis suggested that this is due to loss of structure in clay. They indicate two structure components: bonding and fabric. Bonding is related to physical attachments between soil particles, while fabric is associated with particle arrangement and orientation. They suggest that for a young and lightly overconsolidated marine clays the loss of stiffness due to sampling is due to loss of bonding in clay. That is, under the strains imposed by sampling process the disturbance of interparticle bonding is likely to occur.

7.4 STIFFNESS ANISOTROPY

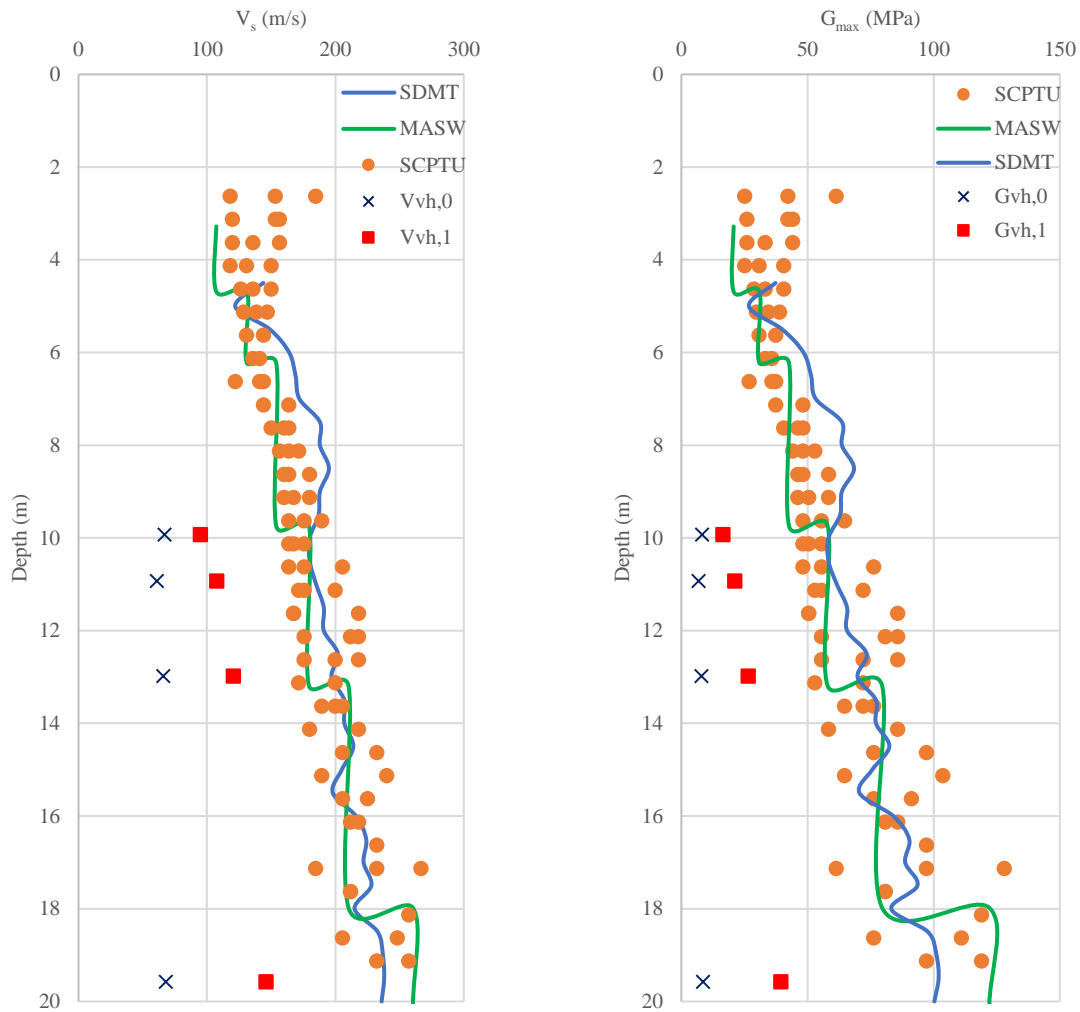


Figure 7.18: Shear wave velocity (V_s) and small strain shear modulus (G_{max}) with depth - comparison between field and laboratory measurements

The determined sample quality indicates that all the samples are of acceptable to very good and excellent quality (see Table 6.4 in section 6.3). However, as mentioned above, the applied isotropic consolidation stress was lower than the anisotropic effective in-situ stress. Therefore, the samples were in fact not reconsolidated to its in-situ stresses. As a result, the amount of expelled water was lower and the sample quality could not be reliably evaluated. Consequently, the samples used in this study could be of lower quality than it was suggested by the amount of expelled water during the tests. Additionally, the long storage time of the mini-blocks between sampling and laboratory investigations contributed to lower quality of the samples. Thus, sample disturbance may have contributed to lower shear wave velocity values obtained in bender elements testing.

7.4 Stiffness anisotropy

In order to investigate the anisotropic behaviour of Flotten quick clay the ratios between shear wave velocities and corresponding small strain shear moduli were determined. Both the ratios vh/hv and hh/hv were calculated. The calculations are summarized in Table 7.2. The ratios for unconfined samples, the end of primary consolidation and after 24 hours of consolidation were included.

7.4 STIFFNESS ANISOTROPY

Table 7.2: Anisotropy ratios for different consolidation stages

Depth (m)	Unconfined				End of primary consolidation				After 24 h consolidation			
	$\frac{V_{vh}}{V_{hv}}$	$\frac{V_{hh}}{V_{vh}}$	$\frac{G_{vh}}{G_{hv}}$	$\frac{G_{hh}}{G_{vh}}$	$\frac{V_{vh}}{V_{hv}}$	$\frac{V_{hh}}{V_{vh}}$	$\frac{G_{vh}}{G_{hv}}$	$\frac{G_{hh}}{G_{vh}}$	$\frac{V_{vh}}{V_{hv}}$	$\frac{V_{hh}}{V_{vh}}$	$\frac{G_{vh}}{G_{hv}}$	$\frac{G_{hh}}{G_{vh}}$
9,75-10,10	0,94	-	0,89	-	0,98	-	0,96	-	-	-	-	-
10,80-11,05	0,97	-	0,94	-	0,96	-	0,91	-	0,98	-	0,96	-
12,80-13,15	1,00	1,02	1,00	1,03	0,99	1,19	0,98	1,42	1,01	1,18	1,02	1,39
19,45-19,70	1,01	1,09	1,03	1,18	0,92	1,30	0,84	1,68	0,93	1,29	0,86	1,66

The ratios between the shear wave velocities and small strain shear moduli in the vertical direction and the horizontal direction with vertical polarization for all consolidation stages are in the range 0,84-1,03, thus around unity. The average value is 0,97. V_{hh}/V_{vh} values are between 1,02-1,09 for unconfined samples. The ratio increases when the samples are subjected to the consolidation stress and it varies between 1,19-1,30 at the end of consolidation, depending on the cell pressure. After 24 hours of consolidation the values slightly decrease and reach 1,18-1,29 at the end of consolidation.

G_{vh}/G_{hv} values are between 0,89 and 1,03 for unconfined samples. For samples subjected to the consolidation stress the G_{vh}/G_{hv} ratio is in most cases lower than 1, meaning that G_{vh} values are lower than G_{hv} values. The ratio between the shear moduli in horizontal direction G_{hh} and the moduli in vertical direction G_{vh} is identified as anisotropy ratio and was defined according to equation 2.20. The results show that anisotropy ratio is always greater than unity, therefore G_{hh} is higher than G_{vh} . The anisotropy of unconfined samples is the least significant with the ratio varying between 1,03 and 1,18. Clear increase in anisotropy was found between unconfined samples and samples subjected to consolidation pressure. At the end of primary consolidation the ratio increased to 1,42-1,68. After the primary consolidation was finished, the anisotropy ratios decrease slightly by 1-2%.

7.4.1 Discussion of stiffness anisotropy in Tiller-Flotten clay

From the above, it can be said that shear waves propagate faster in the plane parallel to the bedding plane than in the normal one. The horizontally polarized S-waves with vertical propagation, and S-waves vertically polarized with horizontal propagation share similar propagation velocities. The average ratio between them is 0,93. It is therefore inferred that Flotten quick clay exhibits stiffness anisotropic behaviour. Since the shear wave velocities were measured under isotropic effective stress conditions, these findings reflect the inherent anisotropy of clay. It is therefore reasonable to conclude that this greater stiffness in horizontal plane than in the vertical plane is result of the clay structure. As found during the investigations, the Tiller-Flotten clay has a varved and laminated structure with the clay minerals oriented in the horizontal direction (section 4.6). Several darker layers of clay were encountered in each mini-block. These are layers with higher organic content and higher water content and they are softer than the homogenous quick clay. According to Sayers and Den Boer (2016) the layered microstructure in clay contributes to strong bonds within the layers and weaker bonds in- between them. Due to the preferred horizontal particle orientation in clay more contacts between the particles lay within the bedding plane, which strengthens the soil structure in response to shearing (Wang and Mok, 2008).

7.4 STIFFNESS ANISOTROPY

The assumption of cross-anisotropy requires $G_{vh} = G_{hv}$. These two values were found to be comparable but not equal to each other. A tendency of G_{hv} greater than G_{vh} is clearly seen in all the samples. Due to these noticeable differences between G_{vh} and G_{hv} , it is suggested that the general assumption of cross-anisotropy cannot be made. Several factors may contribute to these discrepancies. The vertical samples were cut from the top part of the mini-block, while the samples for the measurement of V_{hv} was cut from the lower section. Consequently, the horizontal samples were in reality taken from slightly greater depth and thus had a greater effective in-situ stress and as a result exhibited higher shear wave velocities than the samples from the shallower depths.

The finding of G_{hv} greater than G_{vh} is consistent with this of Pennington et al. (1997). They suggested that this can be due to the layering in clay. The shear wave travelling in the vertical direction has to pass through different layers, whereas the hv wave might travel along layers of higher stiffness and therefore hv is consistently larger than vh . Additionally, the presence of inhomogeneities in clay may contribute to differences between V_{vh} and V_{hv} (Landon and DeGroot, 2006).

The anisotropic behaviour is clearly seen. However, it is not known to what extent the anisotropy determined in laboratory investigations reflects the actual anisotropy present in-situ. This is due to the long storage time of the mini-blocks prior to the laboratory testing and sampling process itself. Sampling contributes to, apart from stress relief, the loss of structure in the soil, and particularly in reduced bonding in clay (Tan et al., 2002). Therefore, as it was suggested that the structure plays a significant role in the anisotropy of quick clay, the stiffness anisotropy investigated on the samples in this study may not resemble the in-situ clay behaviour very well.

7.4.2 Effect of consolidation stress on the anisotropy of G_{max}

Figure 7.19 illustrates G_{vh}/G_{hv} and G_{hh}/G_{vh} ratios versus the average confining pressure. It can be seen that G_{vh}/G_{hv} ratios oscillate around unity with the average of 0,93. Thus, it can be said that the consolidation stress does not influence the ratio G_{vh}/G_{hv} . The G_{hh}/G_{vh} ratios are both significantly greater than unity with the average of 1,54. Additionally, G_{hh}/G_{vh} ratios tend to increase with confining pressure. However, most of the literature presents contradictory results. Degradation of the shear modulus with increasing consolidation stress was found by some researchers. However, according to Masin and Rott (2014) there is no clear dependency of the mean consolidation stress on the anisotropy ratio. Therefore, due to limited number of obtained data points it is not possible to verify the relationship between the anisotropy and confining stress.

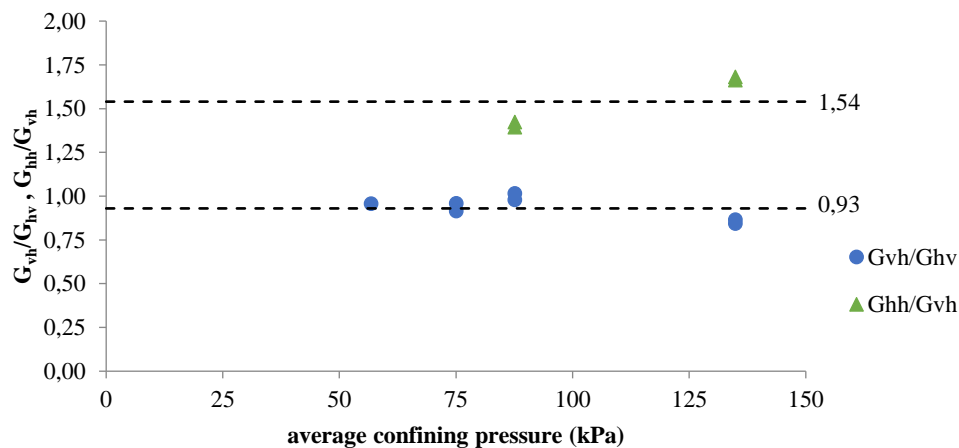


Figure 7.19: G_{vh}/G_{hv} and G_{hh}/G_{vh} ratios versus average confining pressure

7.4.3 Anisotropy with depth

The anisotropy ratios plotted with depth are presented in Figure 7.20. The anisotropy ratio tends to increase with depth. However, the amount of data is not sufficient to consider this relationship conclusive.

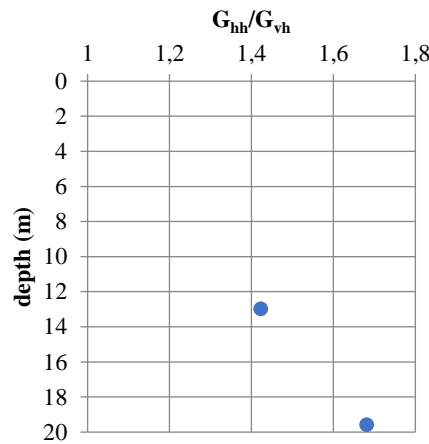


Figure 7.20: Anisotropy ratio versus depth

7.4.4 Effect of consolidation time on the anisotropy of G_{max}

In order to examine the development of anisotropy during time of consolidation the anisotropy ratios were plotted against time. Figure 7.21 shows the relationship between G_{vh}/G_{hv} and time of consolidation. Each of the mini-block samples curves is rather stable. The biggest variations in G_{vh}/G_{hv} are seen in the first 3 hours of consolidation, which corresponds to approximately the primary consolidation time for each of the samples. It can be noticed that G_{vh}/G_{hv} ratio is different for each depth of the sample, however without any distinguishable pattern.

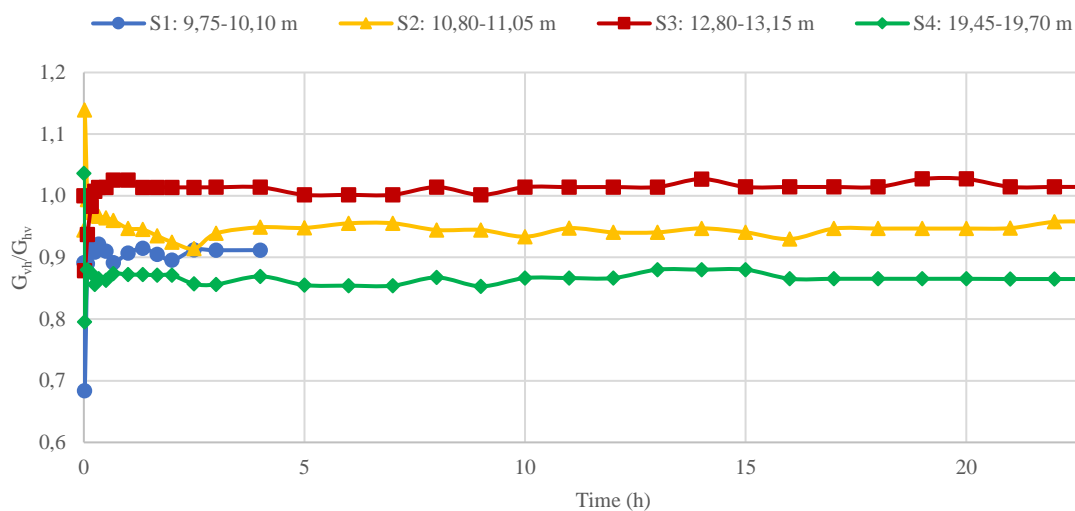


Figure 7.21: G_{vh}/G_{hv} development during sample consolidation

The variation of anisotropy with consolidation time is presented in Figure 7.22. The greatest changes in anisotropy ratio G_{hh}/G_{vh} can be seen during primary consolidation. Anisotropy of sample 4 increased noticeably between the beginning and two first hours of the consolidation. Anisotropy ratio of sample 3 decreased

7.4 STIFFNESS ANISOTROPY

significantly from 1,8 in the beginning of consolidation to approximately 1,45 in the end of primary consolidation. This drop of the anisotropy ratio is suggested to result from relatively faster increase in G_{vh} than in G_{hh} during primary consolidation. During primary consolidation G_{hh}/G_{vh} ratio changed 38% for sample 3 and 40% for sample 4. After the end of primary consolidation anisotropy of sample 3 tends to gradually decrease. The anisotropy of sample 4 showed more distinct variation, however after 16 hours of consolidation the ratio stabilizes. For both of the samples the anisotropy ratios after 24 hours of consolidation are 1-2 % lower than the ratios at the end of primary consolidation and are equal to 1,39 for sample 3 and 1,66 for sample 4.

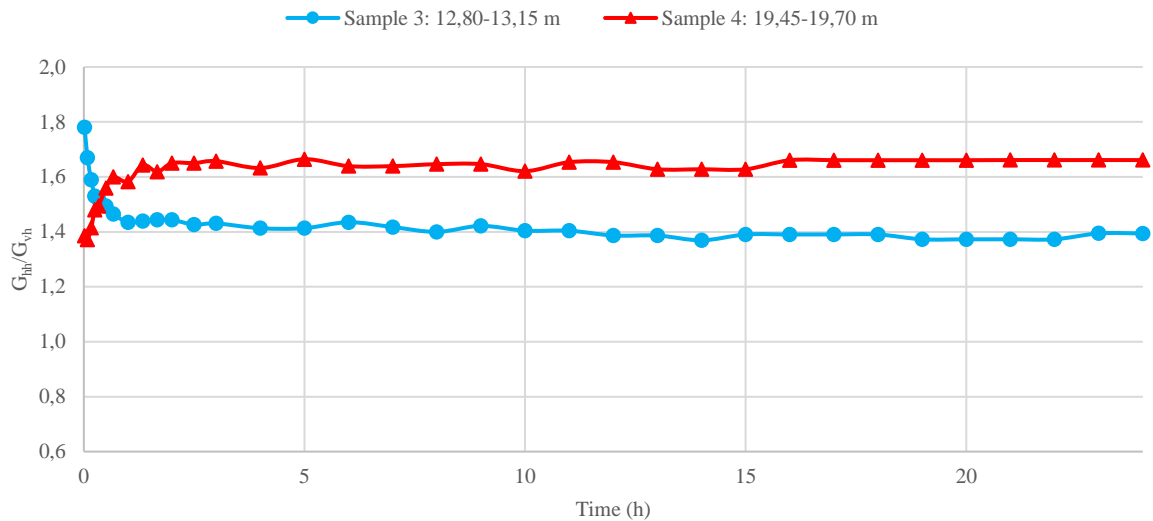


Figure 7.22: G_{hh}/G_{vh} development during sample consolidation

7.4.5 Influence of plasticity index on stiffness anisotropy

Figure 7.23 plots G_{hh}/G_{vh} versus plasticity index. Anisotropy tends to decrease with plasticity index. This relationship is consistent with the study of Berre and Bjerrum (1973). Their research on several Norwegian clays reported that the less plastic the clay, the greater is the anisotropy. The finding by Jamiolkowski et al. (1985) stating that ‘less plastic, and often more sensitive, clays tend to have higher anisotropy than more plastic clays’ therefore appears to be relevant for Flotten quick clay. However, the amount of data is not sufficient to verify this statement. Relationship between anisotropy ratio and plasticity index can be misleading and should not be the base for analysis of anisotropy of different clays (Won, 2013).

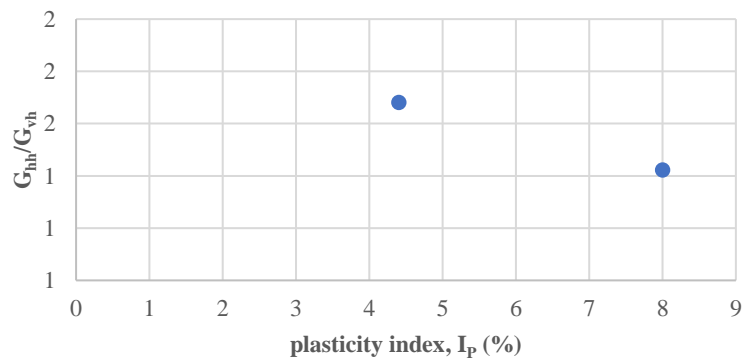


Figure 7.23: Anisotropy ratio G_{hh}/G_{vh} versus plasticity index I_p

Chapter 8

Summary

8.1 Summary and Conclusions

This study focused on laboratory investigations of small strain shear modulus of quick clay from Tiller-Flotten Test Site. The stiffness anisotropy was of main interest. Shear wave velocity measurements were performed using bender element testing technique. Triaxial specimens were obtained from the mini-block samples from Tiller-Flotten NGTS. Vertical and horizontal samples were tested with bender elements, in an unconfined state and during the consolidation in the triaxial apparatus. Index testing was carried out to provide soil identification data. In order to analyse the reliability of obtained shear waveforms, the evaluation of bender element system was performed.

The preliminary findings suggest that the Tiller-Flotten quick clay is inherently anisotropic. Shear waves propagate faster in the plane parallel to the bedding plane than in the normal plane. It is therefore concluded, that the stiffness anisotropy is a consequence of the clay's structure. The clay particles with preferred horizontal orientation, result in greater shear rigidity in the plane of the clay particles than in planes perpendicular to the bedding plane. The varved and layered structure of clay leads to strong bonds within the clay layers and weaker bonds in-between the layers. This contributes to slower shear wave velocities in the vertical direction and therefore to significant anisotropy of the clay structure.

The cross-anisotropic behaviour of Tiller-Flotten quick clay is however, not conclusively supported by the experimental findings of this study. Further investigations are required to verify this assumption. Discrepancies between G_{vh} and G_{hv} are visible in all the samples, with G_{hv} being greater than G_{vh} . This is attributed to several factors, including: the layering within the clay profile, presence of inhomogeneities in clay, and due to the fact that the samples used in the measurement of V_{hv} , were cut from the lower section of the mini-block sample. Nevertheless, the difference between these two shear moduli is not very large. Therefore, the assumption of cross-anisotropy may be relevant, and should be verified in further investigations.

The anisotropic behaviour is clearly seen. However, it is not known to what extent the anisotropy determined in laboratory investigations reflects the actual anisotropy present in-situ. This is due to the long storage time of the mini-blocks prior to the laboratory testing and sampling process itself. Therefore, the stiffness anisotropy investigated on the samples in this study may not resemble the in-situ clay behaviour very well.

Anisotropy was found to increase with depth, whereas the ratio G_{vh}/G_{hv} was rather stable and not affected by depth of the sample. However, the amount of data obtained in laboratory testing was not sufficient to confirm these relationships. Furthermore, anisotropy was found to increase during primary consolidation. During secondary consolidation however, G_{hv}/G_{vh} decreased slightly, and after 24 hours of consolidation the anisotropy ratios were 1-2% lower than the ones at the end of primary consolidation.

8.2 RECOMMENDATIONS FOR FURTHER WORK

Shear wave velocity and small strain shear modulus were found to increase with depth. The comparison between the laboratory determined V_s and G_{max} and the values obtained in in-situ measurements was performed. Laboratory measured values were found to be significantly lower than the ones determined in-situ. This may be attributed to several factors. The first being due to the fact that the isotropic consolidation which was performed does not resemble the in-situ conditions very well since the in-situ stress conditions are anisotropic. Additionally, the applied stress was considerably lower than the stresses present in-situ. Moreover, stress relief and loss of clay structure due to sampling process contributed to lower measured shear wave velocities. Finally, long storage time between sampling and laboratory testing affected sample quality.

A clear increase in the shear modulus with time of consolidation was found. The greatest increase in G_{max} could be seen during primary consolidation. After primary consolidation was completed, the further increase in shear modulus was observed. It is suggested that G_{max} changes during primary consolidation phase are due to void ratio changes, whereas the increase in second phase is believed to result from structure forming process connected with strengthening of bonds in clay. Comparison of results for samples consolidated for 24 hours and 77 hours lead to the conclusion that the isotropic confinement for 24 hours was sufficient time in order to evaluate the long-term effect on small strain shear modulus.

Some clear relationships between small strain shear modulus and index parameters were found. G_{max} was found to decrease with increasing water content. A tendency of decreasing G_{max} with increasing void ratio was seen. Results also showed trend of decreasing G_{max} with increasing plasticity index.

The performance of the bender elements used in this study was found to be significantly influenced by their own mechanical properties. For frequencies greater than 2 kHz the predominant signal frequency at the receiver was lower than the input signal frequency. Therefore, it is inferred that it is the resonant frequency of the bender element-soil system which characterises the response.

The signal distortion was found to be present in all the obtained waveforms. This signal distortion is believed to result from the near-field effect and the interference from the P-wave propagation. The elimination of the dispersion from the received pulse signal was not possible to achieve. The ratio d/λ could not be increased to the value sufficient to reduce the near-field effect. This is attributed to low allowed frequencies, which are in the range 0,5-5 kHz. However, the measurements with excitation frequencies equal to the resonant frequency of the transducer-soil system are deemed appropriate. The resulting d/λ ratio greater than unity is thus believed to give results of sufficient reliability.

8.2 Recommendations for Further Work

This study suggests that the Tiller-Flotten quick clay is inherently anisotropic, however the amount of obtained data was not sufficient. Therefore, in order to verify these preliminary findings, it would be essential to carry out more investigations. Furthermore, the possibility that the soil is cross anisotropic in nature cannot be discarded and further investigations are required to verify the differences between G_{vh} and G_{hv} . Since the results show inherent anisotropy of clay, the clay mineralogy and fabric should be of interest. Thorough investigations on clay microstructure should be carried out.

It would be relevant to investigate if the anisotropy determined in the laboratory testing is comparable to anisotropy present in-situ. In order to achieve this, it is suggested that measurements of in-situ shear wave velocities both V_{vh} and V_{hv} be performed. It is recommended that the measurement of V_{hh} shear wave velocity

8.2 RECOMMENDATIONS FOR FURTHER WORK

should be conducted using bender elements on samples subject to confining pressure in the laboratory. Furthermore, unconfined shear wave velocity measurements should be performed immediately after samples have been extracted from the subsurface. These procedures will be useful when evaluating the reliability of laboratory results. Moreover, it would be interesting to study the influence stress levels have on a clay's anisotropy. This can be done by performing investigations with greater isotropic confining stress.

The mini-block samples used in this study were subjected to long storage time between sampling and laboratory testing. In order to evaluate the influence of this storage time, measurements on fresh samples should be performed. As a result, the mini-block could be used more efficiently, since the disturbance near the edges would be reduced. Additionally, individual samples could be cut both vertically and horizontally from the same level of the mini-block: thus resulting in a more reliable test data.

Moreover, it would be interesting to consolidate the samples to the in-situ effective anisotropic stresses, and compare the obtained $V_{s,v}$ and $G_{\max,v}$ with the data obtained from the in-situ measurements.

Further analysis of bender element system performance should be carried out. In particular, the reasoning for the distortion of the received signal should be investigated. Therefore, numerical analysis of bender elements and the near-field effect would be valuable.

References

- Airey, D., & Mohsin, A. K. (2013). Evaluation of shear wave velocity from bender elements using cross-correlation. *Geotechnical Testing Journal*, 36(4), 1-9. doi:10.1520/GTJ20120125
- Amundsen, H. A., Thakur, V., & Emdal, A. (2016). Sample disturbances in block samples on low plastic soft clays. *Proceedings of the 17th Nordic Geotechnical Meeting*. Reykjavik.
- Anderson, D. G., & Stokoe, K. H. (1978). Shear Modulus: A Time-Dependent Soil Property. *Dynamic Geotechnical Testing*, 66-90. doi:10.1520/STP35672S
- Andresen, A., & Kolstad, P. (1979). The NGI 54 mm samplers for undisturbed sampling of clays and representative sampling of coarser materials. *Proceedings of the International Symposium on Soil Sampling*.
- Arroyo, M., Muir Wood, D., & Greening, P. D. (2003). Source near-field effects and pulse tests in soil samples. *Géotechnique*, 53(3), 337-345. doi:10.1680/geot.2003.53.3.337
- Arulnathan, R., Boulanger, R. W., & Riemer, M. F. (1998). Analysis of Bender Element Tests. *Geotechnical Testing Journal*, 21(2), 120-131. doi:10.1520/GTJ10750J
- Benz, T. (2007). *Small-strain stiffness of soils and its numerical consequences*. Univ. Stuttgart, Inst. f. Geotechnik.
- Benz, T., Schwab, R., & Vermeer, P. (2009). Small-strain stiffness in geotechnical analyses. *Bautechnik Special issue - Geotechnical Engineering*, 16-27. doi:10.1002/bate.200910038
- Berre, T., & Bjerrum, L. (1973). Shear strength of normally consolidated clays. *Proc. 8th ICSMFE*, (ss. 39-49). Moscow.
- Blewett, J., Blewett, I. J., & Woodward, P. K. (2000). Phase and amplitude responses associated with the measurement of shear-wave velocity in sand by bender elements. *Canadian Geotechnical Journal*, 37(6), 1348-1357. doi:10.1139/t00-047
- Brignoli, E. G., Gotti, M., & Stokoe, K. H. (1996). Measurement of Shear Waves in Laboratory Specimens by Means of Piezoelectric Transducers. *Geotechnical Testing Journal*, 19(4), 384-397.
- Camacho-Tauta, J. F., Alvarez, J. D., & Reyes-Ortiz, O. (2012). A procedure to calibrate and perform the bender element test. *Dyna*, 79(176), 10-18.
- Donohue, S., & Long, M. (2010). Assessment of sample quality in soft clay using shear wave velocity and suction measurements. *Géotechnique*, 883-889. doi:10.1680/geot.8.T.007.3741
- Dyvik, R., & Madshus, C. (1985). Lab measurements of Gmax using bender elements. *ASCE Annual Convention on Advances in the Art of Testing Soils under Cyclic Conditions*, (ss. 186-196). Detroit, Michigan.
- Emdal, A., Gylland, A., Amundsen, H. A., & Long, M. (2016). Mini-block sampler. *Canadian Geotechnical Journal*, 53(8), 1235-1245. doi:10.1139/cgj-2015-0628
- GDS. (u.d.). Bender element technical specification.
- Graham, J., & Houlsby, G. T. (1983). Anisotropic elasticity of a natural clay. *Géotechnique*, 33(2), 165-180. doi:10.1680/geot.1983.33.2.165
- Gylland, A., Long, M., Emdal, A., & Sandven, R. (2013). Characterisation and engineering properties of Tiller clay. *Engineering Geology*, 164, 86-100. doi:10.1016/j.enggeo.2013.06.008

- Hardin, B. O. (1978). Nature of stress-strain behaviour for soils. *Proceedings of the ASCE Geotechnical Engineering Division Specialty Conference, 1*, ss. 3-90. Pasadena, California.
- Hardin, B. O., & Richart, F. E. (1963). Elastic wave velocities in granular soils. *Journal of Soil Mechanics and Foundations Division*, 89(1), 33-66.
- Hori, T., Yamashita, S., & Suzuki, T. (2006). Anisotropy of elastic moduli at small strain of sand and clays by bender element test. *Proceedings of the International Symposium on Geomechanics and Geotechnics of Particulate Media*. Ube, Japan.
- ISO. (2014a). *Geotechnical investigation and testing - Laboratory testing of soil - Part 1: Determination of water content*. Switzerland: International Organization for Standardization.
- ISO. (2014b). *Geotechnical investigation and testing — Laboratory testing of soil — Part 2: Determination of bulk density*. Switzerland: International Organization for Standardization.
- ISO. (2015). *Geotechnical investigation and testing — Laboratory testing of soil — Part 3: Determination of particle density*. Switzerland: International Organization for Standardization.
- ISO. (2016). *Geotechnical investigation and testing — Laboratory testing of soil — Part 4: Determination of particle size distribution*. Switzerland: International Organization for Standardization.
- ISO. (2017). *Geotechnical investigation and testing — Laboratory testing of soil — Part 6: Fall cone test*. Switzerland: International Organization for Standardization.
- ISO. (2018a). *Geotechnical investigation and testing — Laboratory testing of soil — Part 9: Consolidated triaxial compression tests on water saturated soils*. Switzerland: International Organization for Standardization.
- ISO. (2018b). *Geotechnical investigation and testing — Laboratory testing of soil — Part 12: Determination of liquid and plastic limits*. Switzerland: International Organization for Standardization.
- Jamiolkowski, M., Ladd, C. C., Germaine, J. T., & Lancelotta, R. (1985). New developments in field and laboratory testing of soils. *Proc. 11th ICSMGE*, (ss. 57-153). San Francisco.
- Jamiolkowski, M., Lancellotta, R., & Lo Presti, D. C. (1995). Remarks on the stiffness at small strains of six Italian clays. *Pre-failure Deformation of Geomaterials*, (ss. 817-836). Balkema.
- Jovicic, V., & Coop, M. R. (1998). The Measurement of Stiffness Anisotropy in Clays with BenderElement Tests in the Triaxial Apparatus. *Geotechnical Testing Journal*, 21(1), 3-10. doi:10.1520/GTJ10419J
- Jovicic, V., Coop, M. R., & Simic, M. (1996). Objective criteria for determining Gmax from bender element tests. *Géotechnique*, 46(2), 357-362. doi:10.1680/geot.1996.46.2.357
- Kartverket. (2019). Available at: <http://norgeskart.no> (Accessed: May 2019).
- Kawaguchi, T., Mitachi, T., & Shibuya, S. (2001). Evaluation of shear wave travel time in laboratory bender element test. *Proceedings of the International Conference on Soil Mechanics and Geotechnical Engineering.*, (ss. 155-158).
- Kim, T., & Finno, R. J. (2012). Anisotropy Evolution and Irrecoverable Deformation in Triaxial Stress Probes. *Journal of Geotechnical and Geoenvironmental Engineering*, 138(2).
- Kokusho, T., Yoshida, Y., & Esahi, Y. (1982). Dynamic Properties of Soft CLay for Wide Strain Range. *Soils and Foundations*, 22(4). doi:10.3208/sandf1972.22.4_1
- Kramer, S. (1996). *Geotechnical Earthquake Engineering*. Prentice Hall, Upper Saddle River, New Jersey.
- Kumar, S. S., Krishna, A. M., & Dey, A. (2013). Parameters Influencing Dynamic Soil Properties: A Review Treatise. *National Conference on Recent Advances in Civil Engineering*.

- Landon, M. M., & DeGroot, D. J. (2006). Measurement of small strain shear modulus anisotropy on unconfined clay samples using bender elements. In: *GeoCongress 2006: Geotechnical engineering in the information technology age*. American Society of Civil Engineers. doi:10.1061/40803(187)20
- Landon, M. M., DeGroot, D. J., & Sheahan, T. C. (2007). Nondestructive Sample Quality Assessment of a Soft Clay Using Shear Wave Velocity. *Journal of Geotechnical and Geoenvironmental Engineering*, 133(4).
- Langø, H. (1991). *Cyclic shear modulus on natural intact clays*. Trondheim.
- Lee, & Santamarina. (2005). Bender Elements: Performance and Signal Interpretation. *Journal of Geotechnical and Geoenvironmental Engineering*, 131(9). doi:10.1061/(ASCE)1090-0241(2005)131:9(1063)
- Leroueil, S., & Hight, D. W. (2003). Behaviour and properties of natural soils and soft rocks. *International Workshop on Characterisation and Engineering Properties of Natural Soils*, (ss. 29-254). Rotterdam, Netherlands.
- L'Heureux, J.-S., & Long, M. (2016). Correlations between shear wave velocity and geotechnical parameters in Norwegian clay. *Proceedings of the 17th Nordic Geotechnical Meeting*. Reykjavik.
- L'Heureux, J.-S., & Long, M. (2017). Relationship between Shear-Wave Velocity and Geotechnical Parameters for Norwegian Clays. *Journal of Geotechnical and Geoenvironmental Engineering*, 143(6).
- L'Heureux, J.-S., Lindgård, A., & Emdal, A. (u.d.). (In press) The Tiller-Flotten research site: Geotechnical characterisation of a very sensitive clay deposit. *AIMS Geosciences*.
- Lings, M. L., Pennington, D. S., & Nash, D. F. (2000). Anisotropic stiffness parameters and their measurement in a stiff natural clay. *Géotechnique*, 50(2), 109-125. doi:10.1680/geot.2000.50.2.109
- Long, M., & Donohue, S. (2007). In situ shear wave velocity from multichannel analysis of surface waves (MASW) tests at eight Norwegian research sites. *Canadian Geotechnical Journal*. doi:10.1139/t07-013
- Long, M., & Donohue, S. (2010). Characterisation of Norwegian marine clays with combined shear wave velocity and piezocone cone penetration test (CPTU) data. *Canadian Geotechnical Journal*, 47, 709-718. doi:10.1139/T09-133
- Lunne, T., Berre, T., Andersen, K. H., Strandvik, S., & Sjørusen, M. (2006). Effects of sample disturbance and consolidation procedures on measured shear strength of soft marine Norwegian clays. *Canadian Geotechnical Journal*, 43(7), 726-750. doi:10.1139/t06-040
- Masin, D., & Rott, J. (2014). Small strain stiffness anisotropy of natural sedimentary clays: review and a model. *Acta Geotechnica*. doi:10.1007/s11440-013-0271-2
- NGI. (2019). Available at: <https://www.ngi.no/eng/Projects/NGTS-Norwegian-Geo-Test-Sites> (accessed: May 2019).
- NGU. (2019). Available at: <http://geo.ngu.no/kart/minkommune/?kommunenr=5001> (accessed: May 2019).
- NTNU. (2015). *Geotechnics. Field and Laboratory Investigations. Lecture notes MSc course TBA 4110*. Trondheim: Geotechnical Division, NTNU.
- Pennington, D. S., Nash, D. F., & Lings, M. L. (1997). Anisotropy of G₀ shear stiffness in Gault Clay. *Géotechnique*, 47(3), 391-398. doi:10.1680/geot.1997.47.3.391
- PLAXIS. (2018). *Material Models Manual. Build 9462*.
- Pusch, R. (1970). Clay microstructure. A study of the microstructure of soft clays with special reference to their physical properties. *Swedish Geotechnical Institute, Proceedings No 24*. Stockholm.

- Rahman, M., Pakrashi, V., Banerjee, S., & Orr, T. (2015). Suitable Waves for Bender Element Tests: Interpretations, Errors and Modelling Aspects. *Periodica Polytechnica Civil Engineering*, 60(2), 145-158. doi:10.3311/PPci.7952
- Rio, J. F. (2006). *Advances in Laboratory Geophysics Using Bender Elements*. PhD thesis, University College London.
- Roesler, S. K. (1979). Anisotropic Shear Modulus due to Stress Anisotropy. *Journal of the Geotechnical Engineering Division*, 105(7), 871-880.
- Sanchez-Salinerro, I., Roesset, J., & Stokoe, K. (1986). *Analytical studies of body wave propagation and attenuation*. Austin: University of Texas.
- Sayers, C. M., & Den Boer, L. D. (2016). The elastic anisotropy of clay minerals. *Geophysics*, 81(5). doi:10.1190/geo2016-0005.1
- Shirley, D. J., & Hampton, L. D. (1978). Shear-wave measurements in laboratory sediments. *The Journal of the Acoustical Society of America*, 63(2), 607-613. doi:10.1121/1.381760
- Shiwakoti, D. R., Tanaka, H., Tanaka, M., & Mishima, O. (2000). A Study On Small Strain Shear Modulus of Undisturbed Soft Marine Clays. *The Tenth International Offshore and Polar Engineering Conference*. Seattle, USA: International Society of Offshore and Polar Engineers.
- Sully, J. P., & Campanella, R. G. (1995, June). Evaluation of in situ anisotropy from crosshole and downhole shear wave velocity measurements. *Géotechnique*, 45(2), 267-282. doi:10.1680/geot.1995.45.2.267
- Tan, T.-S., Lee, F.-H., Chong, P.-T., & Tanaka, H. (2002). Effect of sampling disturbance on properties of Singapore clay. *Journal of Geotechnical and Geoenvironmental Engineering*, 128(11), 898-906. doi:10.1061/(ASCE)1090-0241(2002)128:11(898)
- Teng, F., Ou, C., & Hsieh, P. (2014). Measurements and Numerical Simulations of Inherent Stiffness Anisotropy in Soft Taipei Clay. *Journal of Geotechnical and Geoenvironmental Engineering*, 140(1), 237-250. doi:10.1061/(ASCE)GT.1943-5606.0001010
- Towhata, I. (2008). *Geotechnical Earthquake Engineering*. Springer. doi:10.1007/978-3-540-35783-4
- Viggiani, G., & Atkinson, J. H. (1995a). Interpretation of bender element tests. *Géotechnique*, 45(1), 149-154. doi:10.1680/geot.1995.45.1.149
- Viggiani, G., & Atkinson, J. H. (1995b). Stiffness of Fine Grained Soil at Very Small Strains. *Géotechnique*, 45(2), 249-265. doi:10.1680/geot.1995.45.2.249
- Vucetic, M., & Dobry, R. (1991). Effect of Soil Plasticity on Cyclic Response. *Journal of Geotechnical Engineering*, 117(1), 89-107.
- Wang, Y. H., & Mok, C. M. (2008). Mechanisms of Small-Strain Shear-Modulus Anisotropy in Soils. *Journal of Geotechnical and Geoenvironmental Engineering*, 134(10), 1516-1530. doi:10.1061/(ASCE)1090-0241(2008)134:10(1516)
- Wang, Y. H., & Siu, W. K. (2011). Structure characteristics and mechanical properties of kaolinite soils. II. Effects of structure on mechanical properties. *Canadian Geotechnical Journal*, 43(6), 601-617. doi:10.1139/t06-027
- Won, J. Y. (2013). Anisotropic strength ratio and plasticity index of natural clays. *Proceedings of the 18th International Conference on Soil Mechanics and Geotechnical Engineering*. Paris.

- Wongsaroj, J., Soga, K., Yimsiri, S., & Mair, R. J. (2004). Stiffness anisotropy of London Clay and its modelling: Laboratory and Field. *Advances in Geotechnical Engineering: The Skempton Conference*. London.
- Yamashita, S., Kawaguchi, T., Nakata, Y., Mikami, T., Fujiwara, T., & Shibuya, S. (2009). Interpretation of international paralel test on the measurement of Gmax using bender elements. *Soils and Foundations*, 49(4), 631-650.

Appendices

The following appendices are included:

Appendix A – Bender elements specification

Appendix B – LabVIEW Block Diagram

Appendix C – Grain Size Distribution Curves

Appendix D – Bender elements tests detailed results

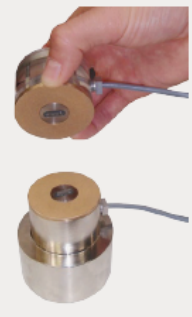
Appendix A

Bender elements specification

This appendix presents bender elements technical specification. It includes the characteristics of bender elements used in this study.



World leaders in the manufacture of laboratory systems for soil & rock



Bender Element System (BES)

The GDS Bender Element system enables easy measurement of the maximum shear modulus of a soil at small strains in a triaxial cell. Measurement of soil stiffness at very small strains in the laboratory is difficult due to insufficient resolution and accuracy of load and displacement measuring devices. The capability exists to regularly carry out measurements of small strain stiffness in the triaxial apparatus using local strain transducers, but this can be expensive and is generally confined to research projects.

The addition of Bender Elements to a triaxial testing system makes the routine measurement of G_{max} , maximum shear modulus, simple and cost effective.

Key Features:	Benefits to the User:
USB interface:	Allows the system to be swapped to any PC in the lab with a USB interface.
Titanium element inserts:	Reduces the weight of the top-cap.
Utilising existing products:	Pedestals and top-caps can be made for other manufacturers' cells as well as GDS cells, so upgrading is potentially simple.
The GDS Bender elements are bonded into a standard insert:	This makes the bender element insert a modular device that can then be easily fitted into a suitably modified pedestal/top-cap. Should an element fail, it is simple and quick for the complete insert to be replaced by the customer
2 Mega Samples/Second, 16bit Data Acquisition:	High speed data acquisition is essential as the sample interval provides the resolution for determining wave speeds.
Elements are manufactured to allow S and P wave testing to be performed:	Determining both S & P wave velocities allows additional specimen parameters to be calculated, such as Youngs Modulus, E.
Vertical and horizontal elements are available:	Specimen anisotropy can be studied with the use of both vertical and horizontal elements on the sample.

Tests that can be Performed:

Determination of Shear Wave Velocity, determination of P-Wave Velocity, vertically propagating horizontally polarised (vertical elements), horizontally propagating horizontally polarised (horizontal elements), horizontally propagating vertically polarised (horizontal elements).

Upgrade Options:

- Combined pedestals for unsaturated testing and bender elements (ie with bonded high air entry porous disc).

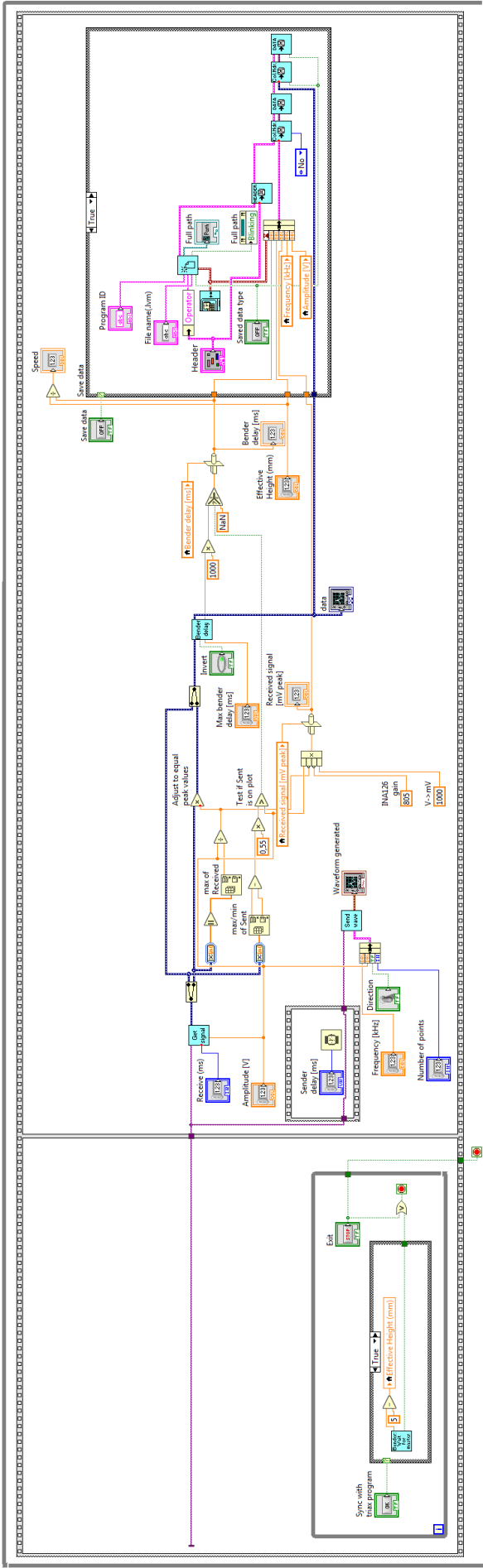
Technical Specification:

Data acquisition speed:	2,000,000 samples/second, simultaneous sampling of both source and received signals.
Resolution of data acquisition (bits):	16
Operating Pressure Range:	Up to 3.5MPa. Above 3.5MPa Acoustic Velocity transducers are required for P&S waves.
Computer Interface:	USB
Available gain ranges for data acquisition:	From x10 to x500
Operating Temperature:	-10°C to 50°C
Sample Sizes:	Up to 300mm

Appendix B

LabVIEW Block diagram

This appendix presents the block diagram from the LabVIEW bender elements program. The algorithm, which is followed by the bender elements program, is illustrated. It includes obtaining input data, waveform generation, receiving the signal, obtaining output data.



Appendix D

Bender elements tests detailed results

In this appendix detailed results from bender elements testing are presented. The following data is included:

- Time from the beginning of consolidation, t (min, h)
- Axial deformation, δ (mm)
- Axial strain, ε_a (%)

$$\varepsilon_a = \frac{\delta}{H_0} \cdot 100\%$$

where $H_0 = 100 \text{ mm}$

- Expelled water, ΔV (mm)
- Volumetric strain, ε_{vol} (%)

$$\varepsilon_{vol} = \frac{\Delta V}{V_0} \cdot 100\%$$

where $V_0 = 229 \text{ cm}^3$

- Frequency, f (kHz)
- Bender delay, t_s (ms)
- Effective height, d (mm)
- Shear wave velocity, V_s (m/s)

$$V_s = \frac{d}{t_s}$$

- Small strain shear modulus, G_{max} (MPa)

$$G_{max} = \rho \cdot V_s^2$$

where ρ is density (g/cm^3)

- Wavelength, λ (mm)

$$\lambda = \frac{V_s}{f}$$

- Ratio d/λ (-)

Time, t		Frequency, f	Bender delay	Effective height, d	Shear wave velocity, V_s	G_{max}	$\lambda=v/f$	d/λ
min	h	kHz	ms	mm	m/s	MPa	mm	-
1	0,02	1,0	1,320	95,00	72,0	9,4	71,97	1,32
5	0,08	1,0	1,150	94,44	82,1	12,3	82,12	1,15
10	0,17	1,2	1,110	94,23	84,9	13,1	70,75	1,33
15	0,25	1,5	1,100	94,21	85,6	13,4	57,10	1,65
20	0,33	1,5	1,070	94,08	87,9	14,1	58,61	1,61
30	0,50	1,5	1,050	94,02	89,5	14,6	59,70	1,58
40	0,67	1,5	1,045	94,01	90,0	14,7	59,97	1,57
60	1,00	1,8	1,025	93,95	91,7	15,3	50,92	1,85
80	1,33	1,8	1,015	93,92	92,5	15,6	51,41	1,83
100	1,67	1,8	1,010	93,91	93,0	15,7	51,66	1,82
120	2,00	1,8	1,010	93,90	93,0	15,7	51,65	1,82
150	2,50	1,8	1,000	93,89	93,9	16,0	52,16	1,80
180	3,00	1,8	0,995	93,88	94,4	16,2	52,42	1,79
227	3,78	2,0	0,990	93,87	94,8	16,4	47,41	1,98

Time, t		Deformation= Axial strain, ϵ_a	Expelled water	Volumetric strain, ϵ_{vol}	Frequency, f	Bender delay	Effective height, d	Shear wave velocity, V_s	G_{max}	$\lambda=v/f$	d/λ
min	h	mm/%	ml	%	kHz	ms	mm	m/s	MPa	mm	-
1	0,02	0,475	1,70	0,741	1,0	1,086	94,53	87,0	13,8	87,04	1,09
5	0,08	0,813	2,63	1,148	1,5	1,070	94,19	88,0	14,1	58,68	1,61
10	0,17	0,951	2,66	1,161	1,5	1,060	94,05	88,7	14,3	59,15	1,59
15	0,25	1,089	2,70	1,179	1,5	1,045	93,91	89,9	14,7	59,91	1,57
20	0,33	1,126	2,88	1,259	1,5	1,025	93,87	91,6	15,3	61,06	1,54
30	0,50	1,144	3,02	1,320	1,8	1,000	93,86	93,9	16,0	52,14	1,80
40	0,67	1,152	3,08	1,347	1,8	0,985	93,85	95,3	16,5	52,93	1,77
60	1,00	1,159	3,12	1,360	1,8	0,975	93,84	96,2	16,9	53,47	1,76
80	1,33	1,162	3,11	1,358	1,8	0,970	93,84	96,7	17,0	53,74	1,75
94	1,56	1,164	3,13	1,367	1,8	0,965	93,84	97,2	17,2	54,02	1,74
100	1,67	1,165	3,13	1,365	1,8	0,960	93,84	97,7	17,4	54,30	1,73
120	2,00	1,167	3,12	1,364	1,8	0,955	93,83	98,3	17,6	54,59	1,72
150	2,50	1,124	3,11	1,358	1,8	0,955	93,88	98,3	17,6	54,61	1,72
180	3,00	1,123	3,11	1,358	2,0	0,950	93,88	98,8	17,8	49,41	1,90
222	3,71	1,170	3,09	1,349	2,0	0,945	93,83	99,3	17,9	49,65	1,89

Depth: 10,80-11,05 m		Vs: vh	Cell pressure: 75 kPa				end of primary consolidation				
Time, t		Deformation= Axial strain, ϵ_a	Expelled water	Volumetric strain, ϵ_{vol}	Frequency, f	Bender delay	Effective height, d	Shear wave velocity, Vs	G_{max}	$\lambda=v/f$	d/ λ
min	h	mm/%	ml	%	kHz	ms	mm	m/s	MPa	mm	-
1	0,02	0,389	1,70	0,744	0,7	1,170	94,61	80,9	11,9	115,52	0,82
5	0,08	0,724	2,41	1,054	1,7	1,150	94,28	82,0	12,2	48,24	1,95
10	0,17	0,916	2,89	1,260	1,7	1,080	94,08	87,1	13,8	51,25	1,84
15	0,25	1,066	3,27	1,430	1,7	1,030	93,93	91,2	15,1	53,65	1,75
20	0,33	1,141	3,62	1,583	1,7	1,005	93,86	93,4	15,9	54,94	1,71
30	0,50	1,233	3,94	1,720	1,7	0,970	93,77	96,7	17,0	56,87	1,65
40	0,67	1,277	4,06	1,772	1,7	0,956	93,72	98,0	17,5	57,65	1,63
60	1,00	1,309	4,13	1,805	1,7	0,937	93,69	100,0	18,2	58,82	1,59
80	1,33	1,323	4,16	1,818	1,8	0,927	93,68	101,0	18,6	56,11	1,67
100	1,67	1,330	4,18	1,824	1,8	0,927	93,67	101,0	18,6	56,11	1,67
104	1,74	1,331	4,18	1,825	1,8	0,927	93,67	101,0	18,6	56,11	1,67
120	2,00	1,339	4,19	1,829	2,0	0,927	93,66	101,0	18,6	50,50	1,85
150	2,50	1,352	4,18	1,826	2,0	0,927	93,65	101,0	18,6	50,50	1,85
180	3,00	1,358	4,18	1,827	2,0	0,915	93,64	102,3	19,1	51,17	1,83
240	4,00	1,366	4,22	1,842	2,0	0,905	93,63	103,5	19,5	51,73	1,81
300	5,00	1,373	4,22	1,842	2,0	0,900	93,63	104,0	19,7	52,00	1,80
360	6,00	1,378	4,23	1,848	2,0	0,892	93,62	105,0	20,1	52,50	1,78
420	7,00	1,382	4,23	1,847	2,0	0,892	93,62	105,0	20,1	52,50	1,78
480	8,00	1,386	4,23	1,847	2,0	0,892	93,61	105,0	20,1	52,50	1,78
540	9,00	1,390	4,22	1,843	2,0	0,892	93,61	105,0	20,1	52,50	1,78
600	10,00	1,395	4,24	1,851	2,0	0,891	93,60	105,0	20,1	52,50	1,78
660	11,00	1,398	4,25	1,854	2,0	0,885	93,60	105,8	20,4	52,88	1,77
720	12,00	1,400	4,24	1,852	2,0	0,883	93,60	106,0	20,4	53,00	1,77
780	13,00	1,401	4,24	1,850	2,0	0,883	93,60	106,0	20,4	53,00	1,77
840	14,00	1,403	4,24	1,851	2,0	0,880	93,60	106,4	20,6	53,18	1,76
900	15,00	1,404	4,23	1,848	2,0	0,883	93,60	106,0	20,4	53,00	1,77
960	16,00	1,406	4,25	1,855	2,0	0,883	93,59	106,0	20,4	53,00	1,77
1020	17,00	1,407	4,25	1,855	2,0	0,875	93,59	107,0	20,8	53,48	1,75
1080	18,00	1,408	4,25	1,855	2,0	0,875	93,59	107,0	20,8	53,48	1,75
1140	19,00	1,409	4,26	1,859	2,0	0,875	93,59	107,0	20,8	53,48	1,75
1200	20,00	1,410	4,23	1,848	2,0	0,875	93,59	107,0	20,8	53,48	1,75
1260	21,00	1,411	4,22	1,844	2,0	0,875	93,59	107,0	20,8	53,50	1,75
1320	22,00	1,412	4,19	1,831	2,0	0,870	93,59	107,6	21,1	53,79	1,74
1380	23,00	1,412	4,20	1,836	2,0	0,870	93,59	107,6	21,1	53,79	1,74
1440	24,00	1,412	4,21	1,838	2,0	0,870	93,59	107,6	21,1	53,79	1,74

Depth: 10,80-11,05 m		Vs: hv		Cell pressure: 75 kPa			end of primary consolidation				
Time, t		Deformation= Axial strain, ϵ_a	Expelled water	Volumetric strain, ϵ_{vol}	Frequency, f	Bender delay	Effective height, d	Shear wave velocity, Vs	G_{max}	$\lambda=v/f$	d/ λ
min	h	mm/%	ml	%	kHz	ms	mm	m/s	MPa	mm	-
1	0,02	0,284	1,96	0,856	1,5	1,250	94,72	75,8	10,4	50,51	1,88
5	0,08	1,218	2,67	1,167	1,5	1,140	93,78	82,3	12,3	54,84	1,71
10	0,17	1,365	3,30	1,440	1,8	1,060	93,63	88,3	14,2	49,07	1,91
15	0,25	1,396	3,71	1,622	1,8	1,010	93,60	92,7	15,6	51,49	1,82
20	0,33	1,425	3,99	1,744	1,8	0,985	93,58	95,0	16,4	52,78	1,77
30	0,50	1,457	4,31	1,883	1,8	0,950	93,54	98,5	17,6	54,70	1,71
40	0,67	1,475	4,52	1,974	1,8	0,935	93,52	100,0	18,2	55,57	1,68
60	1,00	1,496	4,74	2,068	1,8	0,910	93,50	102,8	19,2	57,08	1,64
80	1,33	1,507	4,85	2,118	1,8	0,900	93,49	103,9	19,6	57,71	1,62
100	1,67	1,513	4,90	2,138	1,8	0,895	93,49	104,5	19,9	58,03	1,61
120	2,00	1,518	4,93	2,151	2,0	0,890	93,48	105,0	20,1	52,52	1,78
150	2,50	1,523	4,97	2,169	2,0	0,885	93,48	105,6	20,3	52,81	1,77
158	2,63	1,524	4,98	2,174	2,0	0,885	93,48	105,6	20,3	52,81	1,77
180	3,00	1,526	4,99	2,178	2,0	0,885	93,47	105,6	20,3	52,81	1,77
240	4,00	1,531	5,07	2,213	2,0	0,880	93,47	106,2	20,5	53,11	1,76
300	5,00	1,535	5,16	2,251	2,0	0,875	93,47	106,8	20,8	53,41	1,75
360	6,00	1,538	5,20	2,272	2,0	0,870	93,46	107,4	21,0	53,71	1,74
420	7,00	1,542	5,23	2,284	2,0	0,870	93,46	107,4	21,0	53,71	1,74
480	8,00	1,545	5,27	2,302	2,0	0,865	93,46	108,0	21,2	54,02	1,73
540	9,00	1,548	5,28	2,306	2,0	0,865	93,45	108,0	21,2	54,02	1,73
600	10,00	1,550	5,29	2,311	2,0	0,860	93,45	108,7	21,5	54,33	1,72
660	11,00	1,552	5,29	2,309	2,0	0,860	93,45	108,7	21,5	54,33	1,72
720	12,00	1,554	5,29	2,311	2,0	0,855	93,45	109,3	21,7	54,65	1,71
780	13,00	1,557	5,31	2,319	2,0	0,855	93,44	109,3	21,7	54,65	1,71
840	14,00	1,559	5,30	2,316	2,0	0,855	93,44	109,3	21,7	54,64	1,71
900	15,00	1,560	5,31	2,320	2,0	0,855	93,44	109,3	21,7	54,64	1,71
960	16,00	1,562	5,34	2,330	2,0	0,850	93,44	109,9	22,0	54,96	1,70
1020	17,00	1,563	5,34	2,330	2,0	0,850	93,44	109,9	22,0	54,96	1,70
1080	18,00	1,564	5,34	2,330	2,0	0,850	93,44	109,9	22,0	54,96	1,70
1140	19,00	1,567	5,35	2,335	2,0	0,850	93,43	109,9	22,0	54,96	1,70
1200	20,00	1,567	5,34	2,332	2,0	0,850	93,43	109,9	22,0	54,96	1,70
1260	21,00	1,567	5,34	2,332	2,0	0,850	93,43	109,9	22,0	54,96	1,70
1320	22,00	1,567	5,34	2,332	2,0	0,850	93,43	109,9	22,0	54,96	1,70
1380	23,00	1,567	5,34	2,332	2,0	0,850	93,43	109,9	22,0	54,96	1,70
1440	24,00	1,567	5,34	2,332	2,0	0,850	93,43	109,9	22,0	54,96	1,70

Depth: 12,80-13,15 m		Vs: vh1	Cell pressure: 87,6 kPa				end of primary consolidation				
Time, t		Deformation= Axial strain, ϵ_a	Expelled water	Volumetric strain, ϵ_{vol}	Frequency, f	Bender delay	Effective height, d	Shear wave velocity, Vs	G_{max}	$\lambda=v/f$	d/ λ
min	h	mm/%	ml	%	kHz	ms	mm	m/s	MPa	mm	-
1	0,02	0,158	2,19	0,956	1,2	1,109	94,84	85,5	13,3	71,27	1,33
5	0,08	0,367	2,95	1,289	1,4	1,000	94,63	94,6	16,3	67,59	1,40
10	0,17	0,521	3,54	1,545	1,7	0,945	94,48	100,0	18,2	58,81	1,61
15	0,25	0,611	3,84	1,677	1,7	0,908	94,39	104,0	19,7	61,15	1,54
20	0,33	0,666	4,03	1,760	1,7	0,885	94,33	106,6	20,7	62,70	1,50
30	0,50	0,726	4,27	1,864	1,7	0,865	94,27	109,0	21,6	64,11	1,47
40	0,67	0,755	4,37	1,910	1,7	0,850	94,25	110,9	22,4	65,22	1,45
60	1,00	0,780	4,50	1,963	1,7	0,835	94,22	112,8	23,2	66,38	1,42
80	1,33	0,790	4,51	1,968	1,8	0,830	94,21	113,5	23,4	63,06	1,49
100	1,67	0,796	4,50	1,964	1,8	0,825	94,20	114,2	23,7	63,44	1,49
109	1,82	0,799	4,51	1,969	1,8	0,825	94,20	114,2	23,7	63,44	1,49
120	2,00	0,803	4,54	1,981	1,8	0,825	94,20	114,2	23,7	63,43	1,49
150	2,50	0,812	4,57	1,997	1,9	0,820	94,19	114,9	24,0	60,45	1,56
180	3,00	0,817	4,58	1,998	1,9	0,815	94,18	115,6	24,3	60,82	1,55
240	4,00	0,823	4,59	2,003	1,9	0,810	94,18	116,3	24,6	61,19	1,54
300	5,00	0,827	4,59	2,004	2,0	0,810	94,17	116,3	24,6	58,13	1,62
360	6,00	0,830	4,58	2,000	2,0	0,810	94,17	116,3	24,6	58,13	1,62
420	7,00	0,833	4,61	2,015	2,0	0,805	94,17	117,0	24,9	58,49	1,61
480	8,00	0,836	4,68	2,042	2,0	0,800	94,16	117,7	25,2	58,85	1,60
540	9,00	0,840	4,69	2,049	2,0	0,800	94,16	117,7	25,2	58,85	1,60
600	10,00	0,844	4,73	2,066	2,0	0,795	94,16	118,4	25,5	59,22	1,59
660	11,00	0,847	4,74	2,071	2,0	0,795	94,15	118,4	25,5	59,22	1,59
720	12,00	0,850	4,76	2,078	2,0	0,790	94,15	119,2	25,8	59,59	1,58
780	13,00	0,853	4,77	2,084	2,0	0,790	94,15	119,2	25,8	59,59	1,58
840	14,00	0,855	4,78	2,087	2,0	0,785	94,14	119,9	26,2	59,96	1,57
900	15,00	0,857	4,78	2,088	2,0	0,785	94,14	119,9	26,2	59,96	1,57
960	16,00	0,859	4,78	2,088	2,0	0,785	94,14	119,9	26,2	59,96	1,57
1020	17,00	0,860	4,79	2,092	2,0	0,785	94,14	119,9	26,2	59,96	1,57
1080	18,00	0,861	4,81	2,100	2,0	0,785	94,14	119,9	26,2	59,96	1,57
1140	19,00	0,862	4,82	2,103	2,0	0,780	94,14	120,7	26,5	60,34	1,56
1200	20,00	0,863	4,82	2,103	2,0	0,780	94,14	120,7	26,5	60,34	1,56
1260	21,00	0,866	4,84	2,115	2,0	0,780	94,13	120,7	26,5	60,34	1,56
1320	22,00	0,867	4,81	2,102	2,0	0,780	94,13	120,7	26,5	60,34	1,56
1380	23,00	0,866	4,81	2,099	2,0	0,780	94,13	120,7	26,5	60,34	1,56
1440	24,00	0,866	4,77	2,084	2,0	0,780	94,13	120,7	26,5	60,34	1,56

Depth: 12,80-13,15 m		Vs: vh2	Cell pressure: 87,6 kPa				end of primary consolidation				
Time, t		Deformation= Axial strain, ϵ_a	Expelled water	Volumetric strain, ϵ_{vol}	Frequency, f	Bender delay	Effective height, d	Shear wave velocity, Vs	G_{max}	$\lambda=v/f$	d/ λ
min	h	mm/%	ml	%	kHz	ms	mm	m/s	MPa	mm	-
1	0,02	0,299	1,939	0,847	1,0	1,110	94,70	85,3	13,2	85,32	1,11
5	0,08	0,663	2,630	1,148	1,4	1,030	94,34	91,6	15,3	65,42	1,44
10	0,17	0,821	3,170	1,384	1,4	0,960	94,18	98,1	17,5	70,07	1,34
15	0,25	0,909	3,536	1,544	1,4	0,930	94,09	101,2	18,6	72,27	1,30
20	0,33	0,972	3,969	1,733	1,4	0,900	94,03	104,5	19,9	74,63	1,26
30	0,50	1,047	4,270	1,865	1,6	0,870	93,95	108,0	21,2	67,50	1,39
40	0,67	1,077	4,402	1,922	1,6	0,860	93,92	109,2	21,7	68,26	1,38
60	1,00	1,104	4,563	1,993	1,6	0,845	93,90	111,1	22,5	69,45	1,35
80	1,33	1,114	4,633	2,023	1,6	0,835	93,89	112,4	23,0	70,27	1,34
100	1,67	1,120	4,680	2,044	1,6	0,830	93,88	113,1	23,3	70,69	1,33
120	2,00	1,124	4,726	2,064	1,6	0,830	93,88	113,1	23,3	70,69	1,33
150	2,50	1,128	4,770	2,083	2,0	0,825	93,87	113,8	23,6	56,89	1,65
180	3,00	1,131	4,816	2,103	2,0	0,825	93,87	113,8	23,6	56,89	1,65
228	3,80	1,135	4,887	2,134	2,0	0,820	93,87	114,5	23,8	57,23	1,64
240	4,00	1,136	4,878	2,130	2,0	0,820	93,86	114,5	23,8	57,23	1,64
300	5,00	1,139	4,937	2,156	2,0	0,815	93,86	115,2	24,1	57,58	1,63
360	6,00	1,140	4,965	2,168	2,0	0,815	93,86	115,2	24,1	57,58	1,63
420	7,00	1,143	5,064	2,211	2,0	0,810	93,86	115,9	24,4	57,94	1,62
480	8,00	1,146	5,117	2,234	2,0	0,810	93,85	115,9	24,4	57,93	1,62
540	9,00	1,150	5,156	2,252	2,0	0,805	93,85	116,6	24,7	58,29	1,61
600	10,00	1,152	5,190	2,266	2,0	0,805	93,85	116,6	24,7	58,29	1,61
660	11,00	1,154	5,213	2,277	2,0	0,800	93,85	117,3	25,0	58,65	1,60
720	12,00	1,156	5,222	2,280	2,0	0,800	93,84	117,3	25,0	58,65	1,60
780	13,00	1,158	5,249	2,292	2,0	0,800	93,84	117,3	25,0	58,65	1,60
840	14,00	1,159	5,262	2,298	2,0	0,800	93,84	117,3	25,0	58,65	1,60
900	15,00	1,160	5,279	2,305	2,0	0,800	93,84	117,3	25,0	58,65	1,60
960	16,00	1,162	5,286	2,308	2,0	0,800	93,84	117,3	25,0	58,65	1,60
1020	17,00	1,163	5,324	2,325	2,0	0,800	93,84	117,3	25,0	58,65	1,60
1080	18,00	1,164	5,340	2,332	2,0	0,795	93,84	118,0	25,4	59,02	1,59
1140	19,00	1,164	5,337	2,331	2,0	0,795	93,84	118,0	25,4	59,02	1,59
1200	20,00	1,169	5,310	2,319	2,0	0,795	93,83	118,0	25,4	59,01	1,59
1260	21,00	1,168	5,306	2,317	2,0	0,795	93,83	118,0	25,4	59,01	1,59
1320	22,00	1,168	5,330	2,327	2,0	0,795	93,83	118,0	25,4	59,01	1,59
1380	23,00	1,168	5,341	2,332	2,0	0,795	93,83	118,0	25,4	59,01	1,59
1440	24,00	1,168	5,358	2,340	2,0	0,795	93,83	118,0	25,4	59,01	1,59
1500	25,00	1,168	5,359	2,340	2,0	0,795	93,83	118,0	25,4	59,01	1,59
1800	30,00	1,169	5,576	2,435	2,0	0,790	93,83	118,8	25,7	59,39	1,58
2100	35,00	1,179	5,913	2,582	2,0	0,785	93,82	119,5	26,0	59,76	1,57
2400	40,00	1,186	6,102	2,665	2,0	0,780	93,81	120,3	26,3	60,14	1,56
3000	50,00	1,191	6,484	2,831	2,0	0,780	93,81	120,3	26,3	60,13	1,56
3600	60,00	1,197	7,272	3,176	2,0	0,775	93,80	121,0	26,7	60,52	1,55
4200	70,00	1,212	8,006	3,496	2,0	0,770	93,79	121,8	27,0	60,90	1,54
4620	77,00	1,215	8,731	3,813	2,0	0,770	93,78	121,8	27,0	60,90	1,54

Depth: 12,80-13,15 m		Vs: hv		Cell pressure: 87,6 kPa			end of primary consolidation				
Time, t		Deformation= Axial strain, ϵ_a	Expelled water	Volumetric strain, ϵ_{vol}	Frequency, f	Bender delay	Effective height, d	Shear wave velocity, Vs	G_{max}	$\lambda=v/f$	d/ λ
min	h	mm/%	ml	%	kHz	ms	mm	m/s	MPa	mm	-
1	0,02	0,115	2,27	0,992	1,3	1,040	94,88	91,2	15,1	70,18	1,35
5	0,08	0,179	2,84	1,242	1,3	0,970	94,82	97,8	17,4	75,20	1,26
10	0,17	0,212	3,29	1,438	1,6	0,940	94,79	100,8	18,5	63,02	1,50
15	0,25	0,233	3,59	1,569	1,7	0,915	94,77	103,6	19,5	60,92	1,56
20	0,33	0,247	3,80	1,661	1,7	0,895	94,75	105,9	20,4	62,28	1,52
30	0,50	0,265	4,05	1,767	1,7	0,875	94,74	108,3	21,3	63,69	1,49
40	0,67	0,275	4,15	1,814	1,7	0,865	94,72	109,5	21,8	64,42	1,47
60	1,00	0,288	4,33	1,890	1,7	0,850	94,71	111,4	22,6	65,54	1,45
80	1,33	0,295	4,47	1,953	1,7	0,840	94,71	112,7	23,1	66,32	1,43
100	1,67	0,300	4,57	1,994	1,7	0,835	94,70	113,4	23,4	66,71	1,42
120	2,00	0,304	4,63	2,024	1,7	0,835	94,70	113,4	23,4	66,71	1,42
150	2,50	0,307	4,69	2,049	1,7	0,830	94,69	114,1	23,7	67,11	1,41
180	3,00	0,309	4,76	2,076	1,8	0,825	94,69	114,8	24,0	63,76	1,49
240	4,00	0,314	4,87	2,125	1,8	0,820	94,69	115,5	24,3	64,15	1,48
258	4,31	0,314	4,90	2,140	1,8	0,820	94,69	115,5	24,3	64,15	1,48
300	5,00	0,316	4,96	2,166	2,0	0,815	94,68	116,2	24,6	58,09	1,63
360	6,00	0,319	5,04	2,199	2,0	0,815	94,68	116,2	24,6	58,09	1,63
420	7,00	0,320	5,10	2,228	2,0	0,810	94,68	116,9	24,9	58,44	1,62
480	8,00	0,321	5,18	2,260	2,0	0,810	94,68	116,9	24,9	58,44	1,62
540	9,00	0,323	5,24	2,287	2,0	0,805	94,68	117,6	25,2	58,81	1,61
600	10,00	0,325	5,31	2,318	2,0	0,805	94,68	117,6	25,2	58,80	1,61
660	11,00	0,327	5,39	2,352	2,0	0,805	94,67	117,6	25,2	58,80	1,61
720	12,00	0,328	5,44	2,374	2,0	0,800	94,67	118,3	25,5	59,17	1,60
780	13,00	0,330	5,49	2,398	2,0	0,800	94,67	118,3	25,5	59,17	1,60
840	14,00	0,332	5,55	2,422	2,0	0,800	94,67	118,3	25,5	59,17	1,60
900	15,00	0,333	5,59	2,441	2,0	0,795	94,67	119,1	25,8	59,54	1,59
960	16,00	0,333	5,63	2,460	2,0	0,795	94,67	119,1	25,8	59,54	1,59
1020	17,00	0,334	5,68	2,479	2,0	0,795	94,67	119,1	25,8	59,54	1,59
1080	18,00	0,335	5,76	2,516	2,0	0,795	94,66	119,1	25,8	59,54	1,59
1140	19,00	0,336	5,85	2,553	2,0	0,795	94,66	119,1	25,8	59,54	1,59
1200	20,00	0,337	5,86	2,557	2,0	0,795	94,66	119,1	25,8	59,54	1,59
1260	21,00	0,337	5,90	2,575	2,0	0,790	94,66	119,8	26,1	59,91	1,58
1320	22,00	0,337	5,97	2,605	2,0	0,790	94,66	119,8	26,1	59,91	1,58
1380	23,00	0,336	6,01	2,624	2,0	0,790	94,66	119,8	26,1	59,91	1,58
1440	24,00	0,336	6,13	2,675	2,0	0,790	94,66	119,8	26,1	59,91	1,58

Depth: 12,80-13,15 m		Vs: hh	Cell pressure: 87,6 kPa				end of primary consolidation				
Time, t		Deformation= Axial strain, ϵ_a	Expelled water	Volumetric strain, ϵ_{vol}	Frequency, f	Bender delay	Effective height, d	Shear wave velocity, Vs	G_{max}	$\lambda=v/f$	d/ λ
min	h	mm/%	ml	%	kHz	ms	mm	m/s	MPa	mm	-
1	0,02	0,295	2,53	1,105	2,5	0,830	94,71	114,1	23,7	45,64	2,08
5	0,08	1,462	3,69	1,612	2,8	0,765	93,54	122,3	27,2	43,67	2,14
10	0,17	2,971	4,16	1,814	2,8	0,730	92,03	126,1	28,9	45,02	2,04
15	0,25	3,710	4,56	1,990	2,8	0,710	91,29	128,6	30,1	45,92	1,99
20	0,33	3,727	4,82	2,105	2,8	0,695	91,27	131,3	31,4	46,90	1,95
30	0,50	3,746	4,94	2,155	2,8	0,685	91,25	133,2	32,3	47,58	1,92
40	0,67	3,756	5,01	2,189	2,8	0,680	91,24	134,2	32,8	47,92	1,90
60	1,00	3,766	5,03	2,195	2,8	0,675	91,23	135,2	33,2	48,27	1,89
80	1,33	3,771	5,05	2,204	2,8	0,670	91,23	136,2	33,7	48,63	1,88
92	1,53	3,773	5,06	2,209	2,8	0,670	91,23	136,2	33,7	48,63	1,88
100	1,67	3,774	5,09	2,221	3,0	0,665	91,23	137,2	34,3	45,73	2,00
120	2,00	3,776	5,09	2,225	3,0	0,665	91,22	137,2	34,2	45,73	2,00
150	2,50	3,778	5,15	2,250	3,0	0,665	91,22	137,2	34,2	45,73	2,00
180	3,00	3,779	5,20	2,270	3,0	0,660	91,22	138,2	34,8	46,07	1,98
240	4,00	3,779	5,36	2,339	3,0	0,660	91,22	138,2	34,8	46,07	1,98
300	5,00	3,779	5,46	2,386	3,0	0,660	91,22	138,2	34,8	46,07	1,98
360	6,00	3,779	5,57	2,432	3,0	0,655	91,22	139,3	35,3	46,42	1,97
420	7,00	3,780	5,68	2,482	3,0	0,655	91,22	139,3	35,3	46,42	1,97
480	8,00	3,781	5,78	2,523	3,0	0,655	91,22	139,3	35,3	46,42	1,97
540	9,00	3,782	5,85	2,556	3,0	0,650	91,22	140,3	35,8	46,78	1,95
600	10,00	3,783	5,96	2,603	3,0	0,650	91,22	140,3	35,8	46,78	1,95
660	11,00	3,783	6,09	2,657	3,0	0,650	91,22	140,3	35,8	46,78	1,95
720	12,00	3,784	6,19	2,703	3,0	0,650	91,22	140,3	35,8	46,78	1,95
780	13,00	3,785	6,33	2,762	3,0	0,650	91,21	140,3	35,8	46,78	1,95
840	14,00	3,787	6,52	2,848	3,0	0,650	91,21	140,3	35,8	46,78	1,95
900	15,00	3,789	6,62	2,888	3,0	0,645	91,21	141,4	36,4	47,14	1,94
960	16,00	3,791	6,75	2,947	3,0	0,645	91,21	141,4	36,4	47,14	1,94
1020	17,00	3,792	6,80	2,968	3,0	0,645	91,21	141,4	36,4	47,14	1,94
1080	18,00	3,793	6,91	3,017	3,0	0,645	91,21	141,4	36,4	47,14	1,94
1140	19,00	3,794	6,99	3,051	3,0	0,645	91,21	141,4	36,4	47,13	1,94
1200	20,00	3,795	7,09	3,097	3,0	0,645	91,21	141,4	36,4	47,13	1,94
1260	21,00	3,795	7,21	3,147	3,0	0,645	91,21	141,4	36,4	47,13	1,94
1320	22,00	3,796	7,33	3,200	3,0	0,645	91,20	141,4	36,4	47,13	1,94
1380	23,00	3,796	7,46	3,258	3,0	0,640	91,20	142,5	37,0	47,50	1,92
1440	24,00	3,797	7,60	3,318	3,0	0,640	91,20	142,5	37,0	47,50	1,92

Depth: 19,45-19,70 m		Vs: vh	Cell pressure: 134,9 kPa				end of primary consolidation				
Time, t		Deformation= Axial strain, ϵ_a	Expelled water	Volumetric strain, ϵ_{vol}	Frequency, f	Bender delay	Effective height, d	Shear wave velocity, V_s	G_{max}	$\lambda=v/f$	d/ λ
min	h	mm/%	ml	%	kHz	ms	mm	m/s	MPa	mm	-
1	0,02	0,278	2,58	1,125	1,2	0,830	94,72	114,1	24,1	95,10	1,00
5	0,08	1,138	3,14	1,372	1,4	0,770	93,86	121,9	27,5	87,07	1,08
10	0,17	1,790	3,56	1,555	1,4	0,730	93,21	127,7	30,2	91,20	1,02
15	0,25	1,977	3,80	1,658	1,7	0,715	93,02	130,1	31,3	76,53	1,22
20	0,33	2,029	3,94	1,720	1,7	0,700	92,97	132,8	32,6	78,13	1,19
30	0,50	2,109	4,08	1,782	1,8	0,690	92,89	134,6	33,5	74,79	1,24
40	0,67	2,145	4,15	1,813	1,8	0,680	92,85	136,6	34,5	75,86	1,22
60	1,00	2,164	4,18	1,824	1,8	0,670	92,84	138,6	35,5	76,98	1,21
80	1,33	2,172	4,18	1,825	1,8	0,670	92,83	138,5	35,5	76,97	1,21
91	1,52	2,177	4,19	1,830	1,8	0,665	92,82	139,6	36,0	77,55	1,20
100	1,67	2,180	4,18	1,825	1,8	0,665	92,82	139,6	36,0	77,54	1,20
120	2,00	2,189	4,19	1,827	2,0	0,665	92,81	139,6	36,0	69,78	1,33
150	2,50	2,195	4,17	1,821	2,0	0,665	92,81	139,6	36,0	69,78	1,33
180	3,00	2,199	4,17	1,819	2,0	0,660	92,80	140,6	36,6	70,30	1,32
240	4,00	2,204	4,17	1,822	2,0	0,655	92,80	141,7	37,1	70,84	1,31
300	5,00	2,207	4,19	1,829	2,0	0,655	92,79	141,7	37,1	70,83	1,31
360	6,00	2,211	4,21	1,836	2,0	0,650	92,79	142,8	37,7	71,38	1,30
420	7,00	2,215	4,23	1,846	2,0	0,650	92,79	142,7	37,7	71,37	1,30
480	8,00	2,218	4,25	1,856	2,0	0,645	92,78	143,8	38,3	71,92	1,29
540	9,00	2,223	4,27	1,864	2,0	0,645	92,78	143,8	38,3	71,92	1,29
600	10,00	2,226	4,26	1,858	2,0	0,640	92,77	145,0	38,9	72,48	1,28
660	11,00	2,228	4,27	1,865	2,0	0,640	92,77	145,0	38,9	72,48	1,28
720	12,00	2,231	4,28	1,868	2,0	0,640	92,77	145,0	38,9	72,48	1,28
780	13,00	2,232	4,28	1,868	2,0	0,635	92,77	146,1	39,5	73,05	1,27
840	14,00	2,234	4,27	1,863	2,0	0,635	92,77	146,1	39,5	73,04	1,27
900	15,00	2,235	4,26	1,859	2,0	0,635	92,76	146,1	39,5	73,04	1,27
960	16,00	2,237	4,24	1,852	2,0	0,635	92,76	146,1	39,5	73,04	1,27
1020	17,00	2,238	4,26	1,860	2,0	0,635	92,76	146,1	39,5	73,04	1,27
1080	18,00	2,239	4,24	1,853	2,0	0,635	92,76	146,1	39,5	73,04	1,27
1140	19,00	2,240	4,24	1,853	2,0	0,635	92,76	146,1	39,5	73,04	1,27
1200	20,00	2,241	4,22	1,841	2,0	0,635	92,76	146,1	39,5	73,04	1,27
1260	21,00	2,258	4,18	1,827	2,0	0,635	92,74	146,1	39,5	73,03	1,27
1320	22,00	2,259	4,19	1,829	2,0	0,635	92,74	146,0	39,5	73,02	1,27
1380	23,00	2,261	4,20	1,835	2,2	0,635	92,74	146,0	39,5	66,38	1,40
1440	24,00	2,262	4,24	1,850	2,2	0,635	92,74	146,0	39,5	66,38	1,40

Time, t		Deformation= Axial strain, ϵ_a	Expelled water	Volumetric strain, ϵ_{vol}	Frequency, f	Bender delay	Effective height, d	Shear wave velocity, V_s	G_{max}	$\lambda=v/f$	d/ λ
min	h	mm/%	ml	%	kHz	ms	mm	m/s	MPa	mm	-
1	0,02	0,312	2,40	1,048	1,0	0,740	94,69	128,0	30,3	127,96	0,74
5	0,08	0,785	2,98	1,302	1,6	0,725	94,22	130,0	31,2	81,22	1,16
10	0,17	0,786	3,47	1,513	1,8	0,690	94,21	136,5	34,5	75,86	1,24
15	0,25	0,786	3,71	1,618	1,8	0,670	94,21	140,6	36,6	78,12	1,21
20	0,33	0,787	3,87	1,689	1,8	0,660	94,21	142,7	37,7	79,30	1,19
30	0,50	0,787	4,04	1,762	2,0	0,650	94,21	144,9	38,9	72,47	1,30
40	0,67	0,787	4,11	1,795	2,0	0,645	94,21	146,1	39,5	73,03	1,29
60	1,00	0,786	4,21	1,837	2,0	0,635	94,21	148,4	40,7	74,18	1,27
80	1,33	0,786	4,26	1,862	2,2	0,635	94,21	148,4	40,7	67,44	1,40
100	1,67	0,786	4,32	1,885	2,2	0,630	94,21	149,5	41,4	67,98	1,39
120	2,00	0,786	4,37	1,907	2,2	0,630	94,21	149,5	41,4	67,98	1,39
150	2,50	0,786	4,49	1,960	2,2	0,625	94,21	150,7	42,0	68,52	1,38
180	3,00	0,786	4,53	1,977	2,2	0,620	94,21	152,0	42,7	69,07	1,36
211	3,51	0,786	4,58	2,000	2,2	0,620	94,21	152,0	42,7	69,07	1,36
240	4,00	0,786	4,61	2,011	2,2	0,620	94,21	152,0	42,7	69,07	1,36
300	5,00	0,786	4,68	2,043	2,2	0,615	94,21	153,2	43,4	69,63	1,35
360	6,00	0,786	4,77	2,081	2,2	0,610	94,21	154,4	44,1	70,20	1,34
420	7,00	0,787	4,82	2,103	2,2	0,610	94,21	154,4	44,1	70,20	1,34
480	8,00	0,788	4,87	2,124	2,2	0,610	94,21	154,4	44,1	70,20	1,34
540	9,00	0,789	4,93	2,151	2,2	0,605	94,21	155,7	44,9	70,78	1,33
600	10,00	0,790	5,01	2,188	2,2	0,605	94,21	155,7	44,9	70,78	1,33
660	11,00	0,790	5,05	2,206	2,2	0,605	94,21	155,7	44,9	70,78	1,33
720	12,00	0,792	5,13	2,240	2,2	0,605	94,21	155,7	44,9	70,78	1,33
780	13,00	0,792	5,19	2,267	2,2	0,605	94,21	155,7	44,9	70,78	1,33
840	14,00	0,792	5,27	2,301	2,2	0,605	94,21	155,7	44,9	70,78	1,33
900	15,00	0,793	5,32	2,322	2,2	0,605	94,21	155,7	44,9	70,78	1,33
960	16,00	0,780	5,34	2,333	2,2	0,600	94,22	157,0	45,6	71,38	1,32
1020	17,00	0,780	5,53	2,413	2,2	0,600	94,22	157,0	45,6	71,38	1,32
1080	18,00	0,780	5,61	2,450	2,2	0,600	94,22	157,0	45,6	71,38	1,32
1140	19,00	0,780	5,67	2,476	2,2	0,600	94,22	157,0	45,6	71,38	1,32
1200	20,00	0,780	5,78	2,522	2,2	0,600	94,22	157,0	45,6	71,38	1,32
1260	21,00	0,780	5,93	2,589	2,2	0,600	94,22	157,0	45,6	71,38	1,32
1320	22,00	0,780	6,05	2,640	2,2	0,600	94,22	157,0	45,6	71,38	1,32
1380	23,00	0,780	6,21	2,712	2,2	0,600	94,22	157,0	45,6	71,38	1,32
1440	24,00	0,780	6,40	2,795	2,2	0,600	94,22	157,0	45,6	71,38	1,32

Time, t		Deformation= Axial strain, ϵ_a	Expelled water	Volumetric strain, ϵ_{vol}	Frequency, f	Bender delay	Effective height, d	Shear wave velocity, V_s	G_{max}	$\lambda=v/f$	d/ λ
min	h	mm/%	ml	%	kHz	ms	mm	m/s	MPa	mm	-
1	0,02	0,303	2,17	0,947	2,0	0,705	94,70	134,3	33,4	67,16	1,41
5	0,08	1,498	2,89	1,260	2,4	0,655	93,50	142,8	37,7	59,48	1,57
10	0,17	1,594	3,35	1,461	2,5	0,615	93,41	151,9	42,7	60,75	1,54
15	0,25	1,626	3,66	1,599	2,5	0,590	93,37	158,3	46,3	63,30	1,48
20	0,33	1,656	3,85	1,682	2,5	0,575	93,34	162,3	48,8	64,93	1,44
30	0,50	1,696	4,11	1,794	2,5	0,555	93,30	168,1	52,3	67,25	1,39
40	0,67	1,721	4,24	1,851	2,5	0,540	93,28	172,7	55,2	69,10	1,35
60	1,00	1,743	4,35	1,901	2,5	0,535	93,26	174,3	56,2	69,72	1,34
80	1,33	1,754	4,43	1,934	2,5	0,525	93,25	177,6	58,4	71,04	1,31
100	1,67	1,763	4,46	1,946	2,5	0,525	93,24	177,6	58,3	71,04	1,31
120	2,00	1,767	4,50	1,964	2,5	0,520	93,23	179,3	59,5	71,72	1,30
150	2,50	1,773	4,55	1,988	2,5	0,520	93,23	179,3	59,5	71,71	1,30
162	2,70	1,774	4,56	1,991	2,5	0,515	93,23	181,0	60,6	72,41	1,29
180	3,00	1,777	4,58	2,000	2,5	0,515	93,22	181,0	60,6	72,41	1,29
240	4,00	1,783	4,63	2,020	2,5	0,515	93,22	181,0	60,6	72,40	1,29
300	5,00	1,788	4,65	2,031	2,5	0,510	93,21	182,8	61,8	73,11	1,28
360	6,00	1,791	4,71	2,058	2,5	0,510	93,21	182,8	61,8	73,11	1,28
420	7,00	1,792	4,78	2,089	2,5	0,510	93,21	182,8	61,8	73,10	1,28
480	8,00	1,794	4,83	2,109	2,5	0,505	93,21	184,6	63,0	73,83	1,26
540	9,00	1,796	4,88	2,131	2,5	0,505	93,20	184,6	63,0	73,82	1,26
600	10,00	1,799	4,94	2,155	2,5	0,505	93,20	184,6	63,0	73,82	1,26
660	11,00	1,801	4,98	2,173	2,5	0,500	93,20	186,4	64,3	74,56	1,25
720	12,00	1,803	5,00	2,183	2,5	0,500	93,20	186,4	64,3	74,56	1,25
780	13,00	1,805	5,03	2,198	2,5	0,500	93,20	186,4	64,3	74,56	1,25
840	14,00	1,807	5,10	2,228	2,5	0,500	93,19	186,4	64,3	74,55	1,25
900	15,00	1,809	5,14	2,243	2,5	0,500	93,19	186,4	64,3	74,55	1,25
960	16,00	1,812	5,18	2,262	2,5	0,495	93,19	188,3	65,6	75,30	1,24
1020	17,00	1,813	5,21	2,276	2,5	0,495	93,19	188,3	65,6	75,30	1,24
1080	18,00	1,815	5,30	2,312	2,5	0,495	93,18	188,3	65,6	75,30	1,24
1140	19,00	1,817	5,31	2,321	2,5	0,495	93,18	188,2	65,6	75,30	1,24
1200	20,00	1,818	5,34	2,332	2,5	0,495	93,18	188,2	65,6	75,30	1,24
1260	21,00	1,818	5,44	2,373	2,5	0,495	93,18	188,2	65,6	75,30	1,24
1320	22,00	1,821	5,57	2,434	2,5	0,495	93,18	188,2	65,6	75,30	1,24
1380	23,00	1,822	5,61	2,449	2,5	0,495	93,18	188,2	65,6	75,30	1,24
1440	24,00	1,824	5,65	2,468	2,5	0,495	93,18	188,2	65,5	75,29	1,24

